Experimental study of fluctuations in ultra-narrow superconducting nanowires

Maciej Zgirski
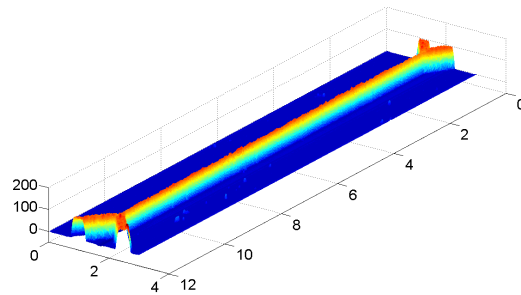
Academic Dissertation
for the Degree of Doctor of Philosophy

To be presented,
by permission of the Faculty of Mathematics and Natural Sciences
of the University of Jyväskylä,
for public examination in Auditorium FYS-1
of the University of Jyväskylä
on September 26, 2008 at 12 o'clock noon

Jyväskylä, Finland
September, 2008

Dla Moniszona

The intellectual attractiveness of a concept
is not sufficient to prove that the concept is right.

PREFACE

My idea, when writing this Thesis, was that it should be understandable for somebody not familiar with the subject. I hope any reader with background in physics will be able to follow it without studying additional references. It is the reason why for an experienced reader some sections of this work may seem slightly too simple. I prefer to discuss simpler formulas which I understand to big extent than to present a priori some complicated equations whose origin is not quite clear to me because of the complexity of the derivation. It was especially the case when I introduced expressions for the finite resistance of 1D superconducting wire in the quantum phase slip regime: I used not fully formal derivation, but instead I presented some plausible arguments to arrive at the final result. In my opinion such approach is better for an experimentalist, not fully conscious of the entire mathematical machinery employed by theorists to get formally clear result. I believe my approach should give one a flavor of the described physics. Formal result is of course the most important, but very often it lacks transparency necessary to get a good grasp of a physical phenomenon. I apologize to all of you who expected to find impressive mathematical expressions. Finally the Thesis is about experiment and all the time I tried to present only that part of the theory which has the direct application in discussed experiments. I also tested my physical intuition trying to find "shortcuts" in some derivations or alternative explanations of the observed phenomena. Physics is full of analogies which lend strong support to the physical intuition. Quantum mechanics has not been born without a good intuition of de Broglie who postulated wave nature of the matter. In physics usually intuition is enough to understand the THING and precedes the mathematical development of the formal theory.

Maciej Zgirski
Jyväskylä, summer 2008

Contents

LIST OF FIGURES

(**T**)

(**O**)

(**W**)

(**S**)

(**E**)

(**A**)

Note: If not indicated in the figure caption the figure is my original contribution.

LIST OF PUBLICATIONS

The Thesis is based on the work contained in the following papers:

1. ***Quantum fluctuations in ultranarrow superconducting nanowires***
   M. Zgirski, K.-P. Riikonen, V. Touboltsev, K.Yu. Arutyunov
   Physical Review B 77, 054508 (2008)
2. ***Ion beam shaping and downsizing of nanostructures***
   M. Zgirski, K.-P. Riikonen, V. Touboltsev, P. Jalkanen, T. Hongisto, K.Yu. Arutyunov
   Nanotechnology 19, 055301 (2008)
3. ***Experimental limits of the observation of thermally activated phase slip mechanism in superconducting wires***
   M. Zgirski, K. Arutyunov
   Physical Review B 75, 172509 (2007)
4. ***Size-dependent enhancement of superconductivity in Al and Sn nanowires: Shape resonance effect***
   A. Shanenko, M. Croitoru, **M. Zgirski**, F. Peeters, and K. Arutyunov,
   Physical Review B 74, 052502 (2006)
5. ***Size Dependent Breakdown of Superconductivity in Ultranarrow Nanowires***
   M. Zgirski, K-P. Riikonen, V. Touboltsev, and K. Arutyunov,
   NanoLetters, V.5, No.6 (2005)
6. ***Resistive state of quasi-one-dimensional superconductors: fluctuations vs. sample inhomogeneity***, **M. Zgirski**, K.Yu. Arutyunov, **Physica E** 40 160-162 (2007)
7. ***Quantum Limitations of Electron Transport in Ultra-Narrow Nanowires***,
   K. Arutyunov, **M. Zgirski**, K.-P. Riikonen, and P. Jalkanen, International **Review of Physics (IREPHY)**, V. 1, N. 1, pp. 28-30 (2007)
8. ***Phase slip phenomena in ultra-thin superconducting wires***
   M. Zgirski, K.-P. Riikonen, T. Holmqvist, M. Savolainen, V. Touboltsev, and K. Arutyunov in *Quantum Computation in Solid State Systems* edited by B. Ruggiero, P. Delsing, C. Granata, Y. Pashkin, P. Silvestrini, pp. 70-75, Springer, 2006

Other author's papers:

1. ***Electrical properties of glass-ceramic composites based on silver-conductive glasses infiltrated into diamond matrix under high pressure***
   M. Zgirski, J. Garbarczyk, S. Gierlotka, B. Palosz, **Solid State Ionics**, V.176**,** issue**:** 25-28**,** special issue: SI (2005)
2. ***Electron-phonon heat transport and electronic thermal conductivity in heavily doped silicon-on-insulator film***, P. Kivinen, A. Savin, **M. Zgirski**, P. Törma, J. Pekola, **Journal of Applied Physics**, 94, 3201 (2003)

Conferences/workshops/seminars:

1. **M. Zgirski**, K.P. Riikonen, V. Touboltsev and K. Arutyunov, *Quantum fluctuations in ultra-narrow superconducting nanowires*, **invited seminar**, 22.01.2008, SPEC-CEA **Saclay**, Quantronics Group, France

2. **M. Zgirski**, K.P. Riikonen, V. Touboltsev and K. Arutyunov, *Quantum fluctuations in ultra-narrow superconducting nanowires*, **invited seminar**, 07.01.2008, **Chalmers** University of Technology, **MC2**, Sweden

3. **M. Zgirski**, K.P. Riikonen, V. Touboltsev and K. Arutyunov, *Quantum fluctuations in ultranarrow superconducting nanowires*, **oral presentation**, European Workshop on Electron Interactions in Ultra 1D Nanostructures, 15-20.05.2007, **Nice,** France

4. **M. Zgirski**, K.P. Riikonen, V. Touboltsev and K. Arutyunov, *Quantum fluctuations in ultranarrow superconducting nanowires*, **abstracts** of International Autumn Seminars on Nanoscience and Engineering in Superconductivity for Young Scientists, 23-29.11.2006, Atagawa Heights, University of Tsukuba, **Japan**

5. **M. Zgirski**, K.-P. Riikonen, V. Touboltsev, K. Arutyunov, *Ion beam assisted method of nanofabrication,* **abstracts** of E-MRS Fall Meeting 2006**,** 04-08.09.2006, **Warsaw,** Poland

6. K. Arutyunov, **M. Zgirski**, K.-P. Riikonen, V. Touboltsev, *Ion beam-assisted methods of nanostructure fabrication*, **abstracts** of International Congress and Exhibition "Nanotechnology in Northern Europe", 16-18 May 2006, **Helsinki**, Finland

7. M. Zgirski, K.-P. Riikonen, V. Touboltsev, and K. Arutyunov, *Experimental evidence of quantum phase slip phenomena in ultranarrow aluminium nanowires*, **oral presentation**, Quantum coherence and decoherence at the nanoscale, 28.08-02.09.2005, **Corfu**, Greece

8. **M. Zgirski**, K.-P. Riikonen, T. Holmqvist, V. Touboltsev and K. Arutyunov, Quantum tunnelling in 1D aluminium nanowires, **proceedings** of the XXXVIV Annual Conference of the Finnish Physical Society, 17-19.03.05, **Espoo**, Finland

9. **M. Zgirski**, K.-P. Riikonen, V. Touboltsev and K. Arutyunov, *Experimental evidence of quantum phase slip phenomena in ultra-narrow superconducting channels,* **oral presentation**, E-MRS Fall Meeting 2004**,** 06-10.09.2004, **Warsaw**, Poland

10. **M. Zgirski**, K.-P. Riikonen, T. Holmqvist, V. Touboltsev and K. Arutyunov, *Experimental evidence of quantum phase slip phenomena in ultra-narrow superconducting channels*, **poster**, TNT 2004, 13-17.09.2004, **Segovia**, Spain

11. **M. Zgirski**, K.-P. Riikonen, M. Savolainen and K. Arutyunov, *Experimental evidence of quantum phase slip phenomena in ultra-narrow superconducting channels*, **proceedings** of the XXXVIII Annual Conference of the Finnish Physical Society, 18-20.03.04, **Oulu,** Finland

I. Introduction (I)

Usually, one associates superconductivity with the sharp drop of resistance down to zero at a certain critical temperature. However, if to look more carefully, the superconducting transition always has some finite width. The common explanation is very often related to inhomogeneity: various parts of the sample have different local critical temperatures T_c. A more interesting explanation utilizes the concept of intrinsic fluctuations of the order parameter to describe the broadening of superconducting transitions. Such fluctuations, quite typically, are more pronounced in smaller structures. With development of fabrication techniques it has become clear that existence of superconducting fluctuations can be established experimentally. It is predicted that in particular case of very narrow wires (with cross-section $\sigma \leq 100$ nm^2) made of superconducting material, zero resistance state can not exist at any temperature due to quantum fluctuations: so called *Quantum Phase Slips* (QPS). Unlike *Thermally Activated Phase Slips* (TAPS) which can affect the superconducting transition only in the immediate vicinity of T_c, *QPS* can wash out the superconducting order completely even at $T \rightarrow 0$. Phase slips are responsible for energy **dissipation in a superconductor** (!!!) and, as such, give rise to **a finite resistance below the critical temperature T_c**. *QPS* phenomenon is often referred to as *MQT* (*Macroscopic Quantum Tunneling*), for it involves collective movement of many Cooper pairs enabling the order parameter (superconducting wave function) to tunnel to a different configuration and to convert the energy of super-liquid into the electromagnetic radiation and Joule heat. The Thesis mainly focuses on the verification of this *QPS* mechanism responsible for breakdown of superconductivity in *1D* channels [1-5]. MQT is not just a hypothesis. In fact it is the phenomenon that is well established in Josephson junctions. The first definitive observation of MQT in Josephson junction was presented by Martinis, Devoret and Clarke [6]. The concept was introduced by Leggett [7]. However it is still debated whether similar process appears in 1D superconducting nanowires.

As continuous miniaturization progresses the components of micro- and nanoelectronic circuits are becoming even smaller. Is then reasonable to expect that physical properties of such elements remain unchanged? Or more precisely, how much a nanoelectronic component can be reduced in size to be still described within the established physics? If it goes beyond the conventional description it is of fundamental importance to understand new rules governing the behavior of the system. The present study sets fundamental limitations for the miniaturization: below a certain scale superconducting structures cannot sustain a dissipationless electric current, because their behavior is governed by fluctuations suppressing the zero resistance state. Is it pessimistic prediction? If one wants to obtain a non-dissipating superconducting nanocircuit the answer is "yes". On the other hand one can take advantage of the new physics originating from the effect e.g. *QPS* can couple quantum states and thus a new type of *qbit* can be

constructed [8]. *QPS* - dominated wires are also good candidates for novel current standard [9].

Apart from being of fundamental importance, this work is also meaningful from the technological point of view. It utilizes the low energy ion sputtering for controllable and predictable reduction of dimensions of nanostructures initially produced with e-beam lithography, just comprising the new approach for *post-processing of nanostructures*. In the context of *QPS* studies, the method provides with powerful tool for observation of a successive development of the *size phenomenon*. After each sputtering session the *R(T)* superconducting transition of a nanowire is measured. Starting from the relatively thick superconducting nanowire one finally arrives at the point when below T_c the ultra-narrow sample exhibit a resistive state governed by the *QPS* mechanism.

The next chapter *Theory of Phase Slips (**T**)* covers the concept of fluctuations in 1D superconducting channels. Then *Existing Experiments on 1D Superconductors (**O**)* are discussed. The methodology of scaling down the dimensions of nanowires will be introduced in chapter *Fabrication of Ultra-Narrow Wires (**W**)*. *Experimental Setup (**S**)* will discuss instruments used to perform experiments, e.g. filters for electrical measurements, thermometry, and cryostat. The most important chapter *Experiments on Ultra-Narrow Superconducting Aluminum Nanowires (**E**)* contains the principal message of the work: experimental evidence of the quantum phase slip mechanism in aluminum nanowires. Also it will be shown that inhomogeneity of the lift-off fabricated aluminum nanowires makes reliable verification of the "orthodox" model of the thermally activated phase slips impossible. Additionally, two accompanying, but not well understood effects will be discussed: negative magnetoresistance and non-monotonous *dV/dI(I)* dependencies. The most important results are summarized in *Conclusions (**C**)*. Some auxiliary information is given in *Appendices (**A**)*.

II. Theory of Phase Slips (T)

Typically, thinking about superconducting transition one has in mind a picture of an abrupt drop in resistance to immeasurably small value at some critical temperature T_c. However experimentally measured $R(T)$ transition always has a finite width. A trivial explanation can be the inhomogeneity of a sample which leads to spatial variation of T_c (cf. *section E.1*). In more interesting case the lack of abrupt transition is the effect of intrinsic fluctuations of the order parameter: above T_c fluctuations can establish superconductivity locally enhancing conductivity of a sample; below T_c fluctuations instantly break the macroscopic coherence at random in different parts of the sample, just giving rise to the measurable resistance.

Above the mean T_c one can consider fluctuations leading to the local establishment of the macroscopic (superconducting) coherence. Then locally superconductivity appears what is observed in experiment as the enhanced conductivity just above the T_c. The effect depends on superconducting dimensionality D of the system. According to Aslamazov-Larkin model [10] correction to conductivity above T_c is: $\delta\sigma \propto (T - T_c)^{-(2-D/2)}$. D is determined by the size of the system and its superconducting coherence length $\xi(T)$. ξ is the smallest distance over which the superconducting order parameter varies significantly. It follows that if the length of a sample along one particular direction is smaller than ξ, the order parameter can not vary appreciably along this direction and dimensionality of the sample is reduced by one. In case of *1D* systems (thin superconducting wires) there are two directions along which the order parameter is uniform. The contribution of the Aslamazov-Larkin term experimentally manifests itself as the "rounding" of the top part of the superconducting transition $R(T)$ above T_c. The effect is qualitatively observed in all systems irrespectively of their dimensionality, being more pronounced for reduced dimensionality D (*2D* films or *1D* wires) [11].

Below the mean T_c the situation is qualitatively different. At the bottom part of the superconducting transition, when the sample "tries" to be in the superconducting state, there are fluctuations leading to local destruction of coherence (local suppression of the order parameter). In *3D* and *2D* these fluctuations do not contribute to a measurable electric signal since the macroscopic coherence responsible for superconductivity is not affected: two ends of a 3D or 2D superconductor are connected coherently although there are "normal islands" situated at random places in the superconductor (*Fig.T.1*). However in *1D* the suppression of the order parameter somewhere along the wire breaks the macroscopic coherence between the two ends giving rise to the measurable resistance. Note that in *1D* wire the order parameter is suppressed in the entire cross-section. The finite resistance observed in *1D* superconducting wires below T_c is the main topic of the Thesis. Particularly it will be shown that behavior of the very narrow *1D* superconductors

is governed by fluctuations even at $T \to 0$ K. Fluctuations responsible for finite resistance of *1D* superconductor below T_c are referred to as *phase slips*.
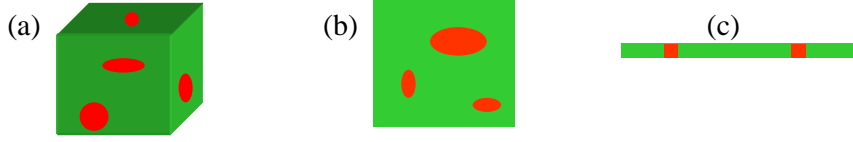
Fig.T.1. *Fluctuations in 3D(a), 2D(b) and 1D(c) samples. Below T_c the red islands correspond to the regions with the locally suppressed order parameter in the "almost" superconducting sample (green).*

T.1. Phase slip process

One of the first who introduced the notion of the phase slips in *1D* superconducting wires was *W. Little* [12]. He considered thermal fluctuations of one dimensional order parameter $\Psi(x)$ around value minimizing the free energy expressed in terms of *Ginzburg - Landau* functional:

$$F(\psi) = \int [a|\psi(x)|^2 + b|\psi(x)|^4 + c|\nabla \Psi(x)|^2]dx \tag{T.1}$$

By minimizing the functional one gets the uniform current-carrying states of the superconductor: $\Psi(x) = \Delta(x) \cdot \exp(i \cdot \phi(x))$ with the phase $\phi(x)$ subject to boundary conditions in the *x* direction. These are the most probable states of the superconductor. However, the interaction with the constant temperature bath allows for the order parameter to diffuse around, visiting states of higher free energies with probability proportional to the Boltzmann factor $\exp(-\dfrac{\Delta F}{k_B \cdot T})$ with ΔF being the departure from the local free energy minimum. As the supercurrent is proportional to the gradient of phase ($j \propto \nabla \phi$), the current-carrying state of the superconductor can be conveniently pictured in *3D* with a helix plotted along the wire (*Fig.T.2(a)*). For each point along the wire such a helix gives the magnitude Δ and phase ϕ of the order parameter Ψ. Each loop in the helix corresponds to 2π change of the phase of the order parameter.

In the vicinity of T_c the order parameter can fluctuate to the state where its magnitude is locally suppressed (close to T_c the order parameter is very small so that it is probable to get extra energy from the constant temperature bath in order to destroy it locally). Then it is energetically favorable for the order parameter to reduce the phase difference locally by 2π (phase slip process). In the picture of helix it corresponds to the removal of one of its loops (*Fig.T2(b)*, [13]). When magnitude of the order parameter is reestablished, the supercurrent is lower and the free energy is smaller.

Im Ψ

t0 = 0

t1 > t0

(a)

t2 > t1

Re Ψ

x-axis along the wire

REAL AXIS

(b)

|Δ(x)|

n = 0

n = 1

A

X ⟶
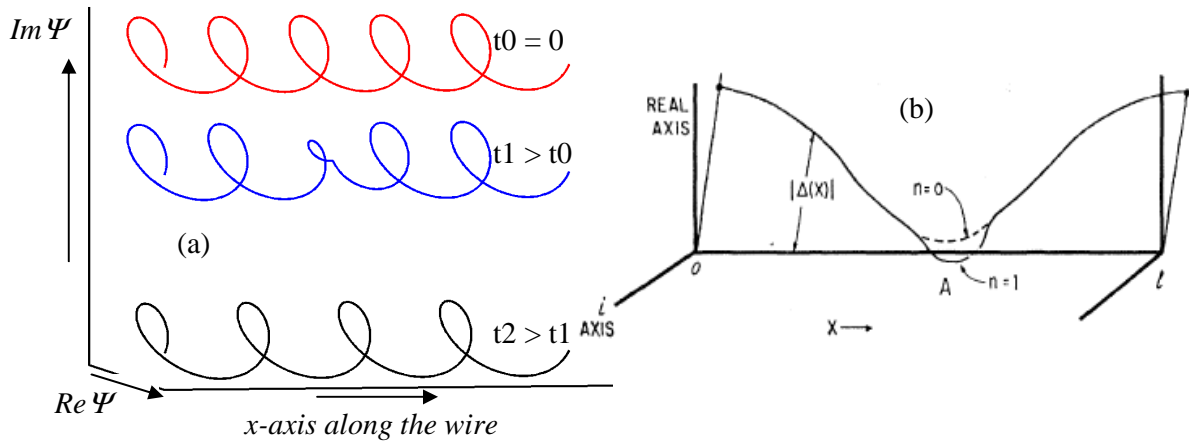
Fig.T.2. *Graphic representation of the phase slip process. (a) Transition between two uniform current-carrying states of a 1D superconducting wire is possible if to assume that the order parameter locally goes to zero allowing for phase to slip by 2π, thus reducing the supercurrent (inspired by [13]). (b) After W. Little [12]. Two possible configurations of the fluctuating order parameter are displayed. They are close in energy, however while for one configuration the order parameter undergoes one complete trip around the horizontal axis (solid line), for another it does not (broken line).*

$\Delta F \propto B_c^2(T) \cdot \Omega,$

$\Omega = \xi(T) \cdot \sigma$

F (free energy)

$\Gamma_{thermal} \propto \exp(\frac{-\Delta F}{k_B T})$

ΔF

$\Gamma_{quantum} \propto \exp(\frac{-\Delta F}{E_{CH}})$

0   2π   *phase φ*   4π
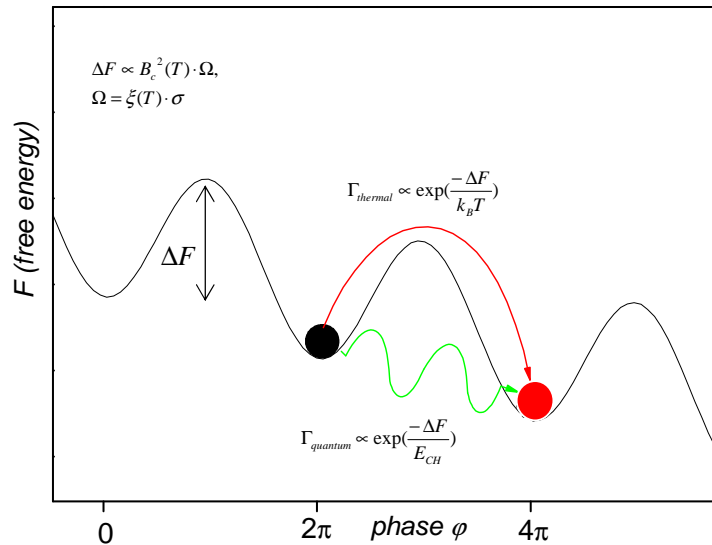
Fig.T.3. *Schematic presentation of the phase slip process. The order parameter can relax to a state of lower energy overcoming the potential barrier ΔF (thermodynamic condensation energy). There are two opportunities: thermal activation and macroscopic quantum tunneling. Γs denote rates for both processes.*

The phase slip process, as described above, involves thermal activation of the order parameter over the free energy barrier between neighboring free energy minima. Assuming for simplicity that phase slips always happen at a fixed point (e.g. weak link), in a full analogy with a Josephson junction, one can present the dependence of the free energy vs. phase as so called *current-tilted washboard potential* (*Fig.T.3*). In this representation the macroscopically coherent system is equivalent to a particle sitting predominantly in one of the local minima of the potential. Classically the particle can change its quantum state "jumping" over the potential barrier. However, there is also "more quantum" mechanism for the order parameter to change its state: tunneling to another potential minimum. It is again accompanied by the 2π change in phase and known as the *quantum phase slip* (*QPS*).

Since phase slip is the main subject of the Thesis it is instructive to see how actually phase "slips" during a fluctuation. The superconducting phase dynamics in phase slip process is presented in *Fig.T.4*. Phase slip happens because difference in phase between two adjacent points of a superconductor, separated by distance smaller than the coherence length ξ, can not be bigger then π. Physical state corresponding to $\pi + \alpha$ phase difference is equivalent to state with $-\pi + \alpha$ phase difference. It is in analogy to physically meaningful k - vectors of electronic waves in a periodic crystal lattice. They are contained exclusively within the first Brillouin zone. If one increases the value of k - vector across the zone boundary, then Bragg reflection occurs with a transfer of momentum to the lattice as a whole (e.g. *umklapp* scattering process). In case of the phase slip the momentum is transferred to the electromagnetic wave and lattice vibrations. Each phase slip generates a voltage pulse on the wire which propagates in the wire as the longitudinal electromagnetic wave known in literature as *Mooij-Schön mode* [14].
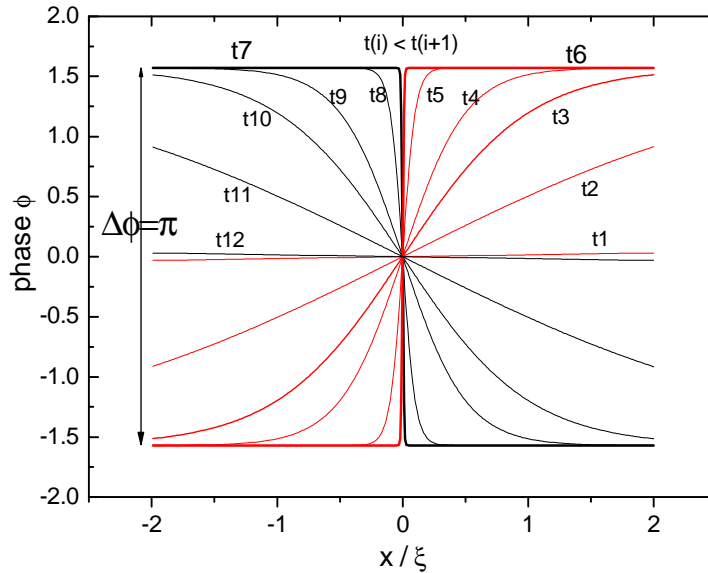
Fig.T.4. *A time sequence of the superconducting phase changes in the phase slip process. Phase slips by 2π in time t such that t7 > t > t6.*

T.2. Steady state of current-carrying dissipating 1D superconductor

Richard Feynman in his famous lectures showed that Schrödinger equation for Cooper pairs in superconductor is equivalent to the equation of motion for the *classical charged ideal liquid* [15]. When the phase slips, the superconducting liquid is not ideal any more. It "scatters" at random in the phase slip process loosing the energy. The kinetic energy of the liquid is converted into energy of the high frequency electromagnetic mode propagating along wire and the Joule heat. If the super-current should flow, the external power source has to compensate for the dissipated energy accelerating the superfluid all over again (*Fig.T.5*). The process is in analogy with the *Drude model* of conductivity in the normal metal where the acceleration-collision cycle is assumed for each electron. Unlike normal electrons, the superconducting liquid exhibits *"collective scattering"* in the phase slip process.

Constant applied voltage increases steadily in time the phase difference between the ends of the superconducting wire, thus increasing the current flowing through it. However **steady state** can be reached if to assume, following *J.S. Langer* and *V.Ambegaokar* [16], that the **phase slips reduce the phase difference at the same average rate as the rate of the increasing phase by the constant applied voltage** (*LA* assumption). Such an assumption allows establishing the connection between the applied voltage *ΔV* and the rate of phase slips via familiar relation (Gor'kov [17] and Josephson [18]):

$$\frac{2e}{\hbar}\Delta V = \frac{\partial(\Delta\phi)}{\partial t} = 2\pi \cdot \Gamma \tag{T.2}$$

where *Γ* is phase slip rate (number of phase slips per second).

It is important to note that typically experiments with superconductors in the resistive state are made in the *current biased mode,* while the *voltage is measured.* The configuration is different from the assumption that a *constant voltage* is applied across wire, as it is often considered in the theory. Whenever a phase slip occurs the supercurrent instantly decreases (*Fig.T.5*). To keep the current flowing, power source should sustain the constant voltage across the wire to keep the bias current at a constant value. In the picture of helix the power source winds the loops steadily in time, while the phase slip process annihilates them at random. In other words, to keep macroscopic current constant an external constant voltage should be applied. The power delivered from the source, dissipated due to phase slips, is then simply current times voltage. In the picture of *LA* assumption, the current bias and the voltage bias modes are equivalent. Anticipating the analogy between a 1D wire governed by superconducting fluctuations and a *1D* chain of Josephson junctions, one can refer to [19], where it was explicitly shown that the low frequency response is exactly the same in the two measuring modes.

There is an interesting analogy between the Josephson junction and the superconducting wire in the resistive state. In the Josephson junction constant voltage generates *AC* current. A wire also behaves like *AC* generator: it converts *DC* power into voltage pulses in the phase slip process.
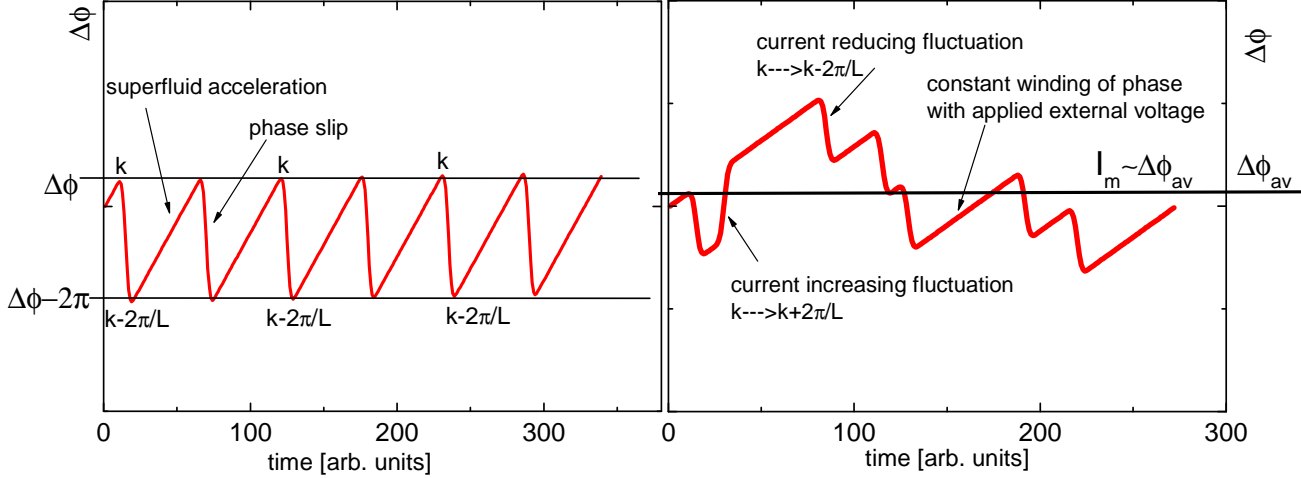
***Fig.T.5.** Phase fluctuations between two ends of a 1D superconducting wire. A constant applied voltage implies a steady increase with time of the relative phase $\Delta\phi$ (Josephson relation). It corresponds to the London picture of the superfluid accelerated by the applied voltage. According to LA assumption [16], a steady state is achieved when the loss of phase in phase slip process, on average, balances out the effect of the applied voltage. Then average constant current can flow in the wire. Unlike left picture showing phase slips appearing at regular time delays, right picture present more realistic situation with phase slips appearing at random and with some of them increasing value of current. Note that these pictures would also describe successive acceleration-collision cycles in the Drude model of normal conductivity, if to replace $\Delta\phi$ with drift velocity of a single electron.*

T.3. Free energy barrier preventing phase slip activation

The usual uniform constant-current solutions for the order parameter Ψ are: $\psi_k = \Delta \cdot \exp(ikx)$, with Δ being the magnitude of the order parameter and $k = \nabla\phi$ being the wave vector subject to periodic boundary conditions $\Psi(0) = \Psi(L)$, where L is the distance between points with the fixed value of the order parameter. These solutions correspond to the local minima of the free energy in the space of functions Ψ. It is possible for the order parameter to pass from one minimum to another via phase slip process in which the k-vector should change by $\pm 2\pi/L$. Recalling that the electric supercurrent density is $j = \dfrac{4 \cdot e}{\hbar} \Delta^2 \cdot k$, the positive phase slip increases the current (one loop is added to helix in *Fig.T.2(a)*), the negative- reduces the current (one loop is removed). Two adjacent minima

8

are separated by the free energy barrier ΔF which can be overcome with probability proportional to $exp(-\Delta F/k_B T)$. Looking for the state locating saddle point of the free-energy functional which is close to Ψ_k (uniform state) everywhere but some finite region Langer and Ambegaokar (*LA*, [16]) calculated the height of the free-energy barrier in the zero current limit:

$$\Delta F_0 = \frac{8 \cdot \sqrt{2}}{3} \cdot \sigma \cdot \xi(T) \cdot (g_n - g_s), \tag{T.3}$$

where σ is wire's cross-section and $\xi(T)$ - temperature dependent coherence length. In the *1D* limit $\sigma^{1/2} < \xi$, where the concept of the phase slip is defined, $\sigma \cdot \xi$ is the smallest volume where the order parameter can change noticeably. The free energy difference between normal and superconducting states is the energy density of the critical magnetic field: $g_n - g_s = \frac{B_c^2}{2 \cdot \mu_0}$. The potential barrier ΔF_0, up to numerical constant, represents the condensation energy of the smallest possible superconducting volume of the wire. Coherence length ξ is the following function of temperature close to T_c:

$$\xi(T) = \xi(T=0) \cdot (1 - \frac{T}{T_c})^{-1/2}, \quad \xi(T=0) = 0.85 \cdot \sqrt{l_{mean} \cdot \xi_0}; \tag{T.4}$$

with l_{mean} being electronic mean free path and ξ_0 - *BCS* coherence length at T = 0 K for clean material (with $l_{mean} >> \xi_0$). Critical magnetic field depends on temperature according to the formula:

$$B_c(T) = B_c(T=0) \cdot \left[1 - (\frac{T}{T_c})^2 \right] \tag{T.5}$$

If a current flows in a wire, the energy barrier ΔF becomes asymmetric: it is more probable to get fluctuation decreasing the current than the one which would increase it. The asymmetric barrier is calculated [16] as the difference in the free energy between two neighboring states locating minima with *k*-vectors differing by $2\pi/L$ (*Fig.T.6*):

$$\Delta F_1 = \frac{dF(\psi_k)}{dk} \cdot \frac{2\pi}{L} = \frac{h}{2 \cdot e} \cdot I, \tag{T.6}$$

with the energy of the uniform state : $F(\Psi_k) = \sigma \cdot L \cdot \left[(k^2 - \alpha)\Delta^2 + \frac{1}{2} \cdot \beta \cdot \Delta^4 \right]$

The same result for ΔF_1 can be obtained even without calling the Ginzburg-Landau formalism by the following observation: ΔF_1 is the energy delivered from the power source per one phase slip event: $\Delta F_1 = I \cdot V \cdot \Delta t = I \cdot \frac{\hbar}{2 \cdot e} \cdot \Delta \phi = \frac{h}{2 \cdot e} \cdot I$, since applied voltage V increases $\Delta \phi$ by 2π in a time Δt defined as an average time between successive phase slips. ΔF_1 is the energy released in the form of electromagnetic radiation when the phase slips by 2π.
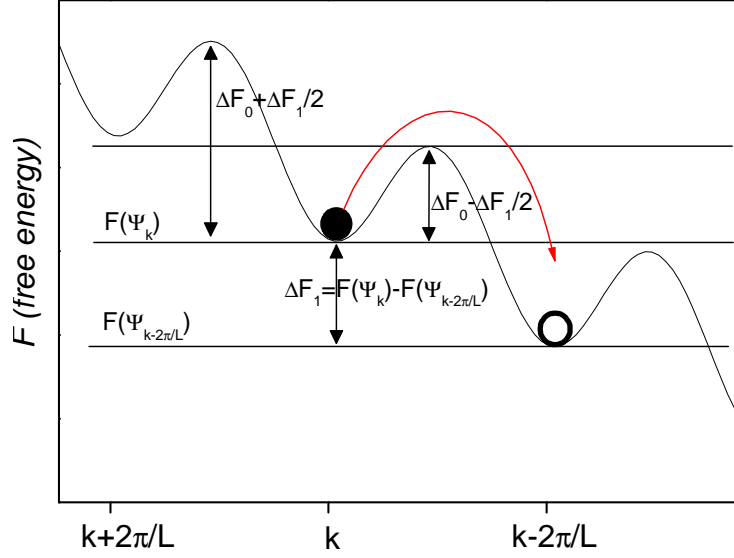
Fig.T.6. *Free energy F vs. wave vector k. In the absence of a current the energy barrier separating neighboring minima is symmetric and equal to ΔF₀. At a finite current the barrier becomes asymmetric favoring Δk = -2π/L fluctuations decreasing the supercurrent.*

T.4. Rate of thermally activated phase slips (LAMH derivation)

The effective rate Γ for phase reduction via phase slips, directly linked to the experimentally measured voltage, is the difference between the rates for *-2π* and *+2π* fluctuations:

$$\Gamma_- = rate(k \rightarrow k - \frac{2\pi}{L}) = \Omega \exp(-\frac{\Delta F_0 - \Delta F_1/2}{k_B \cdot T}) \tag{T.7a}$$

$$\Gamma_+ = rate(k \rightarrow k + \frac{2\pi}{L}) = \Omega \exp(-\frac{\Delta F_0 + \Delta F_1/2}{k_B \cdot T}) \tag{T.7b}$$

$$\Gamma = \Gamma_- - \Gamma_+ = 2 \cdot \Omega \cdot \sinh(\frac{\Delta F_1}{2k_B T}) \cdot \exp(-\frac{\Delta F_0}{k_B T}) \tag{T.7}$$

Being combined with Josephson relation (*eq. T.2*) it yields the expression for the voltage which should be applied by power source in order to keep the average current constant:

$$\Delta V = \Omega \cdot \frac{h}{e} \cdot \sinh(\frac{\Delta F_1}{2k_B T}) \cdot \exp(-\frac{\Delta F_o}{k_B T}) \tag{T.8}$$

In the limit of small currents *sinh* can be replaced by its argument yielding the zero bias expression for the effective resistance of a *1D* superconductor below T_c:

$$R = \frac{\Delta V}{I} = \Omega \cdot R_q \cdot \frac{h}{k_B T} \exp(-\frac{\Delta F_o}{k_B T}); \quad R_q = \frac{h}{4 \cdot e^2} \tag{T.9}$$

Ω is the pre-factor which corresponds to the rate at which order parameter scatters randomly between different states in function space. In *LA* paper [16] it was a priori assumed that $\Omega = \dfrac{\sigma \cdot L \cdot n}{\tau}$, where σ - cross-section of the wire, L - its length, n - number of conduction electrons (then counter would be the total number of conduction electrons in a wire), $1/\tau$ is some characteristic rate for microscopic processes (τ was taken to be the Drude relaxation time defining resistivity ρ_n of the normal state as $\rho_n = m/ne^2\tau$). Later *McCumber* and *Halperin* (*MH*, [20]) using the *Time-Dependent Ginzburg-Landau* (TDGL) equation argued that the correct value for the pre-factor should be:

$$\Omega = \frac{L}{\xi(T)} \cdot \frac{1}{\tau_{GL}} \cdot \sqrt{\frac{\Delta F_0}{k_B \cdot T}} \tag{T.10}$$

This result is understood in the following way. $L / \xi(T)$ is the number of statistically independent subsystems along the wire since $\xi(T)$ sets the relevant scale for variation of the order parameter. In each subsystem the order parameter exhibits diffusive behavior in the function space with the characteristic diffusion time: $\tau_{GL} = \dfrac{\pi\hbar}{8k_B(T_c - T)}$ (so called

GL time). The rate of change of the order parameter is then proportional to $\dfrac{L}{\xi(T)} \cdot \dfrac{1}{\tau_{GL}}$. The

factor of $\sqrt{\dfrac{\Delta F_0}{k_B \cdot T}}$ is the correction for overlapping fluctuations at different places along the

wire, but as it is close to unity it does not affect the magnitude of Ω and can be neglected. Typically *MH* prefactor is more then several orders of magnitude smaller then the one suggested by *LA* and is widely accepted in the scientific community. The *eq. T.8* or *T.9* derived by *LA* with the pre-factor calculated by *MH* (*eq. T.10*) is often referred to as *LAMH theory of thermally activated phase slips* and used to fit resistive transition of the *1D* superconducting wires.

The dominating temperature behavior in the *LAMH* effective resistance is determined by the exponential term in *eq. T.9*. It is important to notice that even small change in the free-energy barrier ΔF_0 (by factor of *2*) could counteract a factor of 10^{10} in the pre-factor [20]. It is up to experimentalist to choose the T_c for observed transition and this fact allows for the fitted pre-factor to differ significantly dependently on chosen T_c [20, *ref.16a*]. The experimental accuracy of determining the value of the pre-factor is very poor. The discussion of its exact value remains only of academic interest.

Since $\Delta F_0 \propto H_c(T)^2 \cdot \xi(T)$, the *LAMH* theory predicts the temperature dependence of resistance below (and close to) T_c of the form:

$$R_{LAMH} \propto \exp(-C \cdot \frac{(1-t)^{3/2} \cdot (1+t)^2}{t}) \xrightarrow{T \to T_c^-} \exp(-4 \cdot C \cdot \frac{(1-t)^{3/2}}{t})$$

with $t = T/T_c$ and C being some constant to be described below. It follows that the thermal fluctuations of the order parameter very quickly become immeasurable as temperature is reduced below the T_c. At $T \to 0$ we still can talk about thermally activated phase slips but their rate is then ridiculously small. LAMH theory explicitly predicts the exponentially strong dependence of the thermal fluctuations on the cross-section σ.

Constant C in the exponent is a product of parameters either measured experimentally, or used to fit data to LAMH model. It reads:

$$C = \frac{\Delta F_0(0)}{k_B \cdot T_c} = \frac{8 \cdot \sqrt{2}}{3 \cdot k_B \cdot T_c} \cdot \sigma \cdot \xi(0) \cdot \frac{B_c^2(0)}{2 \cdot \mu_0}(SI) = \frac{8 \cdot \sqrt{2}}{3 \cdot k_B \cdot T_c} \cdot \sigma \cdot \xi(0) \cdot \frac{H_c^2(0)}{8\pi}(CGS) \qquad (T.11)$$

Important physical quantities are the cross-section of the wire, the critical magnetic field and the coherence length at $T = 0$ K.

T.4.1. LAMH formula with explicit normal state resistance

It is possible to rewrite C in terms of resistance per length R_N/L [21], which may be more convenient for the direct comparison with experiment, for it is much easier measurable quantity then B_c and σ. Derivation will be given in *CGS* units but the final result will be also *SI* compatible. First we need to express $H_c(0)$ in terms of the flux quantum ($\Phi_0 = hc/2e$), coherence length and penetration depth [22]:

$$H_c(0) = \frac{\Phi_0}{2\sqrt{2} \cdot \pi \cdot \lambda_{eff}(0) \cdot \xi(0)} \quad (*)$$

Penetration depth in the dirty limit ($\xi_0 >> l_{mean}$) for $T = 0$ K is:

$$\frac{1}{\lambda_{eff}^2} = \frac{1}{\lambda_L^2} \frac{l_{mean}}{\xi_0} = \{ \lambda_L^2(0) = \frac{4\pi n e^2}{mc^2}(London); \xi_0 = \frac{\hbar \cdot V_F}{\pi \cdot \Delta(0)}(BCS); \rho_N = \frac{m}{ne^2\tau}(Drude);$$

$$\tau = \frac{l_{mean}}{V_F} \} = \frac{8\pi^3\Delta(0)}{\rho_N hc^2} \quad (**)$$

Inserting (*) and (**) into *eq.T.11* for C parameter one gets:

$$C = \frac{\sigma}{\rho_N} \cdot \frac{\Delta(0)}{\xi(0)} \cdot \frac{h\sqrt{2}}{4e^2 \cdot 3 \cdot k_B \cdot T_C}$$

Substituting : $R_N = \rho_N \frac{L}{\sigma}$, $\Delta(0) = 1.76 \cdot k_B T_C$ and $R_q = \frac{h}{4e^2}$ one arrives at the desired result :

$$C = 0.83 \cdot \frac{R_q}{R_N \cdot \frac{\xi(0)}{L}} \qquad (T.12)$$

The big advantage of the derived expression for C is that it does not contain the wire cross-section and the critical magnetic field, but instead the normal state resistance R_N shows up explicitly. Since R_N can be easily measured, *LAMH* formula in this form leaves much less

ambiguity in fitting experimental data. Actually the only possible fitting parameters are now l_{mean} entering $\xi(0)$ and the critical temperature T_c. One can show that *eq.T.12* gives numerically exactly the same result as *eq.T.11* provided that the critical magnetic field at $T = 0$ K is:

$$B_c(0) = \sqrt{0.61 \cdot \frac{k_B \cdot \mu_0 \cdot T_c \cdot R_q}{\xi_0 \cdot K}} \qquad \text{(T.12a)}$$

with the material constant $K = \rho_N \bullet l_{mean}$. For aluminum the tabulated values, $K = 6 \bullet 10^{-16} \,\Omega m^2$, $\xi_0 = 1.6\,\mu m$ and $T_c = 1.18$ K yield $B_c(0) = 9.2$ mT. It is in a good agreement with experimentally determined $B_c(0)_{bulk} \sim 10$ mT.

The LAMH model for small currents can be presented as follows:

$$R_{LAMH} = 4.82 \cdot R_N \cdot (4 \cdot C \cdot \frac{(1-t)^{3/2}}{t})^{3/2} \cdot \exp(-4 \cdot C \cdot \frac{(1-t)^{3/2}}{t}) \qquad \text{(T.13)}$$

where parameter C is given either by *eq. T.12* or *eq. T.11*.

Note that since the normalized resistance R_{LAMH}/R_N depends on the wire cross-section σ and the coherence length $\xi(0)$ only through parameter C, it is sensitive only to the product $\sigma \bullet \xi(0)$ (or alternatively $\sigma \cdot \sqrt{l_{mean}}$) i.e. it is the same for different σ and l_{mean} provided $\sigma \cdot \sqrt{l_{mean}}$ remains unchanged.

T.4.2. Simple model of switching resistors

During the phase slippage the magnitude of the order parameter Δ inside the phase slip core of size $\sim\xi$ reaches zero for the period of time $\sim \tau_{GL}$ (or h/Δ when quantum phase slips are considered). Then one can make an assumption that this part of the wire is driven to the normal state and, hence, can be treated as resistor of value $R_\xi = R_N \xi(T)/L$ (R_N -normal state resistance of whole wire). This resistor is "switched on" only during the phase slip. Then the time averaged value of the resistance is $R = R_\xi \tau_{GL} \Gamma$ (Γ being the rate of phase slippage and $\tau_{GL}\Gamma$ being the fraction of a second when resistor is "switched on"). The simple model does not even call for the Josephson relation to convert Γ into the measurable resistance. It gives proper exponential dependence, however with different value of the pre-factor. Since a quantitative verification of the pre-factor in experiment is problematic the model can be used for interpretation of the data as well as the more rigorous formula derived earlier [1].

T.4.3. Critical current

The application of current reduces the free energy barrier for current reducing fluctuations (*Fig.T.6*). If $\Delta F_0 - \dfrac{\Delta F_1}{2} = 0$ then the barrier disappears and the system "falls down in energy" because its phase can change continuously (it is like continuous phase slip process). This means that the superconducting wire goes to the normal state. It follows that the critical current can be expressed as (*eq. T.3&T.6*):

$$I_c = \frac{4 \cdot e \cdot \Delta F_0}{h} \propto B_c(T)^2 \cdot \xi(T) \propto (1-\frac{T}{T_c})^{3/2} \cdot (1+\frac{T}{T_c})^2 \xrightarrow{T \to T_c^-} \propto (T_c - T)^{3/2}, \tag{T.14}$$

which is the well-known mean-field critical current dependence.

T.4.4. Limitations of LAMH approach

LAMH model is based on the *GL* approach and, as such, applicable only for the zero-gap limit e.g. at temperatures in the immediate vicinity of T_c when the order parameter is vanishingly small but still existing. Existence of the order parameter corresponds to the requirement that the energy barrier is much larger than the thermal energy ($\Delta F_0 >> k_B T$) and, hence, phase slips are rare events. It restricts usage of the *LAMH* model too close to the T_c. Resuming, as a rule of thumb, *LAMH* model should address the part of the resistive transition where the measured wire resistance is below the level of *10%* of the normal state resistance, but not further from T_c then few tens of mK [23].

T.4.5. About two fluid model

When comparing *LAMH* model with an experiment sometimes an additional trick is used to improve the fitting. Namely one assumes existence of the normal electron channel for conductivity in parallel with the superconducting one [16,24,25,26]. This procedure can be justified if to assume the constant voltage applied by external source across the wire. This voltage should compensate the power loses due to phase slips and keep constant super-current on average as described earlier (*section T.2*). It should also affect normal electrons. In the usual treatment [25] resistance of the normal channel is taken to be equal to the normal state resistance of the whole wire R_N. If one is close to T_c then the number of Cooper pairs is small. It follows that the number of normal electrons is actually unaffected, and hence conductance of normal channel can be considered constant and equal to *1/R_N*. However as one departs from T_c almost all electrons are paired and hence conductivity of the normal channel is dramatically suppressed. Far from T_c it is just zero. Thus it is not justified to use the two fluid approach (at least with R_N for the normal channel) when a fit to quantum phase slip data is done, for such data usually involves temperatures far below T_c.

T.5. Macroscopic Quantum Tunneling (MQT)

The tunneling of a single particle through energetically forbidden space is one of the hallmarks of quantum mechanics. This concept can be extended to account for a relaxation of the superconducting order parameter (to state of lower energy) even if there is an energy barrier high enough from the classical point of view to prevent the relaxation. Then we talk about tunneling of the superconducting order parameter in Hilbert space of all possible configurations of the superconducting wave function. Such a tunneling is accompanied by the phase slip process called *quantum phase slip* (*QPS*) to distinguish it from the "classical" *thermally activated phase slip* (*TAPS*). Since the macroscopic number of paired electrons constitutes the superconducting wave function, only their collective behavior can allow for the order parameter to tunnel (one can say that tunneling of the order parameter must be "agreed" between many Cooper pairs). One then talks about the *macroscopic quantum tunneling* (*MQT*) to stress the difference with respect to the single particle tunneling in Euclidean space. Unlike *TAPS* which destroy superconducting order only very close to T_c, frequent *QPS* can appear down to zero temperature washing out superconductivity completely (it is known in literature as the superconductor-to-metal(insulator) transition). First suggestions that phase slip in superconducting nanowires can occur via tunneling date back to *1980s* [27,28,29]. The existing detailed theory of *QPS* is quite complicated and its derivation is difficult to follow. However a lot can be learnt about *QPS* if some basic quantum mechanical principles are applied. First I will give an argument why one should expect *MQT* to appear in superconducting wires and what can be said about its rate. Then I present *Giordano* model which historically was first to describe *MQT* in 1D superconducting wires. Finally the most advanced model derived by *Golubev* and *Zaikin* will be introduced. You will see that although first approach is fairly heuristic it gives qualitatively the same result as the advanced microscopic theory.

T.5.1. Heisenberg uncertainty argument

Heisenberg uncertainty allows for the order parameter to visit states within the energy region $\Delta E \propto h/\Delta \tau$ with respect to the local minimum of the free energy. It creates opportunity for the order parameter to go from one energy minimum to another even if two minima are separated by classically not accessible energy, thus justifying the concept of tunneling. Some physicist used to say that if an event lasts for very short time $\Delta \tau$, a system can borrow energy from "nowhere" to return it to "nowhere" immediately after tunneling happened. Hence if tunneling can happen fast enough, the amount of borrowed energy can be sufficient to overcome potential barrier ΔF. Using this heuristic argument one can formulate the condition for the pronounced *MQT* in the following form: $\Delta F \propto \Delta E \propto h/\Delta \tau$ (analogous criterion for *TAPS* would be $\Delta F \propto k_B \cdot T$). One can claim that just by changing characteristic energy scales in LAMH model of thermally activated

phase slips (k_BT *(thermal)* $\rightarrow h/\Delta\tau$ *(quantum)*) one should get the rate for quantum phase slips. More or less it is what Giordano did trying to interpret his experimental findings.

T.5.2. Giordano heuristic model for macroscopic quantum tunneling

One of the first who observed much wider resistive transitions then predicted by the *LAMH* model was Giordano [28,30]. To interpret his results he used modification of the *LAMH* theory so that it could account for tunneling of the order parameter. Giordano supported his analysis on findings of Caldeira and Leggett [31] who calculated the tunneling rate of the order parameter for Josephson junctions Γ_{JJ}. By generalization of their results Giordano postulated that the rate for *MQT* in case of superconducting *1D* wires can be expressed up to some constant with a *LAMH*-like formula for which thermal energy k_BT should be replaced with "quantum" energy h/τ_{GL}. Giordano assumed *ad hoc* that the time giving uncertainty in energy in the phase slip process should be the Ginzburg-Landau time τ_{GL} since it gives the proper scale for diffusion of the order parameter through different configurations. Performing the described energy scale replacement in *eq. T.9* and *T.10* describing *TAPS* one gets:

$$R_{TAPS} = \frac{\Delta V}{I} = \Omega \cdot R_q \cdot \frac{h}{k_BT} \exp(-\frac{\Delta F_o}{k_BT}), \quad \Omega = \frac{L}{\xi(T)} \cdot \frac{1}{\tau_{GL}} \cdot \sqrt{\frac{\Delta F_0}{k_B \cdot T}} \qquad \text{(T.9 \& T.10)}$$

$$k_BT \leftrightarrow h/\tau_{GL}$$

$$R_{QPS} = \frac{\Delta V}{I} = b \cdot \frac{L}{\xi(T)} \cdot R_q \cdot \sqrt{\frac{\Delta F_0 \cdot \tau_{GL}}{h}} \cdot \exp(-a \cdot \frac{\Delta F_o \cdot \tau_{GL}}{h}) \qquad \text{(T.15)}$$

where *a* and *b* denote numerical constants of the order of unity introduced additionally. Constant *a* arises from uncertainty in the distance under the barrier (or equivalently in the tunneling time), constant *b* reflects approximate nature of the formula. *Eq. T.15* is based on time dependent Ginzburg-Landau equation (*TDGL*) since it is constructed in analogy to *LAMH* theory. For this reason Giordano's approach is not justified for the problem of *QPS* observed at temperatures well below T_c where *GL* formalism is not valid any more. However *eq. T.15* was the first to describe *MQT* process in narrow superconducting wires and is very similar to the simplest version of the detailed microscopic treatment (*cf. eq. T.15* and *T.30* or *T.32*).

We can also take advantage of the derivation of LAMH formula with explicit normal state resistance (*eq.T.13*) to rewrite R_{QPS} in the form convenient for the comparison with experiment. Formally we can do it be replacing term k_BT in R_{LAMH} (*eq.T.13*) with term h/τ_{GL} in R_{QPS}:

$$R_{QPS} = b \cdot 4.82 \cdot R_N \cdot (\frac{C}{4} \cdot (1-t)^{1/2})^{3/2} \cdot \exp(-a \cdot \frac{C}{4} \cdot (1-t)^{1/2}) \qquad \text{(T.16)}$$

where parameter *C*, familiar from R_{LAMH} derivation, is given either by *eq.T.12* or *eq. T.11*.

T.5.3. Detailed microscopic model of Quantum Phase Slips (GZ model)

Golubev and Zaikin (*GZ*) presented microscopic model of *QPS* that involves effect of dissipation inside and outside the phase slip core [32,33,34,35]. Their calculations are based on the imaginary time effective action technique which according to authors properly accounts for the non-equilibrium, dissipative and electromagnetic effects during a *QPS* event. *GZ* argued that *TDGL* approach is not well defined for calculation of *QPS* rates for number of reasons: *TDGL* formalism is valid only close to T_C, while QPS events can take place far below T_c; *TDGL* does not take into account dissipation effects due to quasiparticles inside the *QPS* core; *TDGL* is not adequate to properly describe excitation of electromagnetic waves in the wire and its surrounding during a *QPS* event.

Taking into account the propagating electromagnetic fields is important since the phase slip is not a local event. It is coupled to electromagnetic environment. Each phase slip creates instability which then propagates in the wire in a form of a longitudinal electromagnetic wave (*Mooij - Schön mode* [14]). This plasma mode carries energy away from the phase slip core and dissipates it as the Joule heat far away from the core (e.g. in the normal leads connecting the wire with the outside world or in the environment due to induced dissipative currents). Properly derived *QPS* rate should take into account this dissipation which formally has the effect of increasing energy barrier preventing *QPS* to appear. If the dissipation due to the phase slip generation is huge, then the barrier becomes so large that the rate of *QPS* is negligible. *Duan* in his work actually claimed that *QPS* can not be observed at all because of huge dissipation via electromagnetic fields introduced by a single phase slip event [36]. However *GZ* has arrived to the conclusion more optimistic for experimentalist: *QPS* should be observed in wires with cross-section of the order of *100* nm^2.

QPS rate (single phase slips events)

GZ considered rate of *QPS* to be of the form:

$$\Gamma_{QPS} = \Omega \cdot \exp(-S_{QPS})\tag{T.17}$$

with S_{QPS} being the effective action. *GZ* showed that it is possible to separate action of a single *QPS* into two parts: $S_{QPS} = S_{core} + S_{out}$. The core part S_{core} considers the phase slip center and is determined by the condensation energy and dissipation by normal currents. The hydrodynamic part outside the core S_{out} depends on propagation of electromagnetic fields out of the phase slip center. Outside the phase slip core the absolute value of the order parameter remains equal to some mean value and only the phase of order parameter changes in space and time.

It allowed *GZ* to calculate S_{out} in the form:

$$S_{out} = \mu \cdot \ln\left[\min(c_0 \cdot \frac{h}{k_B T}, L) / \max(c_0 \cdot \tau_0, x_0) \right] \tag{T.18}$$

$$\mu = \frac{\pi}{4\alpha} \cdot \sqrt{\frac{C_1}{L_k}} \tag{T.19}$$

where τ_0 and x_0 are the typical duration of the *QPS* event and the typical size of the *QPS* core, respectively. These parameters are determined from minimization of S_{core}. $L_k = \frac{4\pi\lambda_L^2}{\sigma}$ is the kinetic inductance per unit length, λ_L is the magnetic field penetration depth, $c_0 = 1/\sqrt{L_k C_1}$ is the Mooij-Schön plasmon velocity [14], C_1 is the wire capacitance per unit length, α is the fine structure constant = *1/137* and σ is a wire cross-section. μ is the dimensionless parameter characterizing damping of the electromagnetic excitation (plasmon) inside a *1D* superconductor. In the zero temperature limit $T \rightarrow 0$ K for infinitely long wires, the action S_{out} diverges logarithmically making single *QPS* events unlikely in this limit.

For evaluating S_{core} a choice of trial functions describing dynamics of the phase slip is required. Specifically, *GZ* chose:

$$|\delta\Delta(x,\tau)| = \Delta_0 \cdot \exp(-x^2/2x_0^2 - \tau^2/2\tau_0^2) \tag{T.20}$$

for the departure of the amplitude of the order parameter from the mean value Δ_0 and:

$$\varphi(x,\tau) = -\frac{\pi}{2} \tanh(\frac{x\tau_0}{x_0\tau}) \tag{T.21}$$

for the phase variations of the order parameter. The dynamics is presented in *Fig.T.7*.
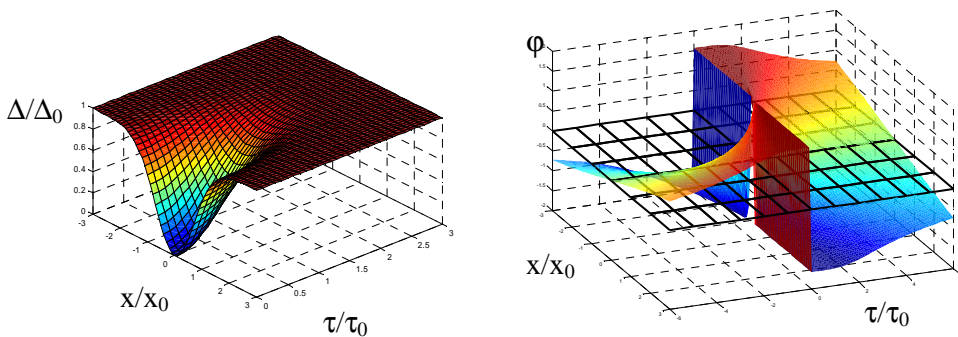
Fig.T.7. *Spatial and temporal evolution of the order parameter amplitude (left) and phase (right) in the core of the phase slip. At $\tau = 0$ the absolute value of the order parameter Δ is suppressed to zero allowing the phase to flip by 2π. It is possible because at $\tau=0$ the phase φ is undefined at $x=x_0$: the system has the same energy for $-\pi$ and $+\pi$ phase difference at $x=x_0$.*

Minimizing the action S_{core} with respect to x_0 and τ_0 *GZ* arrived at the final result for the core parameters and the core action S_{core}:

$$x_0 = a \cdot \sqrt{\frac{hD}{\Delta_0}} = a \cdot \xi \tag{T.22}$$

$$\tau_0 = b \cdot \frac{h}{\Delta_0} \tag{T.23}$$

$$S_{core} = \pi A N_0 \sigma \sqrt{hD\Delta_0} = A \frac{R_q}{R_N} \cdot \frac{L}{\xi} \tag{T.24}$$

where *a, b, A* are numerical constants of order of unity dependent on details of the trial functions used for calculation. The above considerations hold provided the capacitive effects are small i.e. for sufficiently short wires with lengths:

$$L << \xi \cdot \frac{e^2 \cdot N_0 \cdot \sigma}{C_1} \tag{T.25}$$

where N_0 - density of states at Fermi level, σ - wire cross-section. GZ argued that condition *T.25* is satisfied for majority of samples with lengths not exceeding *10* μm.

Hence, for short wires it is possible to separate the full action S_{QPS} into two parts: one accounting for fluctuations of the order parameter and dissipative currents inside phase slip core S_{core}, another describing propagation of electromagnetic wave out of the phase slip center S_{out}. Subsequently it was shown that usually in case of short wires ($L < 10$ μm) the core part exceeds the "hydrodynamic" term. It enables to ignore the S_{out} when minimizing the core part S_{core} with respect to x_0 and τ_0. It follows that the impact of the electrodynamic term on the action is smaller then uncertainty in *A* constant coming from the approximate nature of the trial functions (*cf. T.20, T.21*). Hence S_{out} can be absorbed into *A* constant yielding the result for the full action S_{QPS}:

$$S_{QPS} \approx S_{core} = A \frac{R_q}{R_N} \cdot \frac{L}{\xi} \tag{T.26}$$

The expressions *T.17* and *T.26* give the same dependence which could be extracted from the *TDGL* approach (heuristic Giordano model, *section T.5.2*). However, as argued earlier, *TDGL* is not well defined for the *QPS* problem. It is mandatory to go through proper microscopic derivation taking dissipation effects into account to get a reliable result. Dissipation plays a dominant role during the phase slip event and the correct *QPS* action must take into account the dissipative currents flowing inside the wire when *QPS* appear.

GZ calculated pre-factor Ω for *QPS* rate using the instanton technique in the form:

$$\Omega = B \cdot \frac{S_{QPS} L}{\tau_0 \cdot x_0} \tag{T.27}$$

with *B* being the numerical constant of order of unity. The result for the pre-factor is different from the *TDGL*-based analysis. Equations *T.17, T.26* and *T.27* give the rate of

virtual quantum phase slips (appearing in the wire when there is no current flowing through it) in the limit of short wires (< *10* μm).

Superconductor-to-metal transition

Although the electrodynamic term of the *QPS* action in negligible compared to the core part in case of single *QPS* events (short wire limit: maximum one phase slip in a wire at a time) it can determine behavior of the system when interaction between different *QPS* is considered. For sufficiently long wires in the limit $T \rightarrow 0$ K, *GZ* predicted superconductor - to - metal (insulator) transition similar to *Berezinskii-Kosterlitz-Thouless* (*BKT*) [37] type transition. Unlike *BKT* transition in *2D* superconducting films governed by temperature, the *QPS* transition is driven by the wire cross-section. For thicker wires the electromagnetic interaction between phase slips is sufficiently strong (they are bound in pairs - with opposite topological charges $\pm 2\pi$) and at $T = 0$ K wire should enter superconducting state. However for thinner wires some quantum phase slips are always unbound (they do not have a pair) which causes non-vanishing resistance even at $T = 0$ K.

QPS model for comparison with experiment

Equations *T.17*, *T.26* and *T.27* give the rate of virtual phase slips (in the zero current limit). To find approximate formula for non-zero small current one can express action in the form known from the LAMH model [21] and then proceed analogously as in the derivation of resistance due to thermally activated phase slips. The presented approach is fairly heuristic, but the resulting formula from experimental point of view is the same like the one obtained using advanced calculations ([33], see *eq.T.32*). First we assume action in the form $S_{QPS}=\Delta F_0/E_{ch}$. E_{ch} is characteristic energy scale of the *QPS* process (*see section T.5.1*). It is related to the duration of the phase slip through Heisenberg principle and in the *GZ* derivation corresponds to the superconducting gap $\Delta_0 = h/\tau_0$ (*eq. T.23*; in thermal activation model E_{ch} is $k_B T$). It follows that for the non-zero current the net phase slip rate reads (in analogy for the *TAPS* derivation, *eq. T.7*):

$$\Gamma_{QPS} = \Gamma_- - \Gamma_+ = 2 \cdot \Omega \cdot \sinh(\frac{\Delta F_1}{2 E_{CH}}) \cdot \exp(-\frac{\Delta F_0}{E_{CH}}) \tag{T.28}$$

with $\Delta F_1 = \dfrac{h \cdot I}{2 \cdot e}$

$$\Delta V = \frac{\hbar}{2e} \cdot 2\pi \cdot \Gamma_{QPS} = \Omega \cdot \frac{h}{e} \cdot \sinh(\frac{h}{4 e E_{CH}} \cdot I) \cdot \exp(-\frac{\Delta F_o}{E_{CH}}) \tag{T.29}$$

$$R_{QPS} = \frac{\Delta V}{I} = \Omega \cdot R_q \cdot \frac{h}{E_{CH}} \exp(-S_{QPS}); \quad R_q = \frac{h}{4 \cdot e^2}, \text{ for } I < \frac{4 e E_{CH}}{h} \tag{T.30}$$

One can see that finally the exponent is not affected by the choice of E_{ch}, for the action can be substituted back to it. E_{ch} explicitly appears only in the pre-factor Ω. We can rewrite R_{QPS} in the form convenient for comparison with experiment introducing temperature dependence of the coherence length and putting $E_{ch} = \Delta_0$ (eqs. T.26, T.27, T.30):

$$R_{QPS} = D \cdot (1-t) \cdot \exp(-C(1-t)^{1/2});$$ (T.31)

$$t = \frac{T}{T_c}; \quad C = S_{QPS}(T=0) = A \cdot \frac{R_q}{R_N} \cdot \frac{L}{\xi(0)}; \quad D = B \cdot C \cdot \frac{L}{\xi(0)} \cdot R_q; \quad \xi(0) = 0.85 \cdot \sqrt{\xi_0 \cdot l_{mean}}$$

D and C are constants (used as fitting parameters when comparing model to data) characterizing property of sample at $T = 0$ K and *(1-t)* terms correspond to temperature dependence.

The more rigorous expression for R_{QPS} in the linear limit of small bias currents $I < 4e\Delta_0(T)/h$ takes the form [35]:

$$R_{QPS}(T) = \frac{V(T)}{I} = B \frac{\Delta_0(T) \cdot S_{QPS}^2 L}{\xi(T)} \cdot \exp(-2 \cdot S_{QPS}) \cdot T^{\kappa}$$ (T.32)

where $B \sim 1$. Parameter $\kappa = 2\mu-3$ with μ determined in *eq. T.19*. The power dependence on temperature $\sim T^{\kappa}$ in practice can be neglected being negligible compared to the strong exponential dependence. Note that the dominating dependence on temperature comes from the variation of the energy gap $\Delta(T)$ defining the coherence length $\xi(T) = \sqrt{hD/\Delta(T)}$. At temperatures significantly below the critical temperature, $\Delta(T)$ is actually constant and hence *eq. T.32* predicts much weaker dependence on temperature then the *TAPS* model (*eq. T.9*). From experimental point of view *eq. T.32* gives quantitatively the same results as *eq. T.30* or *eq. T.31*.

Note that the expression for the effective resistance R_{QPS} (*eq. T.31* or *T.32*) is additive with respect to the wire length. If we increase the wire length twice then we increase its normal state resistance twice. Hence the change of the sample length has no effect on the action since the exponential term is determined only by the resistance per unit length or, in other words – by the wire cross-section ($R_N / L = \rho_N / \sigma$). On the other hand the pre-factor will increase twice doubling the rate (resistance). In the part of my thesis devoted to obtaining wires with sputtering (*Chapter IV (W)*) I show that small variations in cross-section affect normal state resistance a lot if the wire is sufficiently narrow. It follows that resistance per unit length in different parts of the wire can be drastically different making phase slips to nucleate in the narrowest constrictions preferentially (so called weak links). One can argue that variations of the order parameter are averaged over the distance of the order of ξ. Constrictions with length smaller then ξ should not be "visible" and the wire should behave as a homogenous *1D* channel (provided that the constriction is not so severe that the local current density is significantly higher than in the other parts of the wire). However if the length of the non-uniform wire is much longer then

the coherence length, it is possible to divide the wire into $N \sim L/\xi$ independent domains each with slightly different value of the cross-section. As the rate of phase slip depends exponentially on the cross-section (see section *T.5.4*) one can assume that *the narrowest part of the wire provides the overwhelming contribution to the measured resistance R_{QPS}.* Hence it is quite natural to consider a realistic (= inevitably non-uniform) experimental wire as consisting of two parts connected in series: one exhibiting *QPS* behavior of the length $L_{eff} < L$ and the normal state resistance $R_{N,eff} < R_N$, and another one behaving actually like an ordinary superconducting wire (without *QPS* behavior) of the length *(L-L_{eff})* and the normal state resistance *(R_N-$R_{N,eff}$)*. Accepting this argument, $R_{N,eff}$ and L_{eff} should be used as the fitting parameters when comparing experimental *R(T)* with *QPS* model. We know the upper limits for them which are easily experimentally measurable quantities: R_N and *L*.

T.5.4. Criteria for the observation of QPS in experiments

The experimental manifestation of quantum phase slips fully relies on the value of action S_{QPS}. If $S_{QPS} >> 1$ then *QPS* mechanism is completely frozen. Only for $S_{QPS} \sim 1$-*10* one can hope to observe a measurable resistance below T_c. It is instructive to investigate what are general requirements to conduct successive experiment on *QPS*. One can rewrite the action in the following way:

$$S_{QPS} = A \frac{R_q}{R_N} \cdot \frac{L}{\xi} = \frac{A \cdot R_q \cdot \sigma}{\rho_N \cdot \xi} = \frac{A \cdot R_q \cdot \sigma \cdot l_{mean}}{\rho_N \cdot l_{mean} \cdot 0.85\sqrt{\xi_{BCS} \cdot l_{mean}}} = \frac{A \cdot R_q \cdot \sigma \cdot \sqrt{l_{mean}}}{0.85 \cdot K \cdot \sqrt{\xi_{BCS}}} \tag{T.33}$$

where ξ_{BCS} and $K = \rho_N \bullet l_{mean}$ are constants for the given material (for *K* constant see *Appendix A.3*). Since $S_{QPS} \sim \dfrac{1}{K \cdot \sqrt{\xi_{BCS}}}$, the best material for observation of *QPS* is the one with the large *BCS* coherence length ξ_{BCS} and large *K* constant. Having selected the material, it is highly desirable to make a wire with small cross-section and with the short mean free path, for $S_{QPS} \sim \sigma \cdot \sqrt{l_{mean}}$. It may seem suspicious that a long coherence length is an advantage in observation of *QPS*. It increases volume where order parameter is suppressed which at first sight may seem to reduce probability of *QPS* activation. However, since $\xi_{BCS} = \dfrac{\hbar \cdot V_F}{\pi \cdot \Delta}$, long coherence length implicates small superconducting gap what is favorable for superconducting fluctuations. Alternatively one can say, being based on equation $\dfrac{1}{2} \cdot N_F \cdot \Delta^2 = \dfrac{B_c^2}{2\mu_0}$ (N_F - density of states in the normal state at Fermi level), that materials with long coherence lengths have small critical magnetic fields what implicates small condensation energy and again is in favor for observation of fluctuations.

One may also claim using BCS gap formula: $\Delta(0) = 1.76 \cdot k_B T_c$, that material with low T_c is more likely to exhibit QPS behavior.

The action S_{QPS} (*eq. T.33*) depends linearly on the wire cross-section if the elastic mean free path l_{mean} of a sample is not affected by the cross-section variations (case of amorphous wires). However for wires studied in this work, the dependence on the cross-section is stronger then linear: for l_{mean} scales approximately linearly with the cross-section for the smallest wires studied in my experiments $l_{mean} \sim \sigma$. In this limit the mean free path is fully determined by scattering at sample boundaries. I need to recall here that the cross-sections of the wires exhibiting *QPS* behavior obtained with sputtering look like "flat pancakes" and their l_{mean} can be considered to be roughly equal to the height h of the wire. One can say that thin wires are reduced in size with sputtering because their height gets smaller while their width actually remains constant. It follows that resistance due to *QPS* process R_{QPS} depends on the wire cross-section σ in the following way:

$$\log(R_{qps}) \propto -\sigma^n \qquad \begin{aligned} &n = 1 \text{ if } l_{mean} \text{ does NOT depend on } \sigma \\ &1 < n \le 3/2 \text{ if } l_{mean} \text{ depends on } \sigma \\ &n = 3/2 \text{ if } l_{mean} \propto \sigma, \text{ case of wires studied in my experiments} \end{aligned} \tag{T.34}$$

Above formula implicates a sharp superconductor-to-metal (or insulator) transition: a crossover between superconducting and insulating behavior governed by the wire cross-section. Simulation presented in *Fig.T.8*, based on *eq. T.31* with $R_N = \dfrac{K \cdot L}{\sigma \cdot l_{mean}}$, shows that reduction of the wire diameter by *1* nm leads to a tremendous enhancement of the *QPS* rate. Also it shows that *QPS* should be observed experimentally only if the wire diameter falls below the *10* nm range. However this last conclusion can be untrue if to assume different values of *A* and *B* than *1* (*A* is in the exponent and from modeling point of view it is indistinguishable from σ). Slight variation of the actual values of parameter *A* and *B* can relax/tighten experimental conditions of *QPS* observation. One should remember that in *GZ* theory effects of electromagnetic environment on *QPS* rate are absorbed into constant *A* since they are too small to be distinguished from the effects described in the "core" part of the action. Nevertheless the constant *A* is dependent on electromagnetic environment (see *eq.T.33* and discussion preceding it). Hence one can argue that *A* is different for slightly different cross-sections σ. This fact usually is not taken into account in experimental interpretations: *A* is considered to be the same constant for the whole family of superconducting transitions [2,26]. I believe that *Fig.T.8* would not change qualitatively if the unknown $A(\sigma)$ dependence was taken into account.
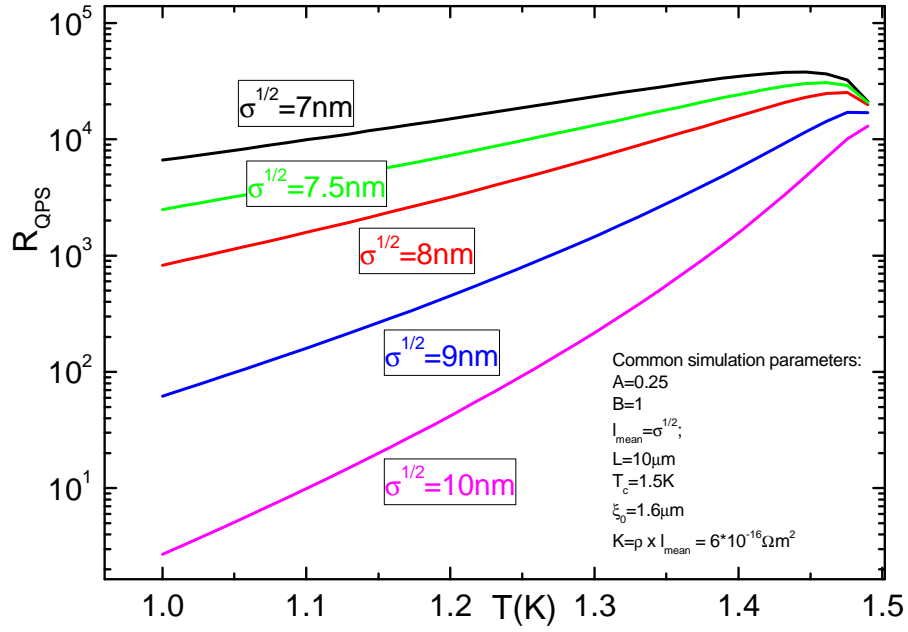
Fig.T.8. *Strong dependence of Quantum Phase Slip rate on the wire cross-section as simulated with GZ model (eq. T.31) for aluminum nanowire.*

III. Existing Experiments
on 1D Superconductors – Overview (O)

O.1. Thermal phase slips: Experiments on tin whiskers

The model of *thermally activated phase slips* (*TAPS*) [16,20] currently has the status of a well-established theory. Since its development in *late 1960s* it has been used in a number of experiments. To get rid of the trivial broadening of the experimentally measured *R(T)* transition due to the sample inhomogeneity, one should study extremely pure samples. The first experiments [38,39] were made on naturally-grown tin *1D* crystals (*whiskers*) with typical dimensions of *~ 0.5 μm x 0.5 μm x 1* mm like the one presented in *Fig.O.1* [40]. The crystals were literally hand-picked from the ingots and the electric contact were made either by soldering with Wood's metal or squeezed with indium. Note that both materials are superconductors with T_c higher and lower than that of tin, respectively. The experiments revealed that the experimentally observed width of the superconducting transition can be described by the *TAPS* model (*Fig.O.2*). Note that the measured resistance drops by *5* orders of magnitude over *~1* mK range.
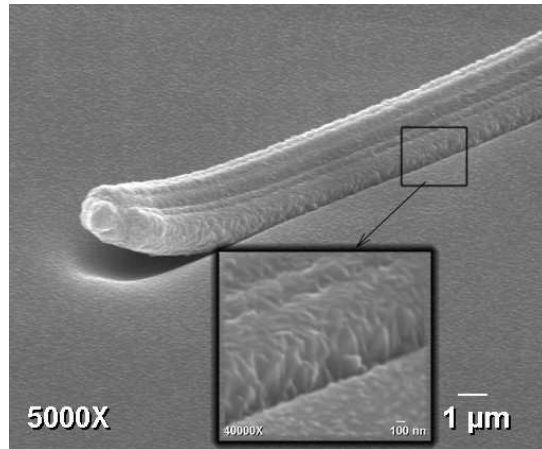
Fig.O.1. *Tin whisker on the surface of the spin-on-glass [40].*

A remarkable feature of the TAPS model is the hyperbolic sine dependence of the phase slip rate (effectively measured voltage) on the bias current (*eq.T.6 & eq.T.8*). It was claimed to be confirmed also in one of the early experiments on tin whiskers ([38], *Fig.O.3*). In the experiment the *V(I)* dependence should be measured at a well - stabilized temperature below T_c. Even *ΔT ~ 0.1* mK instability might spoil the measurement (*cf. Fig.O.2*). Such experiment requires thermal stability by far much better then *1* mK, which is not a trivial task.
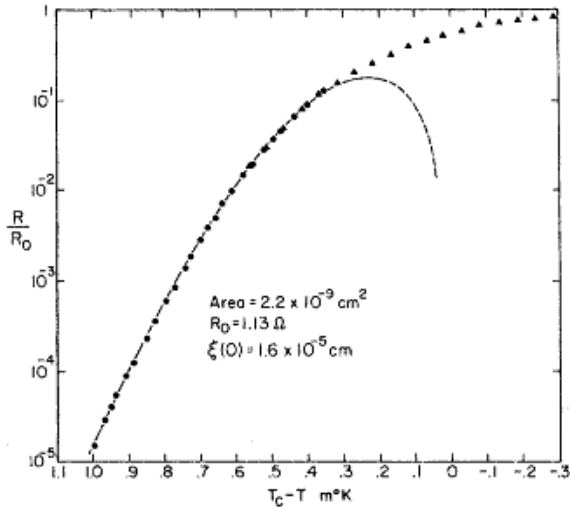
Fig.O.2. *After [38]. One of the first verifications of TAPS model. Notice 4 orders of magnitude reduction of resistance in 0.7 mK interval.*
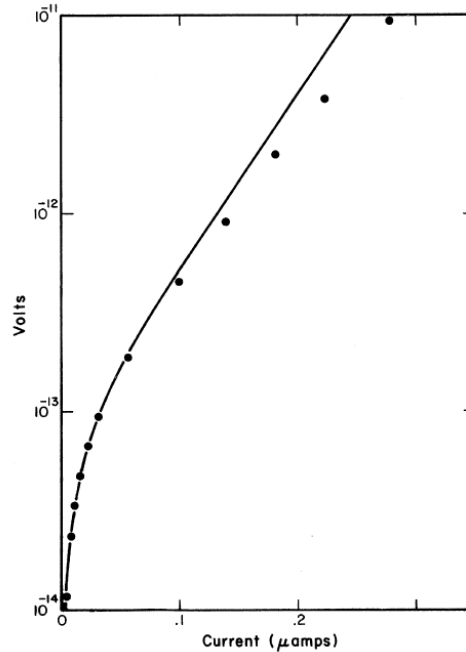
Fig.O.3. *After [38]. Experimental verification of the hyperbolic sine dependence of voltage on the bias current in TAPS regime at fixed temperature just below T_c.*

O.2. Considerations concerning verification of the TAPS mechanism in real nanowires

In this section I will discuss some other factors which may influence the experimentally observed superconducting transitions of realistic *1D* samples expected to confirm validity of the *TAPS* model.

<u>1. Dependence of the T_c on the wire cross-section, defects and proximity effects</u>

In general, the critical temperature T_c of low dimensional superconductors may deviate from the bulk value being dependent on the wire size and morphology. Each real wire is inhomogeneous to some extent. This inhomogeneity involves finite *geometry*, *defects*, various *proximity effects* (e.g. proximity of measuring leads). Typically the smaller the sample, the stronger the relative geometrical non-uniformity is. All these effects can easily account for broadening of the *R(T)* transition. My considerations on this subject are presented in section *E.1. Experimental limit on observation of phase slips…* With respect to the cited experiments on tin whiskers [38,39] I would like to note that many factors have not been addressed yet: e.g. what is the influence of the contacts made of stronger/weaker

superconductors? What is the T_c dependence on the whisker cross-section? Particularly one can ask what will happen if you cut whisker into two parts? Will T_c of two parts will be the same within accuracy ~ *0.1* mK? It would be interesting to compare *R(T)* transitions for *3D* crystals and *1D* whiskers to see if for the *3D* structures transitions are steeper. One should bear in mind that here we speak about very fine effects capable of broadening the superconducting transition width by ~ *1* mK.

2. Overheating

The *overheating* of the wire by the finite bias current might bring another uncertainty to the experiment. Experimentally the effect may manifest itself as hysteresis: transition to the superconducting state happens at a lower temperature compared to the transition to the normal state. The Joule heating can lead to a situation when temperature of a part of wire (say, the one which is still above T_c) keeps slightly growing as we increase the bias current. This part behaves then as, the so called, *hot-spot*, which grows in size as current is increased. The non-linearity of the *V(I)* dependencies (*Fig.O.3*) can be interpreted as the hot-spot formation [41,42,43].

There are two mechanism of cooling for electron subsystem heated by external power: *diffusion* of energetic electrons out of the wire and *phonon emission*. Decoupling of the electron and phonon temperatures is only observed at sub-Kelvin temperatures. It follows that at *3.7* K, which is T_c for tin whiskers, electron and phonon temperatures should be in principle the same. However, due to *Kapitza resistance*, the phonon temperature inside the wire can differ from the substrate temperature (the bath temperature). It can be especially pronounced for long or suspended wires coupled thermally to the bath only through electrical connections at the ends serving as reservoirs (the surface over which the heat can be exchanged in such case is rather small: two cross-sectional areas of the wire). One should note that the ends of the wire close to the "cold" reservoirs (contact pads, leads) can get rid of the excess heat (via diffusion) more effectively than the central parts [44]. It actually can lead to the situation when the ends of the wire are already in the superconducting state, while its middle part is still in the normal state. It is just one more reason why the superconducting transition in *1D* wire can have some finite width.

Myself I have never measured *R(T)* transitions for aluminum wires which could be reasonably fitted with the *LAMH* model of *TAPS*: experimental dependencies are always noticeably wider and usually exhibit some "kinks". It happens because of the $T_c(\sigma)$ dependence, ensuring that thicker parts of an aluminum wire (e.g. node regions) undergo superconducting transition at lower T_c. For detailed discussion see section *E.1.Experimental limit on observation of phase slips…*

O.3. Early experiments on quantum phase slips (QPS)

Probably the first who observed departure from the *TAPS* – like behavior in superconducting transitions of *1D* wires was Giordano. He used his heuristic model (*section T.5.2*) to explain data for *In* and $Pb_{0.9}In_{0.1}$ wires obtained with a step-edge technique in which ion milling was used to pattern previously deposited thin film [28,30]. These wires showed finite resistance far below T_c (*Fig.O.4*). However, in the light of the earlier discussed background, there are several unclear points in that pioneering work. For example: what was the homogeneity of the samples; why the two wires of different cross-section in *Fig.O.4* exhibit the same slope associated with resistance produced by quantum phase slips (*cf. eq.T.34 and Fig.T.8*)? Finally, one should expect that the wire with smaller cross-section should display smaller slope which is not so obvious here.

The well known experimental demonstration of quantum phase slips as being responsible for the finite resistance of narrow wires below T_c was provided by Harvard group ([26,45], *Fig.O.5*). Their wires were obtained by deposition of $Mo_{0.79}Ge_{0.21}$ onto carbon nanotubes (or ropes) suspended across slits on *Si/Si0$_x$/SiN* substrates. Thus the nanotubes were used as templates for nanowires. In the first *Nature* paper the authors claimed that the wires were superconducting or insulating (not reaching zero resistance) dependently on the ratio of their total normal-state resistance R_N to the quantum resistance for Cooper pairs $R_q=6.45$ kΩ. For $R_N < R_q$ wires should remain superconducting while for $R_N > R_q$ quantum phase slips destroy the long-range superconducting order (insulating state).

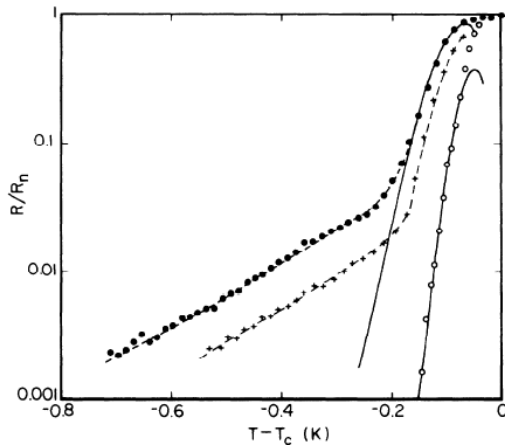*Fig.O.4*. After [28]. One of the first experiments claiming observation of Quantum Phase Slip (QPS) phenomenon in 1D wires. The sample diameters were: 41 nm (full dots), 50.5 nm (crosses) and 72 nm (open dots). Solid lines are predictions of TAPS model.
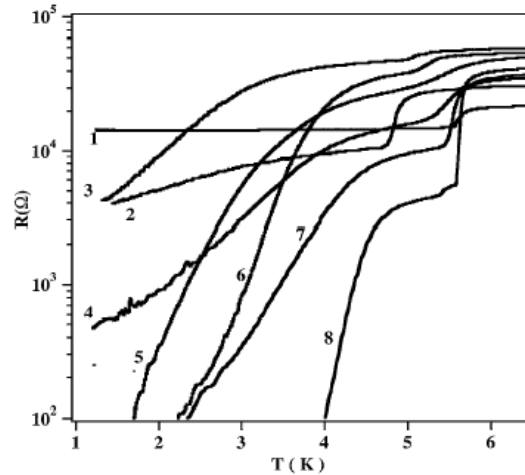
Fig.O.5. After [26]. Narrow MoGe nanowires deposited onto carbon nanotubes exhibit broadening of the superconducting transitions.

Later, in *Phys. Rev. Lett.* [26] the authors revised their conclusions: the relevant parameter controlling the superconducting transition is not the ratio of R_q/R_N, but appears to be the resistance per unit length, or equivalently, the cross-sectional area of the wire.

In the recent review [46] *A. Bezryadin* summarizes the experimental data on *MoGe* nanowires and comes to the following conclusions:

- *Short* homogeneous nanowires ($L < 200$ nm) exhibit a clear dichotomy: they demonstrate either "weakly insulating" behavior with clear features of weak Coulomb blockade, or relatively steep superconducting transition *R(T)* with the resistance controlled by thermal fluctuations (LAMH model of TAPS). In this regime no sample shows a crossover between two types of behavior. The actual parameter governing the behavior of short homogeneous wires is R_N with $R_N = R_q$ setting the transition point.

- *Long* nanowires (200 nm $< L < 1$ μm) typically exhibit a crossover between the regimes of small and large *QPS* rates giving the rise to superconducting and normal behavior, respectively. The *R(T)* transitions of long wires show a decrease of the resistance with cooling even those which satisfy $R_N > R_q$. The crossover between normal and superconducting behavior of the long samples is controlled by the wire cross-section σ or, equivalently, by the ratio R_N/L with the overall picture consistent with the *QPS* scenario (*section T.5*).

The author also stresses the fact that measurements of wires, which are made inhomogeneous (granular) on purpose, show that such wires, even if they are short in the sense stated above, do not show a clear dichotomy [47]. Appreciating results on *MoGe* nanowires one should mention that since carbon nanotubes are known to be insulating, metallic or even superconducting it is not clear how and to what extent they can alter superconducting properties of the nanowires deposited onto them [26,45]. However, the most recent results [47,48] were obtained using fluorinated single-wall nanotubes, which are known to be insulating. These results appeared qualitatively the same to those obtained with regular nanotubes.

A systematic experimental study on *Pb* nanowires of different thicknesses and widths has been reported [11]. The method enabled *R(T)* measurements on in situ grown samples with progressively increased thickness at a constant width. It was found that the superconducting transition of sufficiently thick and wide wires can be fitted with the *LAMH* model; while with decreasing the wire cross-section the width of transitions systematically deviate from predictions of the model (*Fig.O.6*). The authors attributed this behavior to 1D Coulomb correlation effects. One may argue that the effect can be actually related to *QPS* mechanism. However, in my opinion, inhomogeneity of the studied samples could equally well account for the observed *R(T)* broadening, although the authors pointed out that it is unlikely. They claimed that similar modulation of wire width, independent of wire thickness, should give rise to the same deviation from the *LAMH* model for all samples of the same width. Since it is not the case for presented data (*Fig.O.6*), the authors assumed that geometrical imperfection (e.g. edge roughness) does not affect *R(T)*

transitions. In my opinion the argument is not correct. First, as one reduces the size of a wire the relative inhomogeneity increases even if absolute roughness is kept unchanged. It may happen that thick wires with some given roughness can be considered homogenous while thin wires with the same roughness are already inhomogeneous. What really matters is the dependence of the T_c on the cross-section (or more generally on geometry). For example: in case of aluminum the magnitude of the slope $dT_c/d\sigma$ for smaller σ is higher implicating stronger broadening of transition for the same absolute roughness (see section *E.1. Experimental limit on observation of phase slips...*). From the provided data (*Fig.O.6*) one may conclude that in lead $dT_c/d\sigma > 0$. Hence, the thinnest parts of the sample exhibit the superconducting transition at the lowest temperatures, thus trivially contributing to the broadening of the *R(T)* transition. Second, usually when you try to obtain really narrow metallic lines their absolute inhomogeneity usually gets worse. In the discussed work [11] there is no evidence (e.g. *SPM* picture) how roughness changes with the size of the samples. Resuming, in my opinion, data on *Pb* nanowires [11] is not conclusive to claim observation of the *QPS* phenomenon.
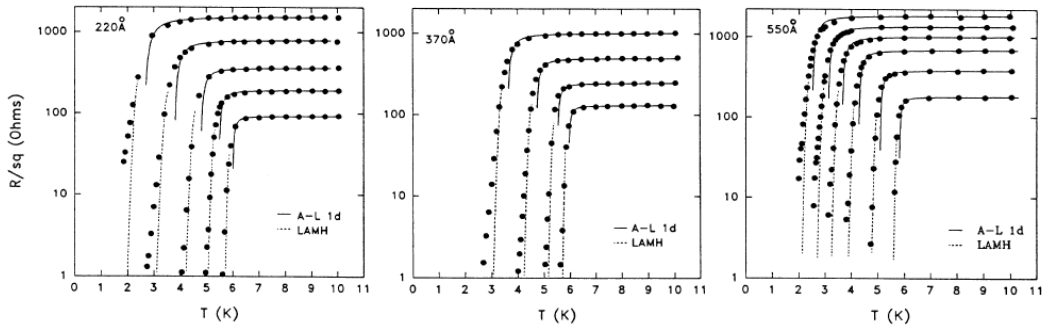
Fig.O.6. *After [11]. Resistance per unit area R/sq vs. temperature for several lead nanowires of different widths: 22 nm (left panel), 37 nm (middle panel), 55 nm (right panel). For the same width, the thickness is varied. Dotted lines are fits to the LAMH model of TAPS. Deviations from the model are more pronounced with decreasing thicknesses and wire width.*

From other scientific papers reporting observation of *QPS* observation in nanowires I will mention two. One addresses electrical transport measurements made on the *ensemble of single-crystal Sn* nanowires fabricated by electrodeposition technique and embedded inside the membrane [49]. Another presents the evidence for QPS in *long 1D aluminum wires* [50].

Resuming experimental overview, I can say that before I started my PhD activity, there existed some experimental evidence of non-thermal mechanism responsible for broadening the *R(T)* dependencies in superconducting nanowires. However, the *QPS* phenomenon in ultra-narrow channels was far from being experimentally established.

IV. Fabrication of Ultra-Narrow Wires (W)

It may seem that there are many different fabrication methods which allow one to obtain thin metallic wires in the nanometer range. Probably the most common are lithographical techniques in which patterns are written on a substrate with a masked or finely focused optical (*UV*), *X-ray*, electron beam (*EB*) or focused ion beam (*FIB*). Whereas *UV* photolithography, being compatible with mass production, is good for industrial applications it can not compete with *EBL* or *FIB* in resolution. State-of-the art *EBL* has been proved to deliver line width ~*10* nm (being limited by a size of organic molecules of resist used for mask fabrication). Alternatively one can use *Scanning Probe* for nanoindentation [*51*], manipulation of small objects [*52*] or controlling chemical reactions locally (e.g. oxidation of silicon [*53*]). The *SPM* nanolithography is under development and at the moment lacks universality. There are also chemical methods, e.g. electrodeposition [*54,55,56*], relying on self-assembly properties of crystals. In my work I have used the different approach: *sputtering*. I utilize idea of *scaling down pre-fabricated structures* using ion beam. Wires initially obtained with *EBL* (however any other method for initial sample fabrication would work as well) were exposed to the low-energy ion beam and eroded down in homogeneous way assisted by removal of initial roughness. There are many advantages of such approach:

1. One can measure *the same* structure with successively reduced size. It opens up a great opportunity to follow *the progressive development* of a size-dependent phenomenon in nanostructures. Even if one claims that it is possible to get the desired line width by other means, still he has to produce many different samples to trace the development of the size phenomena. Each such sample should be characterized independently to a large extent representing a unique system being produced with slightly different fabrication parameters and giving more room for artifacts.

2. Sputtering allows for shrinking *the same* sample in predictable way meaning that we can *tailor* the structure with nanometer accuracy.

3. The method preserves homogeneity. It is much more difficult to obtain with EBL a long and very narrow line with constant cross-section than a thicker one. But having initially a homogeneous thick wire you can sputter it to get a homogeneous narrow sample.

4. The big advantage is accessibility. Not many researchers have an access to state-of-the-art *EBL* systems, while starting from a "modest" system with ~ *100* nm resolution one can still get the desired feature size utilizing ion sputtering.

In the following, I will describe the morphology and the size of pre-fabricated and sputtered wires determined with *SPM* and *SEM*. Sputtering strategy will be treated. I will introduce simple geometrical model describing the shape and the size evolution of the sputtered wires and compare it against the experimental data. Then I will present a little more complex model allowing understanding and predicting the change in resistance of a sputtered wire being based on its material and initial geometrical parameters. This model

will be compared against the *4-probe* measurements of wires' normal state resistance. Finally, I will compare two estimations for a wire's cross-section: direct - based on *SPM* data and indirect – based on normal state resistance.

W.1. Initial sample fabrication

Wires produced with e-beam lithography followed by thermal evaporation of *99.995*% pure aluminum are granular (polycrystalline). They were processed in *UHV* chamber in which magnetic materials have never been evaporated. From *SPM* and *SEM* measurements linear grain size can be estimated to be in the range of *20-100* nm. (*Fig.W.1*). Obtained wires were studied with *SPM* microscope to determine their geometry and homogeneity. Typical cross-sectional area distribution of a wire is displayed in *Fig.W.2.* For the purpose of the reliability of ultrasonic bonding the contact pads were covered with *~50* nm of copper. The deposition was made in such a way (high angle evaporation) that the thinnest parts of the nanostructure were left purely aluminum (see also *Fig.S.2*). The nomenclature of the samples reflects the presence of copper on the pads.
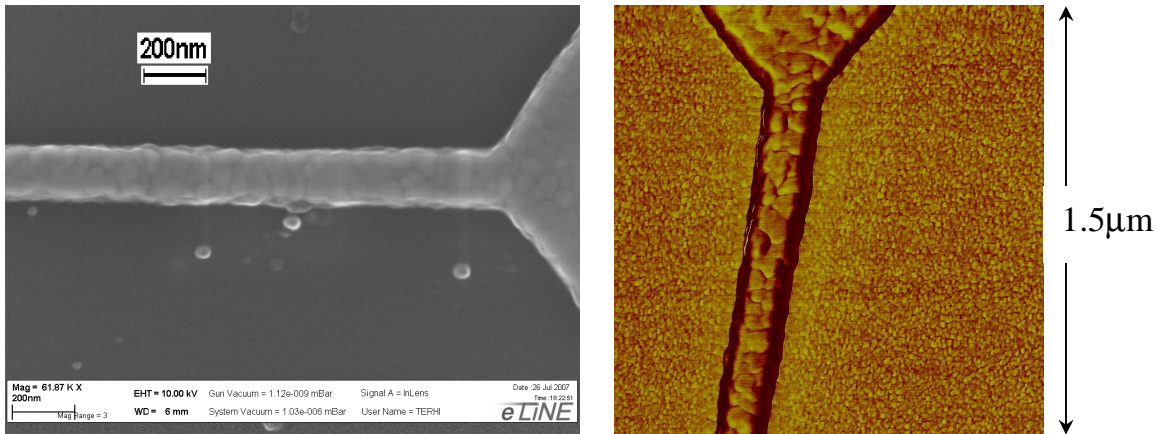
Fig.W.1. Polycrystalline nature of aluminum wires produced with e-beam lithography: (a) SEM picture (Cu5μm2no4); (b) SPM phase mode picture (Cu5μm1no5). Grain size ranges from 20 to 100 nm. The wider parts seen in pictures are electrodes allowing for 4-probe resistance measurements. The same electrodes are on the other side of the wire.

W.2. Sputtering as a method of scaling down nanowires

Ion beam sputtering can be thought as an erosion of a surface due to primary ions bombardment: each projectile ion behaves like a cannon ball kicking out atoms from the bombarded material. As a result, the ion beam sputtering provides powerful tool for gentle, layer-by-layer removal of the target. The method can be used whenever successive reduction of dimensions of the structures initially produced by other methods (e.g. e-beam
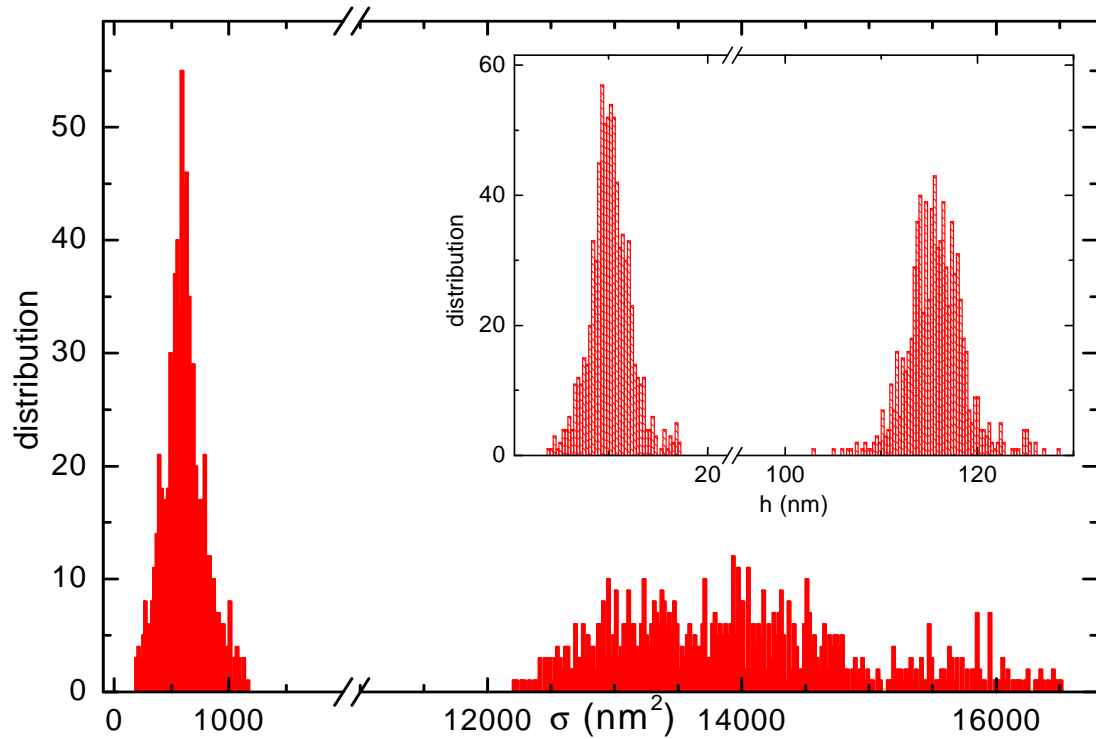
Fig.W.2. *Distribution of the wire cross-section for the 5μm long aluminum wire (Cu5μm1no1) produced with e-beam lithography (right histogram) and the same wire after sputtering (left histogram). One can observe narrowing of the histogram due to sputtering. However relative inhomogeneity gets worse. In the inset, corresponding height evolution is presented. The images of this wire before and after sputtering can be found from Fig.W.9. The representative cross-sectional profile of this wire is presented in Fig.W.11(c).*

lithography) is required. It allows tracing the size-dependent physical properties of a material. Previously the method has been shown to work successfully to reduce the diameter of nanowires and the size of the island of *SET* transistors [*57*]. In other research group sputtering was also utilized to pattern the previously deposited thin film to obtain wires [*58*] or to decrease thickness of *high-T_c* layered superconductor bringing it to the limit when only one layer was left [*59*]. In my work I used the sputtering to investigate the effect of the wire's cross-section on the shape of its superconducting transition *R(T)*. As my final goal was to obtain wires in the range of *10 x 10* nm^2 I had to control sputtering with high accuracy. Numerous experiments performed on wires (mainly made of aluminum) allowed me to develop the phenomenological sputtering model which gives reasonable insight into evolution of the shapes and the sizes of wires initially produced with e-beam lithography. I have shown that it is possible to reduce nanowires cross-sections in predictable and controllable way. Starting with different initial sectional profiles of the wires and using different sputtering angles it is possible to control the aspect ratio (height to width ratio) of the wire cross-sectional profile.

W.2.1. Issue of damage introduced by sputtering

As bombarding ions penetrate material the question of destruction arises. Hence it is justified to ask to what extent physical property of material is altered as it is bombarded by ions. Some answer to this question can be based on simulation with *SRIM* software (*The Stopping and Range of Ions in Matter*) [*60*]. In my experiments the nanowires were sputtered with low energetic (*0.2 - 1* keV) argon ion beam. At such low energies only the very surface of the target is affected as the ions' projected range and associated collision cascades in aluminum are at the level of few nanometers (*Fig.W.3*). Obviously, the smaller energy used, the smaller the range of the material which can be possibly damaged by the bombardment. Using our ion gun it takes a lot of time (~ few hours) to sputter noticeably an aluminum wire with *200* eV. Mainly energy of *1* keV has been used. *1* keV Argon ions can penetrate as deep as *5-6* nm. It is negligible for thick wires (with transverse size ~*100* nm), but can be crucial for very thin wires. We performed one set of sputterings with energy *200* eV (see *section E.3.1*) and found no difference compared to experiments where *1* keV ion beams were used. For *200* eV the penetration depth is below *2* nm. This very surface does not contribute to electrical

Fig.W.3*. Projected range of argon ions penetrating aluminum amorphous target (a) and range of collision cascades induced by impact of argon ions (b) at energies* 1 keV, 0.5 keV *and* 0.2 keV. *Recoil is defined as an aluminum atom removed from its initial position. Curves were calculated with SRIM software for perpendicular bombardment.*

properties as it is immediately oxidized when the wire is taken from the sputtering chamber to ambient conditions. The thickness of the naturally created aluminum oxide is at the level of few nm. Hence we conclude that the results obtained for wires bombarded with *200* eV do not suffer from ion beam induced damage. As no difference in experiments performed for *1* keV and *200* eV has been observed we conclude that generally the ion beam method for energies below *1* keV is non-destructive in the sense that it does not alter the intrinsic electrical properties of the studied wires. It is also possible that for *1* keV the *5-6* nm thick surface of aluminum is amorphized under the ion beam bombardment, but recrystallizes after the sputtering is stopped.

W.2.2. Rutherford backscattering (RBS) analysis of sputtered aluminum films

Aluminum films deposited on silicon substrates have been analyzed in RBS experiment employing *1* MeV $^4He^+$ as incident ions. Backscattering angle of *168°* has been used. Samples have been tilted to avoid channeling of ions in silicon. The experiment was conducted to see what kinds of impurities are introduced to aluminum when it is sputtered. *RBS analysis* of as-received aluminum films (not subjected to sputtering) revealed no measurable amounts of any impurities (*Fig.W.4*). However it is important to note here that impurities lighter then aluminum e.g. oxygen or carbon could have not been detected in the analysis.
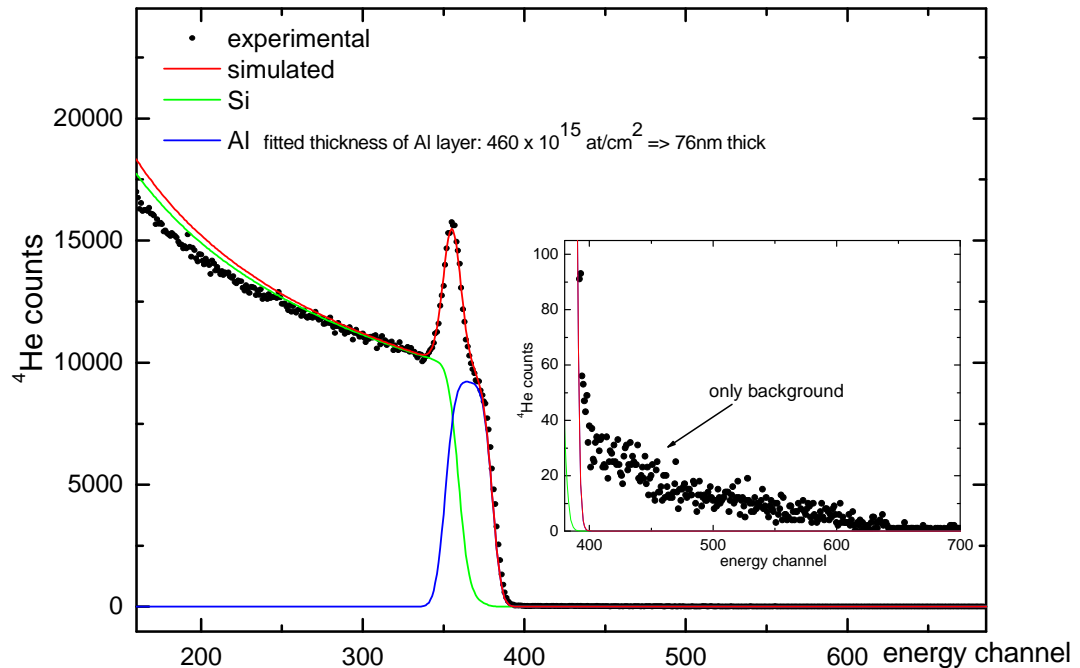
Fig.W.4. *RBS spectrum of the as-received aluminum film evaporated on the silicon substrate. Red line is the simulation. It is the sum of back-scatterings that appeared on aluminum atoms (blue line) and silicon atoms (green line). Inset shows the magnified fragment of the spectrum. No evidence for elements heavier then aluminum can be found.*

The RBS spectrum of aluminum films sputtered with *1* keV *Ar$^+$* ions to remove *~ 35* nm of aluminum is reach in impurities: *Ar, Cu, Fe, Ni, Mo, Sn* (or *Ag*) and *Au* (*Fig.W.5*). However they can be found only on the very surface layer of ~ *2* nm. Very probably the appearance of these elements in the originally pure sample (*Fig.W.4*) comes from the re-deposition of the co-sputtered environment: copper comes from sample holder, iron and nickel from stainless steel walls of vacuum chamber, molybdenum from the ion gun aperture, silver from the epoxy used to fix contacts. Since surface layer of ~ *2 - 3* nm of aluminum films is covered with aluminum oxide I do not expect detected impurities to alter electron transport properties of the studied films/wires.
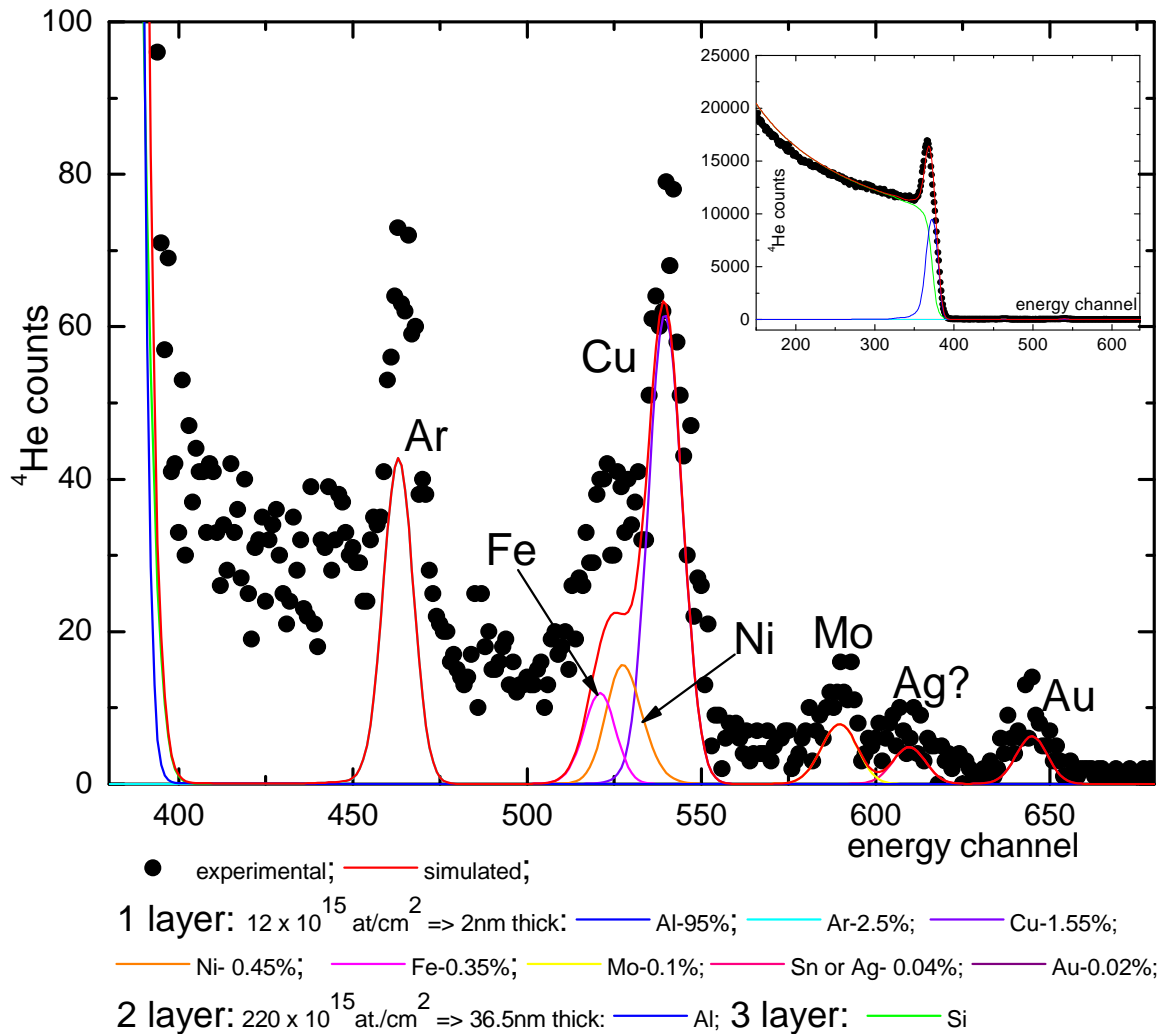
Fig.W.5. *RBS spectrum of aluminum film sputtered with* 1 keV Ar$^+$. *Inset shows the full spectrum dominated by the back-scatterings on aluminum and silicon atoms. Enlargement of the spectrum for higher energies (central picture) reveals the presence of elements heavier then* Al *and* Si.

W.2.3. Sputtering yield and sputtering rate

It is a known fact that sputtering *yield* (number of atoms ejected from the target per one incident ion) depends on the angle between the target's surface and the projectiles' trajectory. The effect originates from the fact that at glancing angles more projectiles' energy is deposited near the surface enabling the enhanced sputtering yield. I calculated the expected dependence of the yield on the impingement angle θ for aluminum bombarded by *1* keV *Ar*$^+$ ions [60]. The result is presented in *Fig.W.6*. It should be noticed that density of projectiles at slopes is suppressed by factor *cos(θ)*. Since the amount of the removed material is the product of the density of the projectiles and the yield, one may expect that the rate of the material removal is represented by the dependence given in *Fig.W.6* with green dots (lower curve). If to apply this dependence to particular structure being irradiated with ion beam at fixed direction, one can notice that different sides of the structure are sputtered with different rates (*inset of Fig.W.6*).
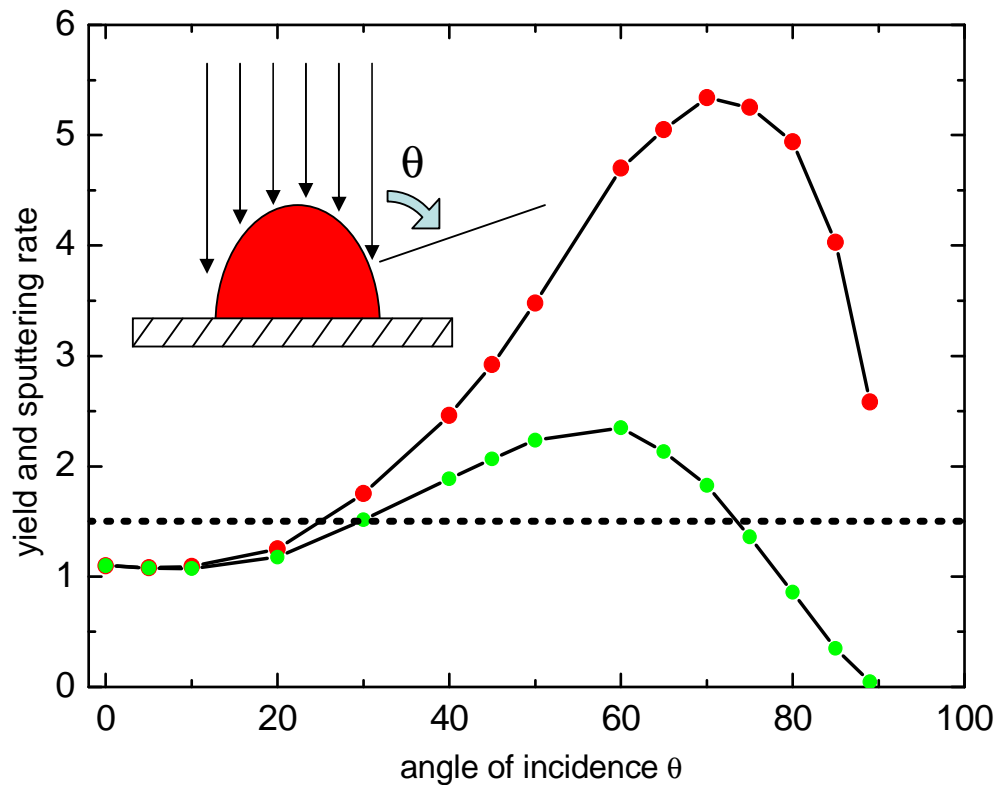
Fig.W.6. *Angular dependence of the yield (upper curve) for 1 keV Ar$^+$ ions hitting an amorphous aluminum target calculated with SRIM [60]. Lower curve represents the actual efficiency of the aluminum removal (sputtering rate) as it takes into account the reduction of the ion density at slopes by factor of cosθ. The angle θ is measured from the normal to the surface (see the inset). Horizontal dashed line is the effective sputtering rate averaged over all possible impinging angles.*

W.2.4. Geometry of sputtering

Experimentally I found that perpendicular bombardment makes a wire less and less homogeneous (*Fig.W.7*). I associate this effect with angular dependence of the sputtering rate. Also, since I considered polycrystalline wires it is not excluded that different grains within the wire can be sputtered with different rates dependent on their crystallographic orientation with respect to the ion beam axis. This effect obviously is not taken into account in *SRIM* calculations (*SRIM* considers amorphous targets) and can give rise to inhomogeneity development in studied wires when perpendicular ion beam is used.

A good remedy to get rid of this kind of preferential sputtering is to use rotating sample stage tilted with respect to the beam axis (*Fig.W.8*). Such geometry enables the averaging of the sputtering rate over different angles so that all parts of the wire are affected similarly by bombarding ions, and the whole nanostructure is eroded down in homogeneous fashion. The rotation of the sample eliminates differences in sputtering rate related to anisotropy of polycrystalline wire. It can be thought that bombarding ions "see" on average an amorphous structure of the target material. One can notice that in this kind of arrangement the top part of wire is sputtered all the time, while sides are bombarded by ions only for half of the time (being in shadow for another half). The approximate average sputtering rate is shown in *Fig.W.6* with horizontal dashed line.
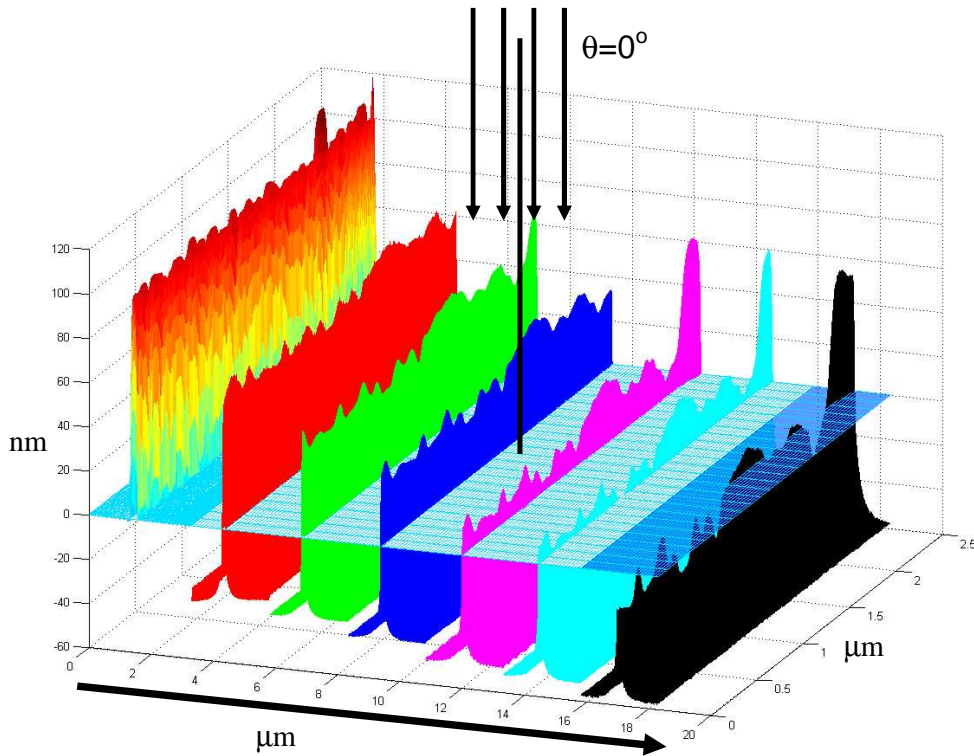
Fig.W.7. *SPM pictures of the same single aluminum nanowire scaled down with* 1 keV Ar$^+$ *beam for perpendicular bombardment. One can observe the development of inhomogeneity. As silicon substrate is sputtered faster then aluminum, finally the wire is located at the top of the silicon pedestal. Plane with grating (height = 0) separates silicon from aluminum.*
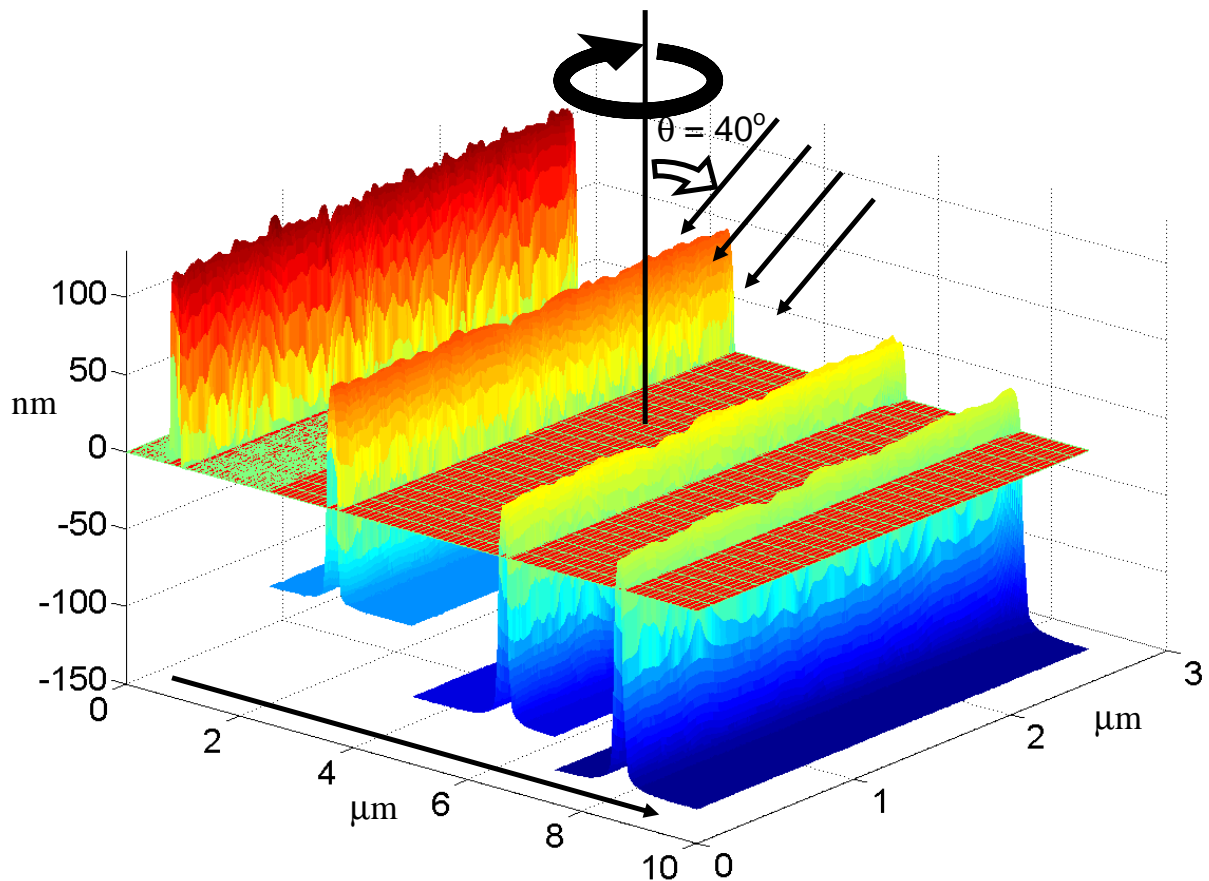
Fig.W.8. *SPM pictures of the same single aluminum nanowire scaled down with 1keV Ar+ beam at rotating sample stage tilted at* θ = 40° *with respect to the beam axis. One can observe "polishing effect" of the ion beam bombardment on wire's shape. As silicon substrate is sputtered together with aluminum finally the wire is located at the top of the silicon pedestal. Plane with grating (height=0) separates silicon from aluminum. Notice removal of the initial roughness (high frequency Fourier components of height). However smooth variation in height (low frequency Fourier components) can not be eliminated.*

W.2.5. Effect of sputtering on wire morphology

Sputtering not only preserves initial homogeneity at smooth sections of the wire but also gradually removes the roughness in less even sections (*Fig.W.8*). It is not excluded that observed smoothing of wires can be associated with the ion beam induced downhill currents responsible for redeposition of the bombarded material as it is calculated in work of *Moseler* [61]. However it should be stressed that his simulation considers amorphous targets as diamond-like carbon or amorphous silicon. Wires studied in my work are granular (polycrystalline) and it would be required to redo the mentioned simulation for polycrystalline structure with random beam direction to insure that downhill currents are indeed responsible for the observed smoothing. One can consider sputtering as a low pass filter. It removes high frequency components (= sharp spikes) from the Fourier spectrum of

the surface topography. It does not affect smooth variations. Particularly, it can not prevent development of extended constrictions with smooth variation of the cross-section along the wire (*Fig.W.9*).
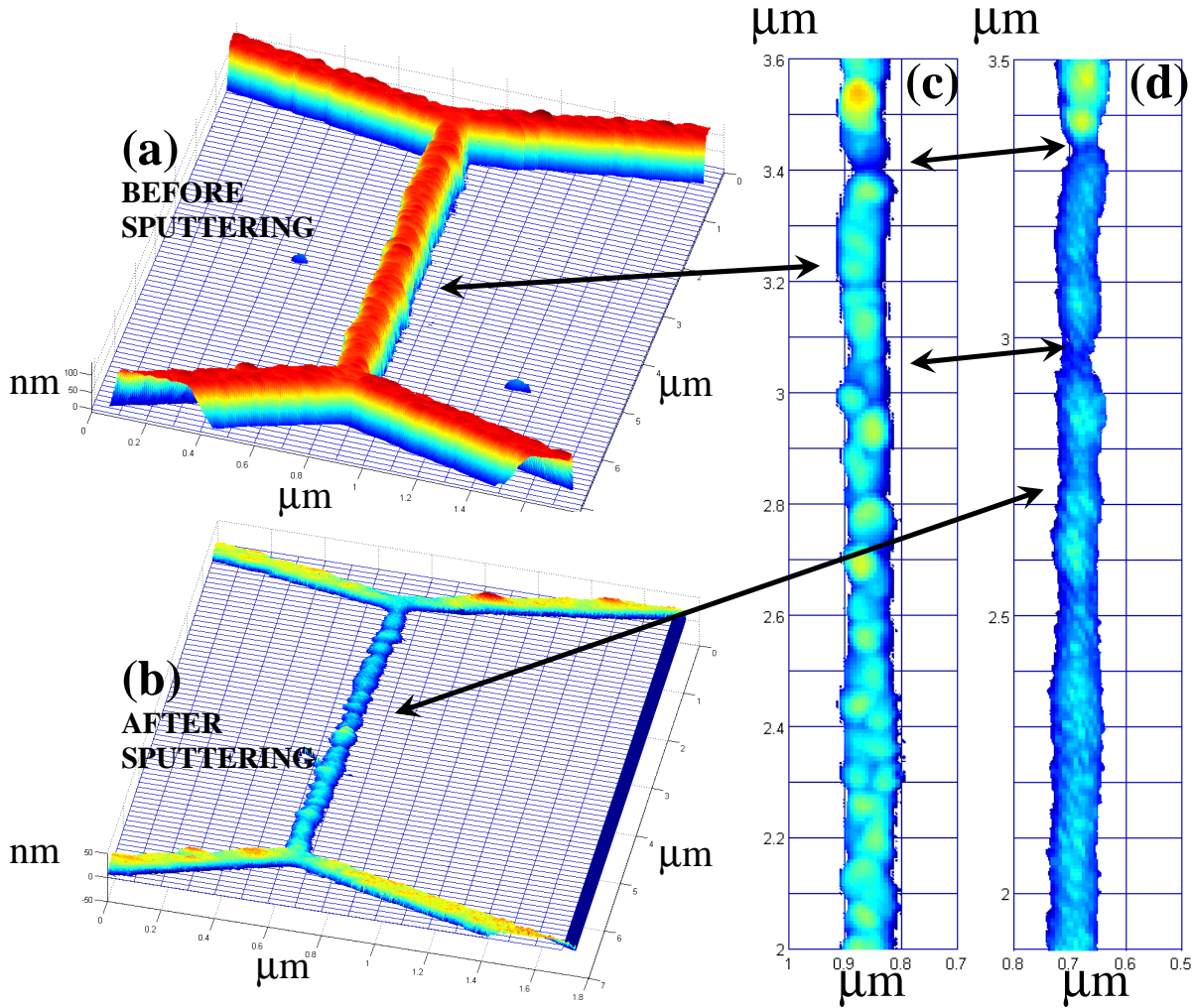
Fig.W.9. *The same aluminum wire (Cu5μm1no1) before* **(a,c)** *and after* **(b,d)** *sputtering (SPM data). Topography of the top part of the initial wire reveals its granular nature* **(c)**. *After sputtering the absolute roughness is reduced* **(d)** *(color resolution in picture* **(b)** *is much higher than in* **(a)** *which may lead someone to an opposite wrong conclusion), however the relative inhomogeneity is increased (cross-section histograms for this particular wire are presented in Fig.W.2). In course of sputtering one can observe the development of "smooth" constrictions denoted in* **(c)** *and* **(d)** *with arrows. These are the places where the wire breaks first if sputtering is continued even further. For corresponding representative profiles for this particular sample refer to Fig.W.11(c). In* **(b)** *the silicon pedestal has been subtracted to demonstrate the morphology of the wire with better resolution. Similarly in* **(c)** *the bottom part of the wire has been subtracted to demonstrate the granularity.*

W.2.6. Evolution of structure under ions bombardment (model)

In order to control the shape and size of structures treated with the ion beam I created a simple geometrical model describing their evolution. Typical cross-section of a lift-off fabricated nanowire can be approximated by a trapezoid (*Fig.W.10*). This assumption allows us to predict some trends governing evolution of the wire shape when it is bombarded by the ion beam. For trapezoid we have two different slopes which in general
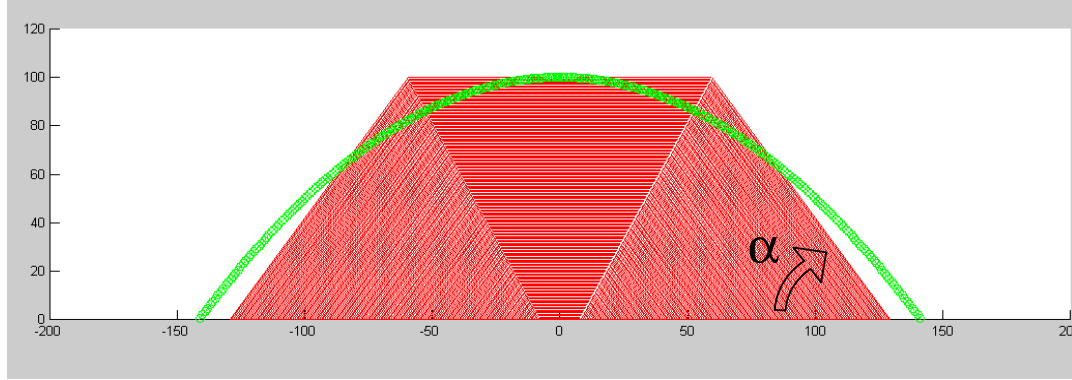
Fig.W.10. *Modeling of a real wire cross-section (shown with the smooth rounded line) with trapezoid of the same height, cross-sectional area and side wall angle* α.

can be sputtered with different rates. In the geometry utilized in my experiments the top part of the trapezoid is bombarded all the time with the ion beam tilted at $\theta = 40^o$, while the sides of the trapezoid are treated with the ion beam incident at different angles only for the half of this time (being in shadow for another half; it is true when side-wall angle α of a wire is larger then $\theta = 40^o$, which was the case for my wires). It follows that sputtering rate at the sides V_α is suppressed with respect to the sputtering rate at the top part of trapezoid V_{per} by factor $V_\alpha/V_{per} \approx 0.4$ (approximately for the case of aluminum). This can be easily verified from the data presented in *Fig.W.6* if to assume the averaging of the sputtering rate over the angles θ in the range 0°-90°. It can be shown that depending on the initial aspect ratio and the side-wall angle α there might be two scenarios of the trapezoid shape evolution: sharpening or flattening (*Fig.W.11*). In the context of our discussion "sharpness" corresponds to the aspect ratio AR being defined as the ratio of height to width. It can be shown that condition for *"sharpening scenario" (Fig.W.11(b))* is:

$$AR_{ini} > \frac{\sin \alpha}{2} \cdot \frac{V_{per}}{V_\alpha} \tag{W.1}$$

where AR_{ini} denotes the initial aspect ratio and α is the side-wall angle of the trapezoid. The condition for the *"flattening scenario" (Fig.W.11(a))* is:

$$AR_{ini} < \frac{\sin \alpha}{2} \cdot \frac{V_{per}}{V_\alpha} \tag{W.2}$$

If to put "=" sign in the above inequalities trapezoid becomes triangle only in the limit when its cross-section approaches zero. Considering this limit is also the easiest way to get the inequalities.

Hence it is sufficient to know the initial trapezoid shape to know whether after sputtering it will end as a "flat pancake" or as a "spiky triangle". Both opportunities are presented in *Fig.W.11*, *W.12* and *W.13*. We can conclude that to get the "sharpening scenario" for the used sputtering geometry $\theta = 40^o$ one would need to fabricate the wire-trapezoid with the initial aspect ratio larger than *1.25* and the side-wall angles α approaching 90°. In general for particular side wall angle structure with aspect ratio higher then $tan(\alpha)/2$ can not be produced (it would correspond to triangle with side wall angle α). This allows to evaluate range of angles for which "sharpening scenario" could possibly take place (*Fig.W.12*). In practice all produced wires ended up as flat pancakes ("flattening scenario"). This statement is supported with the *SEM* and *SPM* pictures (cf. *Fig.W.11(c)*, *Table W.1-p.54* and *Fig.W.20*) of a typical nanowire used in my experiments.

It is possible to show that the area of the trapezoid σ in the discussed model decreases parabolically with the ion dose ϕ (*fluence*). In the "flattening" case it is just parabola, in the "sharpening" case it is the curve consisting of two parabolas connecting gently (first derivative continuous) at the point where the triangle is formed (*Fig.W.11(b)*). In the case of a *2D* film it is just a linear dependence.

The equations describing the evolution of the cross-section σ in flattening case are (derivation is given in *Appendix A.1*):

$$\sigma = a \cdot \phi^2 + b \cdot \phi + \sigma_0, \qquad (W.3)$$

$$a = \frac{-\sigma_0 - b \cdot \phi_0}{\phi_0^2}$$

$$b = \frac{d\sigma}{d\phi}\Big|_{\phi=0} = V_{per}(w_0 - \frac{2 \cdot \sigma_0}{h_0}) - V_\alpha \cdot \frac{2 \cdot h_0}{\sin \alpha}$$

$$w_0 = \frac{\sigma_0}{h_0} + \frac{h_0}{tg\,\alpha}$$

where:

h_0 - initial height of trapezoid, σ_0 - initial cross-section, α - side-wall angle, w_0 - initial width, V_{per} – speed of sputtering of top part of trapezoid (*nm / fluence*),

V_α - speed of sputtering of sides of trapezoid (*nm / fluence*),

ϕ − *fluence* defined as the flux of projectiles (Ar^+ ions) integrated over time of sputtering,

$\phi_0 = h_0 / V_{per}$ – fluence required to sputter the whole trapezoid,

$V_\alpha / V_{per} \approx 0.4$ (*SRIM* simulation-based estimation for aluminum and rotational sample stage).
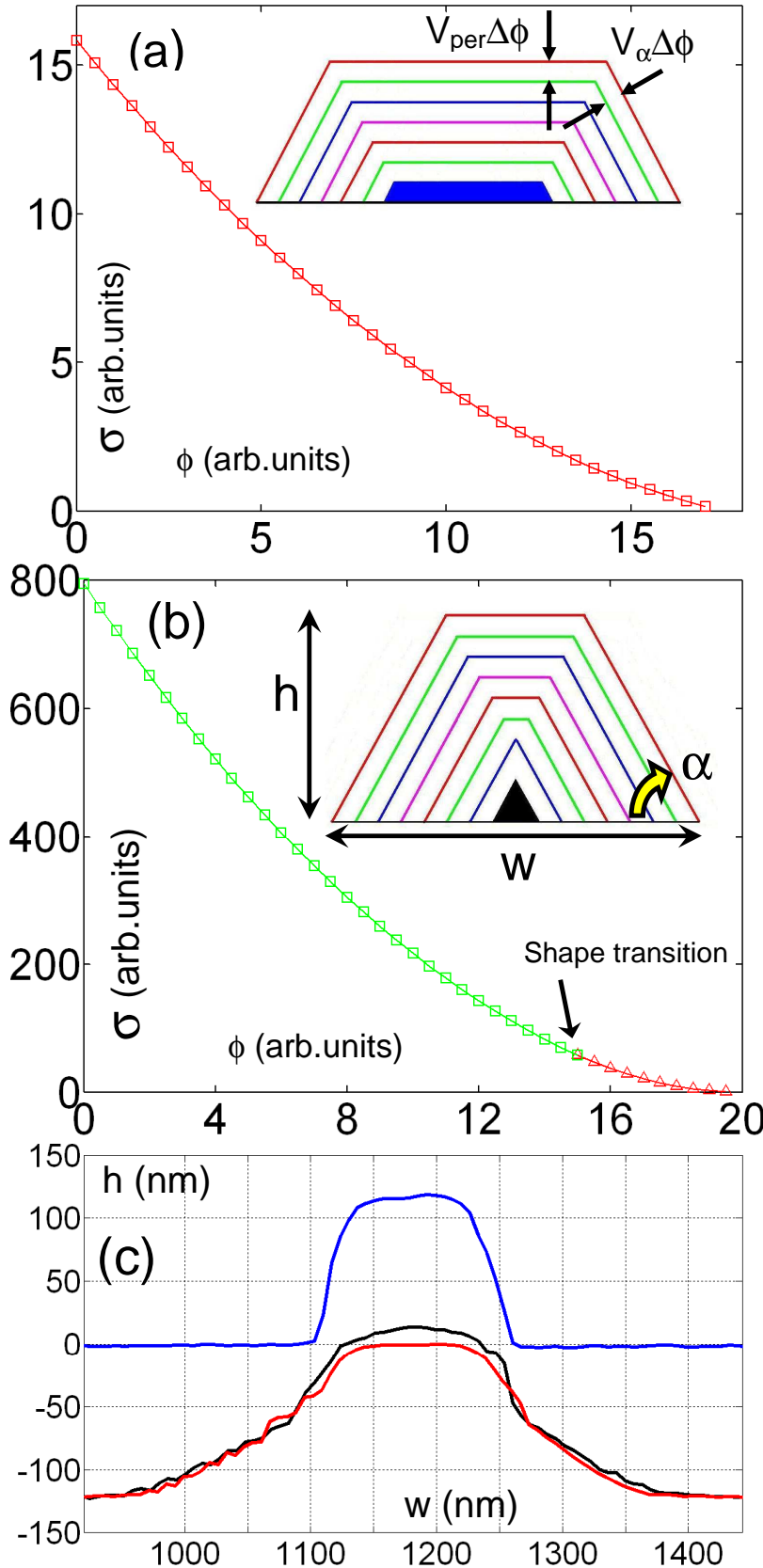
Fig.W.11. Modeling of the wire cross-section as the function of the ion fluence ϕ. *Dependently on the initial aspect ratio and the ratio* V_{α}/V_{per} *there are two possibilities:* flattening *(a) and* sharpening *(b). In both cases the cross-section decreases parabolically with the ion dose* ϕ. *The curves were calculated for the case* $V_{per}=V_{\alpha}$.

In (c) the real wire (Cu5μm1no1) cross-sectional profile evolution is shown as recorded with SPM. The units for the both axes in (c) are the same to stress real geometry of studied wires. Red profile corresponds to the silicon pedestal left after the removal of aluminum with HCl *acid.*
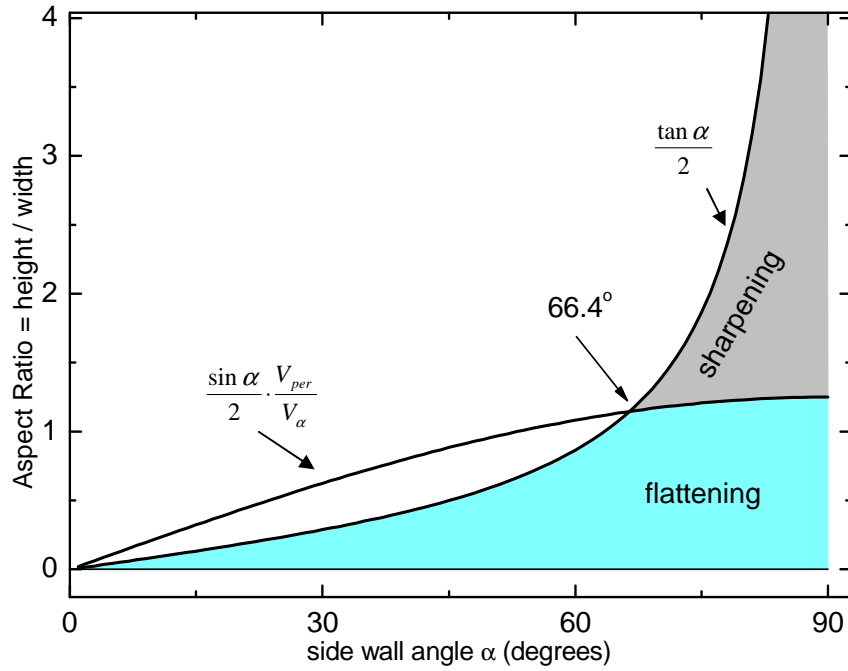
Fig.W.12. *Dependently on the initial aspect ratio and the side wall angle* α *the sputtered wire can become sharper or flatter. In practice all studied wires could have been considered within the "flattening scenario".*
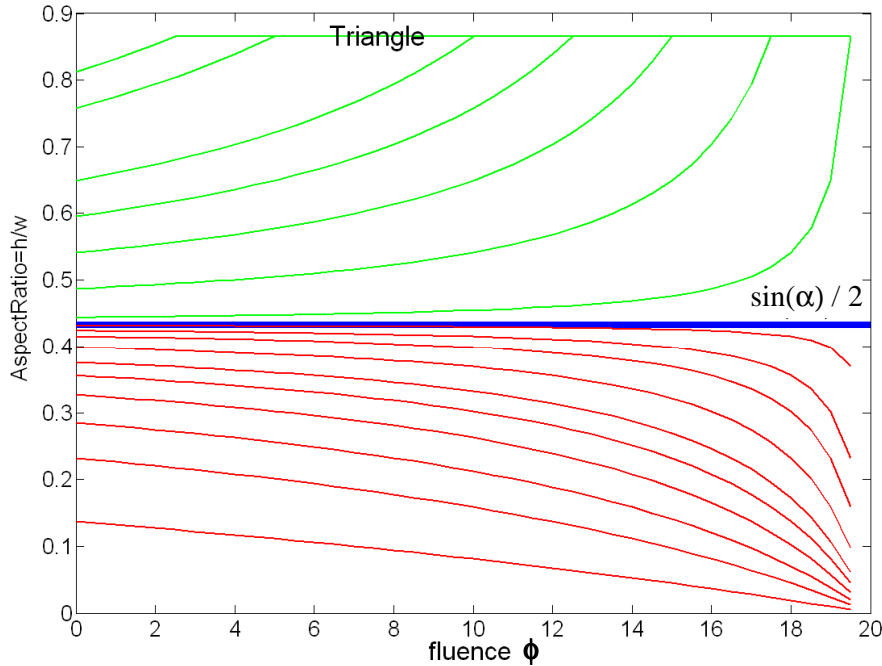
Fig.W.13. *Evolution of the aspect ratio (AR) for the sputtered trapezoid with the side wall angle* α=60°*. If* AR=sin(α) / 2 *then the trapezoid does not change its shape while sputtering (we obtain sequence of similar figures) – it is represented with thick blue line. If initial* AR > sin(α) / 2 *then the trapezoid gets sharper and finally it degenerates into a triangle with the side wall angle* α = 60°*. If* AR < sin(α) / 2 *then the trapezoid gets flatter until it disappears completely. In calculation the same sputtering rates at the sides* V$_\alpha$ *and at the top* V$_{per}$ *of trapezoid are assumed.*

An important consequence of the parabolic dependence of the sputtered cross-section on the ion fluence is that as the structure gets smaller, it is also sputtered slower (the magnitude of the parabola derivative for smaller cross-sections is smaller). The effect can be qualitatively understood in terms of smaller area exposed to the bombarding ions. It follows that for particular fluence less target atoms are removed from a smaller structure compared to a larger one.

Armed with the presented geometrical model one can predict the evolution of the shape of the real wires under the ion-beam treatment. *Fig.W.14* shows experimental data based on SPM measurements and the corresponding simulation. The only fitting parameter is the sputtering rate for the top part of trapezoid V_{per}. Within *10%* the V_{per} was found to be the same for all samples. For the sputtering rate at the sides I used $V_\alpha / V_{per} = 0.4$ (case of aluminum nanowires). It should be mentioned that all wires presented in *Fig.W.14* satisfy the "flattening scenario".
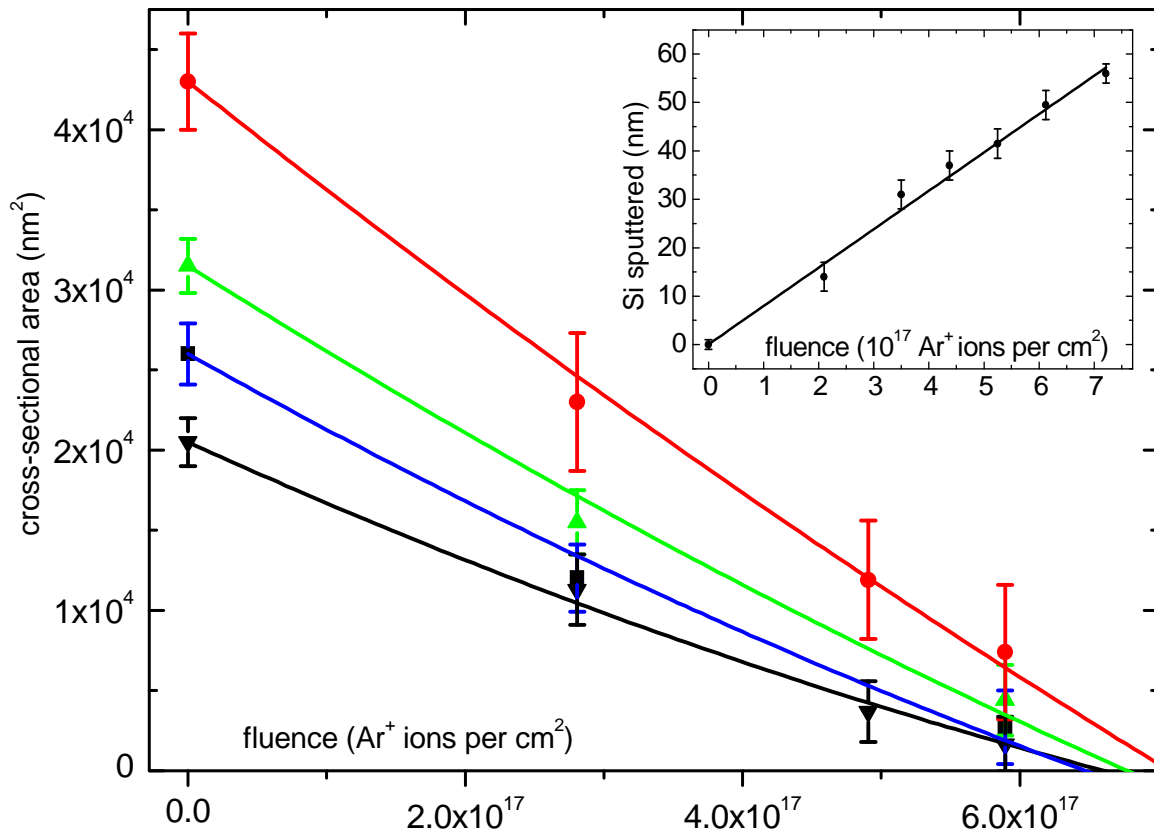
Fig.W.14. *Evolution of the aluminum nanowires cross-section with fluence. Experimental points were calculated as averages from SPM data. Error bars are mainly set by the uncertainty (~ 10%) in estimation of the silicon substrate sputtered. Solid lines are parabolic fits to the geometrical model discussed in the text (flattening case). Inset shows calibration of the sputtering rate for the Si substrate. Data points were obtained from SPM measurements of the thresholds defining the border between the areas of the silicon substrate exposed to the ion beam and the areas covered with the protective layer during the whole sputtering experiment, hence unaffected by the ions (cf. section W.2.7).*

W.2.7. Determination of the border between the wire and substrate in the sputtered samples

Usually sputtering of metallic wires is accompanied by sputtering of the supporting substrate. Since metallic structure acts as a mask for the silicon, finally the wire is located at the top of the silicon pedestal (*Fig.W.7, W.8, W.11(c)*). Then the following experimental problem arises: how to determine the interface between the substrate and the wire to get a reliable estimation of wire geometry? In early stages of my work I used tiny droplets of conductive carbon glue (*Leit-C CCC Neubauer Chemikalien*) distributed over the substrate before each ion beam treatment and serving as masks protecting the substrate underneath from being sputtered. After experiment was finished the droplets were removed with acetone leaving behind the steps in the silicon substrate to be scanned with SPM to know their height. The method allows for determination of the height of the sputtered silicon with accuracy *~10%* (values for the droplets that should give the same number were different up to *10%* dependently on the location of the droplet on the substrate). The measured heights should fall on a straight line if sputtering conditions remain constant during entire experiment (see *Fig.W.14, inset*). The *10%* accuracy in the silicon height determination results in a rather poor estimation of the wire height. For example, you measure the height of the whole structure (silicon + wire) after experiment to be *100* nm. Then from "droplet calibration" of the sputtered silicon you get value *90 ± 9* nm. It yields a poor estimate for the wire height: $h_{wire} = 10 ± 9$ nm.
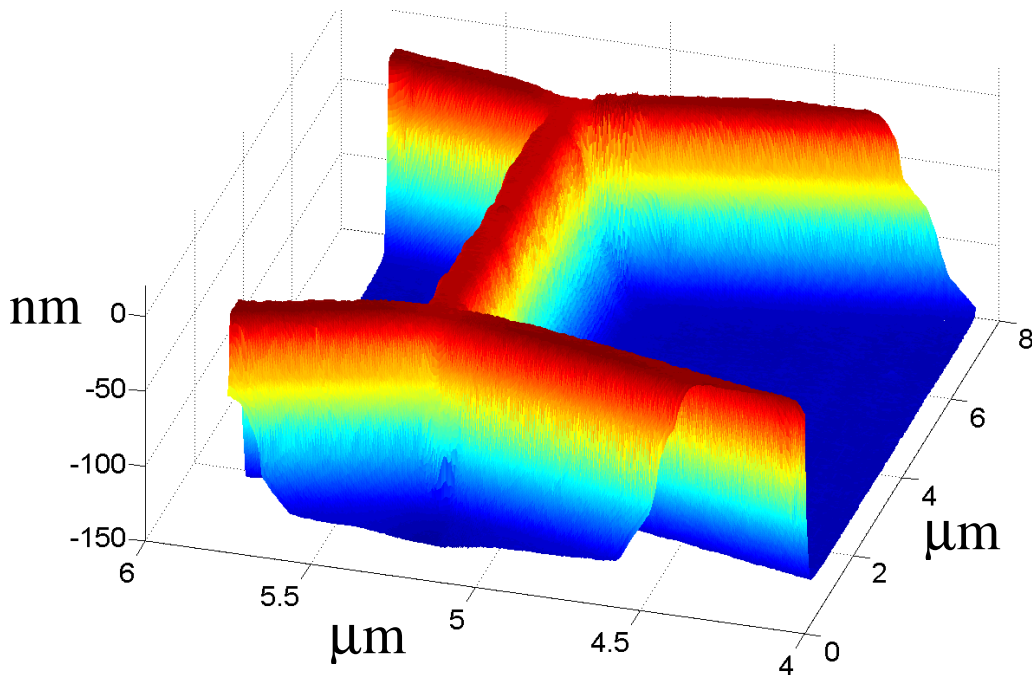
Fig.W.15. *SPM image of atomically smooth silicon pedestal (surface roughness ~ 0.5 nm) left after removing of the aluminum nanowire with 7% HCl. The corresponding cross-sectional profile is given in Fig.W.11(c).*

More accurate approach is to use some etchant (*7% HCl* works well for aluminum) to remove the metal, but not the substrate. The method is obviously destructive, but it enables the determination of the wire height with *~1* nm accuracy. What is needed is to compare two topography SPM data: before (silicon pedestal with wire at the top of it) and after (only silicon pedestal) sputtering. SPM can provide *sub - 1* nm accuracy in height measurements. The picture of an almost atomically smooth silicon pedestal (with roughness at the level of *0.5* nm) is given in *Fig.W.15.*

To summarize the sputtering section I would like to add that we performed similar experiments on *Sn* and *Bi* nanowires and obtained qualitatively similar results as in case of aluminum. Hence, we believe that the presented method can be utilized for various materials whenever there is a need to reduce their size in predictable and homogenous way.

W.3. Normal state resistance of the wires

According to the *Ohm's law* the normal state resistance of a wire is:

$$R = \rho \cdot \frac{L}{\sigma} = \rho \cdot l_{mean} \frac{L}{l_{mean} \cdot \sigma} = K \cdot \frac{L}{l_{mean} \cdot \sigma} \tag{W.4}$$

where:

L - length of the wire, ρ - resistivity, σ - cross-section, l_{mean} - elastic mean free path, $K = \rho \cdot l_{mean}$ - constant characteristic for a given material (see *Appendix A.3*).

Using *Matthiessen rule* resistance can be divided into two components (at low temperatures $T \sim 4.2K$ phonons can be neglected):

$$\frac{1}{l_{mean}} = \frac{1}{l_{mean\_bulk}} + \frac{1}{l_{mean\_meso}} \quad \text{(see *Appendix A.4*)} \tag{W.4a}$$

$$l_{mean\_bulk} = \frac{\sqrt{3}}{3} \cdot l_{gb} \quad \text{scattering by grain boundaries and impurities}$$

$$l_{mean\_meso} = \frac{\sqrt{3} \cdot \sigma}{(\sigma/h + h)} \quad \text{scattering by sample boundary, h - height, } \sigma \text{ - cross - section}$$

First component produces resistance as if it was *NO scattering* on the sample boundaries (*bulk term*), another gives resistance as if it was *ONLY scattering* on the sample boundaries (*mesoscopic term*). First term describes resistance of polycrystalline structure with linear grain size $l_{gb} <<$ *linear size of structure*, second term describes resistance dominated by the surface of the structure (*linear size of structure $<< l_{gb}$*). As a wire cross-section is reduced one goes from the bulk to mesoscopic limit. For the thinnest wires bulk term can be practically neglected. In smaller wires the mean free path l_{mean} is significantly reduced due to the scattering on sample boundaries, but then resistivity ρ is enhanced in such a way that the product $K = \rho \cdot l_{mean}$ remains constant.

In *Fig.W.16* resistivity data for several wires fabricated using e-beam lithography has been collected. Resistance was measured with four-probe method eliminating the

influence of the electrodes. Values for the cross-section σ were obtained with SPM. Resistivity ρ for the thickest samples is around *1.7 • 10^{-8}* Ωm and it rises for the smaller wires. An increase of the resistivity ρ results from the decrease of the mean free path but also can be the effect of the *SPM* overestimation of the wires cross-section for the thinnest samples due to the convolution of the real image and the *SPM* tip. It is understandable that when the size of the wire starts to be comparable to the size of the *SPM* tip, the quantitative analysis is problematic. The height of a nanostructure can be measured with good accuracy (~ *0.5* nm) while the lateral dimensions can be affected by the finite tip shape. Another source of error is due to the fact that the surface of aluminum samples is oxidized; hence a conducting wire cross-section is smaller than the total one. The last contribution results in a systematic overestimation of the conducting cross-section from the *SPM* data. l_{mean} in sufficiently thick wires is of the order of the average grain size ($l_{mean} \propto$ *grain size ~ 20 - 50* nm, cf. *Fig.W.1*). It follows that constant $K = \rho • l_{mean}$ can be estimated to be $K = (6.0 \pm 2.5) • 10^{-16}$ Ω m^2. This is in good agreement with data given in literature for aluminum films [62].

The resistance ratio $R_{273K}/R_{4.2K} \sim 4$ for the thickest wires ($\sigma \sim$ *20000* nm^2) typically was measured. In the very thin wires resistance was dominated by the non-temperature dependent scattering – the phonon scattering was negligible resulting in $R_{273K}/R_{4.2K} \sim 1$.
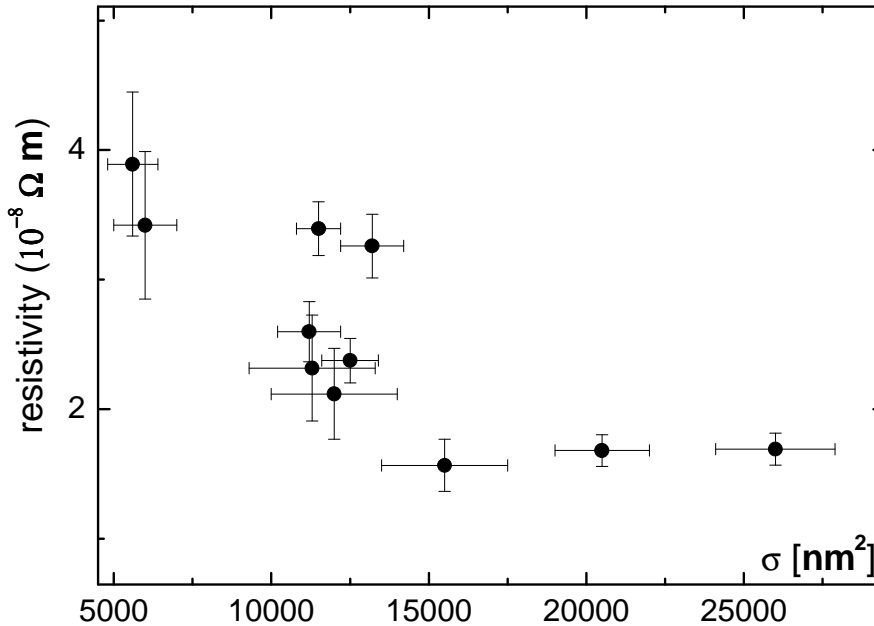
Fig.W.16. *Dependence of the resistivity* ρ *of aluminum wires on their cross-section* σ *calculated as* $\rho = R • \sigma / L$ *measured at* 77 K. *The error bars reflect experimental difficulty to estimate the cross-sections of the wires.*

W.3.1. Evolution of a wire resistance and cross-section with sputtering

The formula for the normal state resistance of a thin wire (eq. W.4) together with the model of sputtering (*"flattening case"*, W.3) enables to predict the evolution of the wire resistance if the initial sample geometry and the applied fluence are known. I applied the model to fit experimental points: wire resistance vs. ion beam dose (*Fig.W.17*). I used V_{per} (sputtering rate of the top part of trapezoid) and $K = \rho \bullet l_{mean}$ as the fitting parameters. Initial geometry (length, cross-section, height, side-wall angle) was known from *SPM* measurements and I assumed that $V_\alpha = 0.4V_{per}$ (see discussion in *W.2.6*). Additionally I could vary l_{gb} within reasonable values. Fitting made to first *5* points in *Fig.W.17* gives $K = 5.9 \bullet 10^{-16} \Omega m^2$ and $l_{gb} = 39$ nm. Only the *5* first points were taken because of the thin layer of aluminum oxide covering the surface which is sputtered at much lower rate than
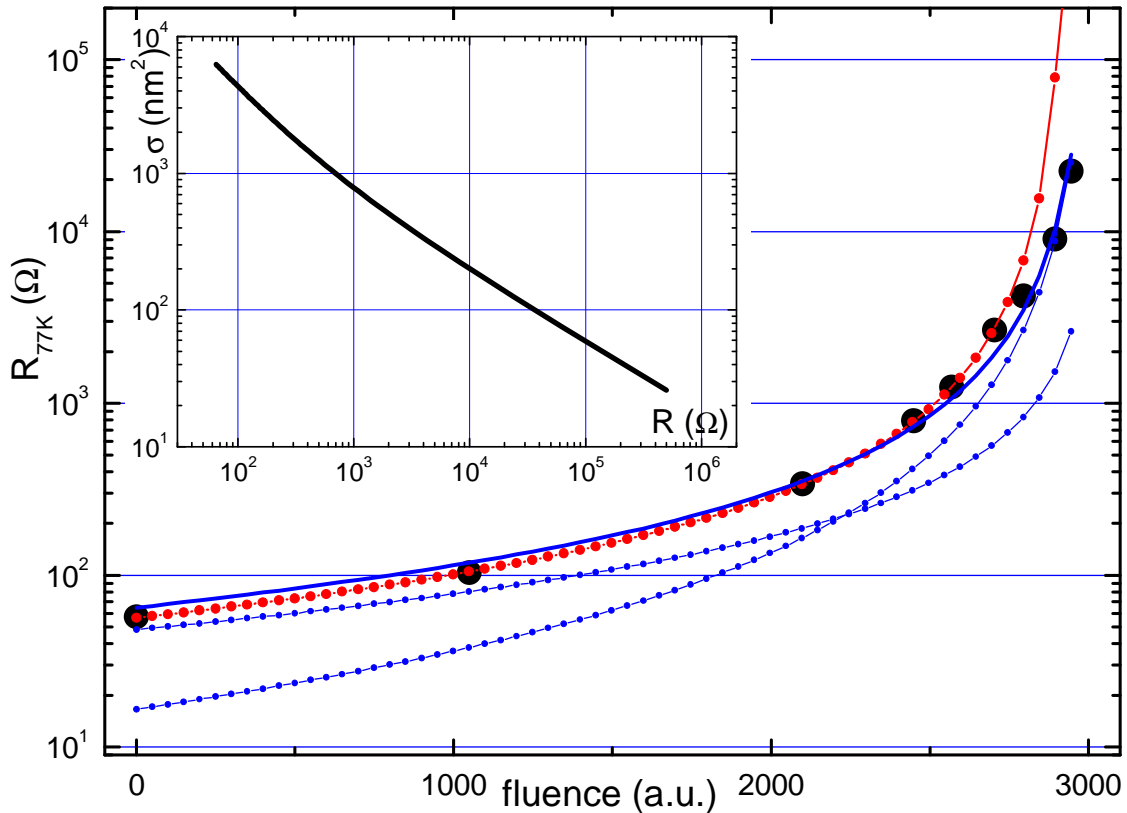
Fig.W.17. *Evolution of the wire resistance with applied fluence. Black dots are experimental points, while solid blue line is the fit to the data based on formula (W.4) and "the model of flattening" W.3 (SPM data for this wire are:* s = 6200 nm^2, h = 58 *nm*, $\alpha = 65^o$, L = 10 μm). *The fit is divided into two parts: dotted solid blue lines, representing resistance resulting from the scattering at the grain boundaries and impurities* ("bulk resistance"), *and from the scattering at the sample boundary* ("mesoscopic resistance"). *Red curve is the fit only to the first 5 experimental points (see comment in text). The inset shows the evolution of the mean wire cross-section as a function of its resistance.*

the aluminum. If the applied fluence in a given sputtering session is not too large as it happens for thin wires (in *Fig.W.17* these are points corresponding to the highest resistances), then significant amount of it is "wasted" to remove aluminum oxide layer and only afterwards aluminum can be removed at a higher rate. It follows that the smaller amount of material is removed compared to the case if it was no oxide layer. Hence, the resistance of the wire is smaller than the model predicts. However, taking into account all data points does not change fitting parameters significantly (solid blue curve in *Fig.W.17*). The constant K resulting from such fit is $K = 6.8 \cdot 10^{-16} \, \Omega\text{m}^2$ (if $l_{gb} = 39$ nm is assumed). Changing l_{gb} in the range from *20* nm to *60* nm yields $K = (6 \pm 2) \cdot 10^{-16} \, \Omega\text{m}^2$ in agreement with the previous result based on the normal state resistivity and the average grain size (*Fig.W.16* and *Fig.W.1*). The fit done to all experimental points can be divided into *bulk-* and *mesoscopic resistance* (*eq. W.4&W.4a*). It can be observed that as the wire shrinks its resistance starts to be produced entirely due to scattering at sample boundaries and the bulk term can be neglected. The dependence of the wire cross-section on its resistance is plotted being calculated self-consistently within the fitting procedure in the inset of *Fig.W.17*. This data, however, must be treated with certain skepticism as the calculation was made using the assumption that wire is ideally uniform. What happens if it is not the case is discussed in the next section. One should be conscious that what I call the cross-sectional area is the surface area of a flat trapezoid as discussed in the sputtering model (see *section W.2.6*). Hence *200* nm^2 means that the wire cross-section is a *"flat pancake"*, say of width of *50* nm and height of *4* nm (cf. histograms in *Fig.W.2* for representative wire profile). It is important to notice that the value of the conductive cross-section for the thinnest wires determined from the *SPM* measurements has a large uncertainty due to the finite size of the tip and the oxide layer at the sample surface. The data obtained from *SPM* can thus be treated only as upper-limit estimation. The determination of the cross-section based on measurement of the normal state resistance can provide complementary information (cf. *section W.4*). For some applications the resistance of a microstructure or a nanostructure can be measured *in situ* just in the sputtering chamber, providing a powerful tool for monitoring the sample processing. In fact, an increase in the electrical resistance of thin films due to ion bombardment was used already many years ago to determine sputtering yield of different materials [63]. There are no principal objections against integration of a measuring circuit and sputtering system in a single setup.

W.3.2. Effect of inhomogeneity of wires

A real wire is never homogenous. It has some cross-section and height distribution when it is initially produced with e-beam lithography. In course of sputtering this inhomogeneity can be reduced only partially. There is always place along wire where its cross-section is smaller. This place will be sputtered away quicker then the other segments of the wire. As it has been discussed in the previous section, variation of the sputtering

angle enables the effective removal of the "sharp spikes", but it cannot remove the inevitable "smooth" variations of the cross-section along the wire. For sufficiently thick wires, say with height of order of *50* nm and variation of the height *dh = 3* nm, the wire can be considered smooth and homogenous. Putting *h = 50* nm or *53* nm to formula for resistance (eq. W.4) will not change its value dramatically. But for the wire with the mean value of height h_{mean} = *7* nm and the variation of the height *dh = 3* nm the wire can be considered as highly inhomogeneous. What can be considered as a measure of the wire's homogeneity is the ratio *dh / h*. The thinnest section of the thin wire provides the dominant contribution to the resistance. This section is responsible for the observed abrupt increase of resistance as a function of fluence.

As an example let us consider the wire of length *10* μm consisting of two parts connected in series:

-*9* μm of wire with cross-section *11500* nm^2 and height *84* nm,

-*1* μm of wire with cross-section *10500* nm^2 and height *80* nm (constriction).

For both segments of the wire I assumed side wall angle *65°*. We want to follow evolution of the wire resistance as a function of the ion beam fluence.
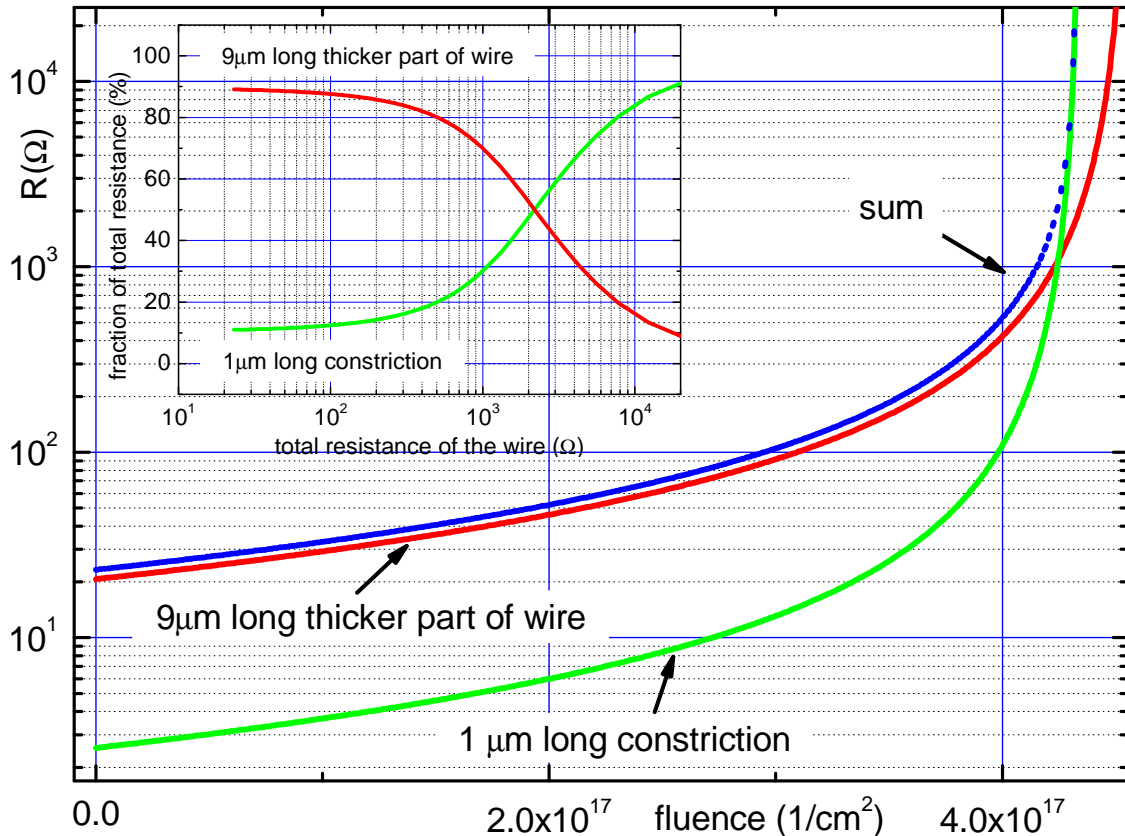
Fig.W.18. *Evolution of the total resistance (sum, blue curve) for the* 10 *μm long wire consisting of two segments of slightly different geometrical parameters: the thicker part (red curve) and the thinner part (constriction, green curve). As sputtering is progressing constriction is formed which determines the total resistance. Inset shows the fraction of the total resistance produced by each segment. At* 2 *kΩ the* 1 *μm long constriction produces the same resistance as the* 9 *μm long rest part of the wire.*

In *Fig.W.18* the result of such simulation is presented. It can be seen (*inset Fig.W.18*) that when the sample is sufficiently thick the thinner part of the wire produces actually the same resistance per length like the thicker part. However, when the dimensions are reduced, the situation changes. At *2* kΩ half of the total resistance comes from the thin part of the wire. As one continues to reduce the size, the thinner segment dominates the total measured resistance. This result is no surprise if to look at the plot showing the dependence of the cross-section σ on total resistance (*Fig.W.19*). At the total resistance equal to *2* kΩ the cross-sectional area of the constriction is below *200* nm^2, while the cross-section of the thicker part is still around *600* nm^2. The result originates not only from the reduction of σ, but also is the effect of the reduction of the mean free path in the constriction (cf. *eq. W.4a*).
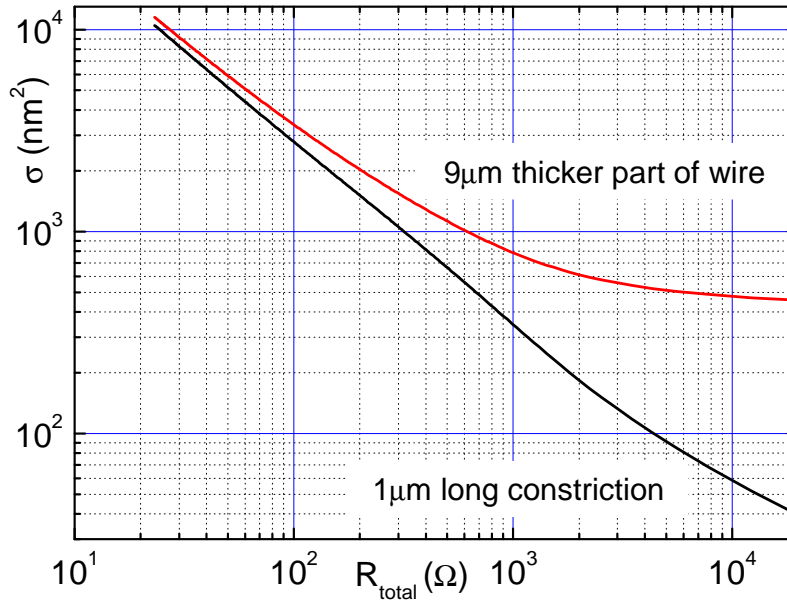
Fig.W.19. *Dependence of the cross-section on the total resistance for two segments of the wire (thin and thick). Data were obtained along with the calculations of the evolution of the resistance presented in Fig.W.18.*

The above example and the corresponding calculations, though might seem obvious, are of significant importance for the interpretation of the experimental results on *quantum phase slips* (*QPS*). As it has been shown (*eq.T.41*), the probability of the phase slip event depends exponentially on the wire cross-section (or resistance per length). It follows that *QPS* happen in constrictions (so called weak links) predominantly. The wire can be considered to be the series connection of the constriction (independent of the wire length, with large resistance per length), where *QPS* nucleate, and the wider classical superconductor (whose normal state resistance is length dependent), which does not contribute significantly to the *QPS* process. Hence, as long as we consider single phase slips in inevitably inhomogeneous polycrystalline nanowires they produce similar effect in wires of different lengths.

W.4. Determination of wires' cross-section (the case of the particular samples)

As a wire becomes thinner the quantitative determination of its cross-section starts to be not a trivial task. For sufficiently thick sample one can rely on *SPM* measurements. But for thin wires (with cross-section falling below ~ *30 x 30* nm^2) the finite tip size can bring about pronounced convolution effects. In principle one can estimate the height of the structure *h* with *SPM* quite reliably. Additionally, if the scanned feature is flat (with the side wall angles smaller then the side wall angles of the *SPM* tip) then the estimation of the lateral dimensions resulting from SPM should be also correct. One can use *SEM* (*Fig.W.20*) to determine the width of the wire and hence provide the check for the data measured with *SPM*. In chapter devoted to sputtering technique I have already shown that the investigated wires within typically fell into the *"flattening limit"* meaning that the wires in course of sputtering became very flat (*Fig.W.11(c), Table W.1* and *Fig.W.20*). Hence it was possible to determine their cross-sections with *SPM*. Such estimation must rely on the well-defined border between the metallic wire and the silicon pedestal supporting it. Practically the border can be determined with *1 - 2* nm accuracy (*W.2.7*). Below I will present the microscopy-based estimation for the cross-section of the nanowires. I will show that the results are consistent with those derived from the normal state resistance.

In *Table W.1* the *SPM* data for two representative *5* μm long nanowires obtained with the ion beam treatment are presented. For both samples the width is much bigger then the height (wires are very flat). This data were obtained by averaging *~1000* SPM scans across the particular wire. On subtracting *2 - 3* nm thick surface layer of the naturally formed oxide one can obtain the cross-section of the conducting aluminum core.

Alternatively, the wire cross-section can be obtained from the normal state resistance assuming that the mean free path is of the order of the smallest dimension (the height *h*). Utilizing expression: $R = K \cdot \dfrac{L}{l_{mean} \cdot \sigma}$ (*eq. W.4*) I calculated resistance-based cross-section (*Table W.1*) taking K = *(6 ± 2)* • *10^{-16}* Ωm^2.

SPM- and resistance-based approaches for determining cross-section are coherent. Analyzing data from *Table W.1* one should remember that it is a big challenge to determine dimensions of artificial *3D* nanoobjects when their sizes fall into the range of few nanometers and, hence should not be surprised with the large relative errors.

	σ-SPM Al+Al$_x$O$_y$ nm^2	h$_{max}$ SPM nm	w SPM nm	σ-SPM Al only nm^2	l$_{mean}$ nm	R$_{77K}$ Ω	σ-R Al nm^2
Cu5 um1 no1	600 ± 200	10 ± 2	90 ± 14	**< 500**	4 ± 2	4005	**190 ±160**
Cu5 um1 no2	1200 ± 500	11 ± 2	160 ± 15	**< 1200**	5 ± 2	715	**800 ±600**

Table W.1. *Comparison of two methods of the cross-section determination for two representative samples. Columns with "SPM" added to the symbol represent SPM-based data. Mean free path estimation is based on the SPM-measured height of the wire. Normal state resistance is measured with the 4 - probe method.* σ-R *is the estimation for the cross-section based on the resistance and the mean free path.*
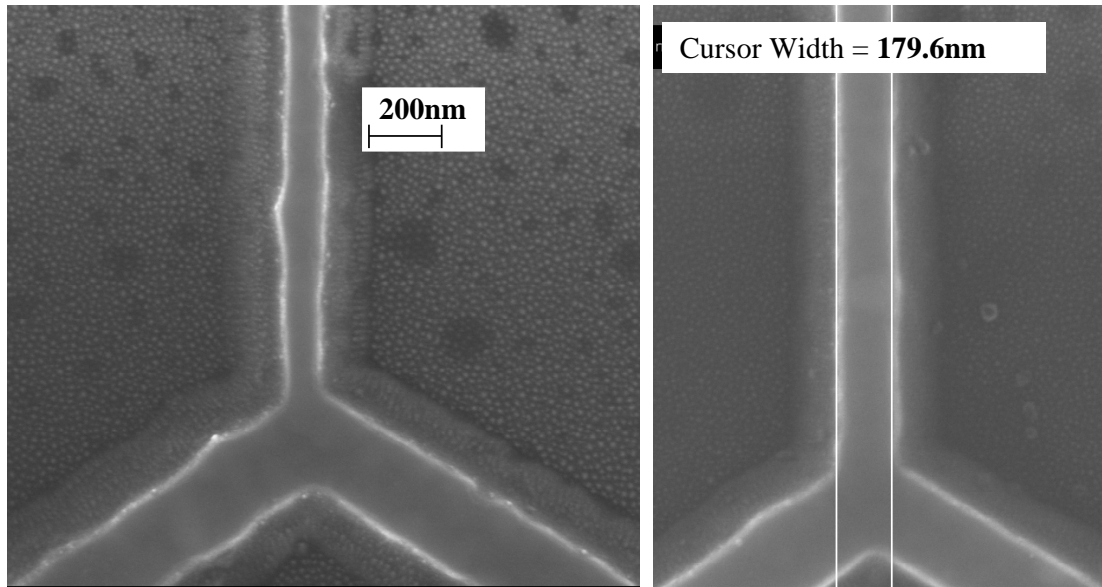
Fig.W.20. *SEM pictures of two sputtered wires discussed in the text. Cu5um1no1 is* 100 *nm wide (left picture). Cu5um1no2 is* 180 *nm wide (right picture). These values should be directly compared to the values presented in Table W.1. One can also observe shadows around the wires which are the sides of the silicon pedestal formed in course of the bombardment of the rotating sample stage with the ion beam incident angle* θ = 40°.

V. Experimental Setup (S)

S.1. Low temperature measurements

S.1.1. 1K Helium cryostat (Fig.S.1. – see p. 57 for figure caption)

(a)

liquid
nitrogen
can

magnetic coils
($B_{max} \sim 120mT$)

(b)

by-pass

diffusion
pump

rotary pump

(c) Dip-stick

(d) glass Dewar

(e)

(f)

(g)

(h)

S.1.2. Sample stage and sample (Fig.S.2.-see p. 57 for figure caption)

5μm long wire

(f)

(a)

Contact pads

Shunting wire for
installation →
bonding wires

(e)

(d)

filter box

thermometer

(b)

(c)
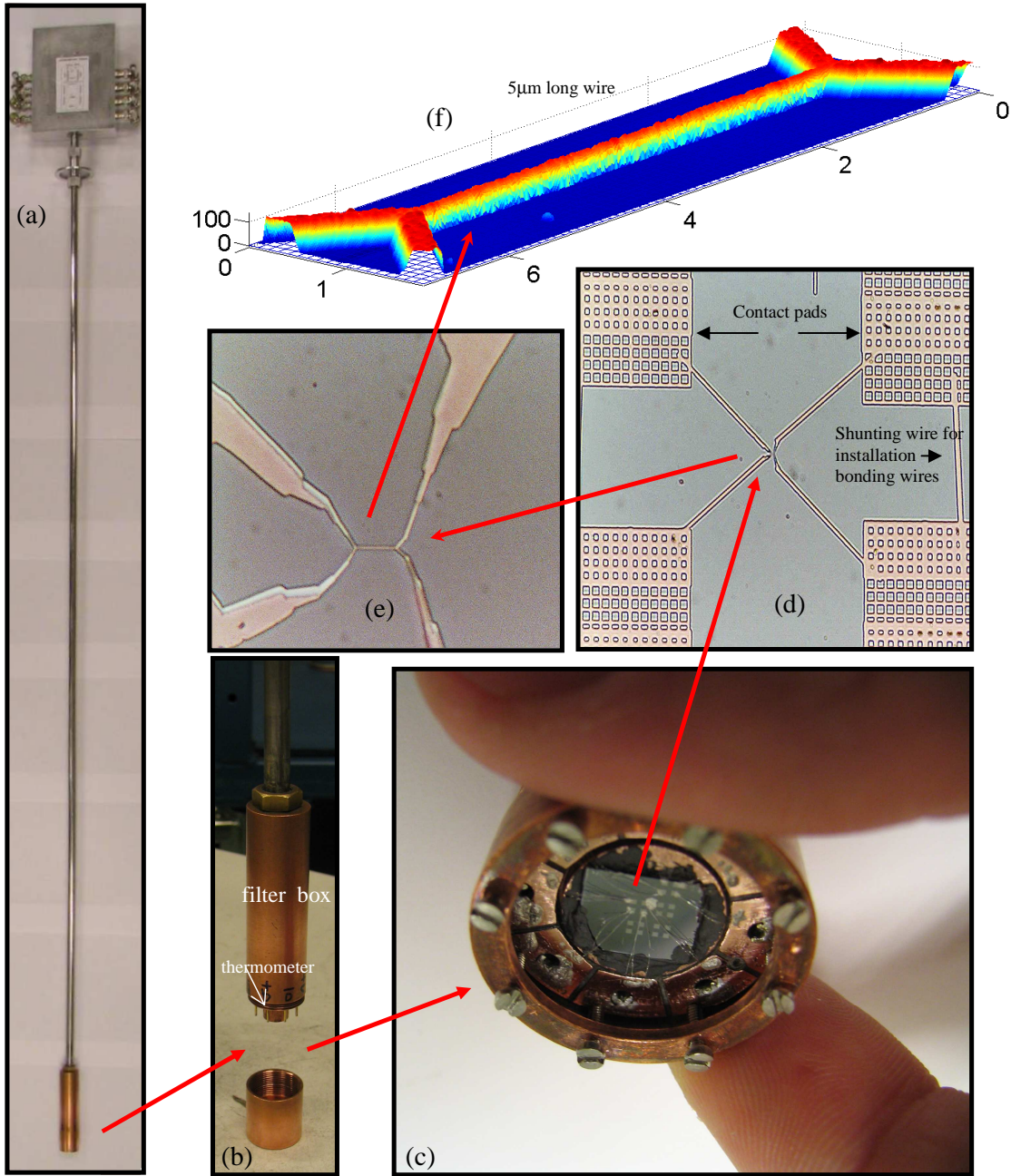
Fig.S.1. *1K direct pumping Helium cryostat. Dip-stick with sample is inserted into the double-walled glass Dewar filled with liquid* ^{4}He. *The Dewar is mounted in the liquid nitrogen can. By pumping away the most energetic helium atoms we could achieve temperature* ~ 1.2 K *with the rotary pump and* ~ 0.97 K *with the diffusion pump. Below the* λ–*point temperature can be stabilized with accuracy* ± 0.1 mK *using either manual valves or* PID *controller with the heater increasing helium evaporation (and pressure).* (a) *The picture of the entire cryostat.* **(b)** *Pumps on the other side of the wall.* **(c)** *Top part of the dip-stick.* **(d)** *The double-walled glass Dewar.* **(e,f)** LI-75A *Low Noise Preamplifier for the AC Lock-In measurements, DC Nanovoltmeter EM Model* M31**. (g)** *The pipe (orange) is to evacuate the gas from the in-between walls space of the glass Dewar (to provide thermal isolation).***(h)***Clean helium valve for venting the cryostat and "dirty helium line" serving as the output for pumps.*

Fig.S.2. *Performing four-probe low temperature measurements on microscopic-size sample.* **(a)** *Dip-stick with* 4 *pairs of RF-filtered BNC inputs.* **(b)** *Detail of the low temperature part of the dip-stick***. (c)** *Sample holder with the glued sample (glue - conductive Leit-C CCC (Neubauer Chemikalien)). Notice the shunting ring (with* 8 *screws) used to ground the sample during installation to the dip-stick.* **(d,e)** *Optical microscope images of a sample obtained with e-beam lithography by evaporation of* ~100 nm *of aluminum at 0° angle followed by evaporation* ~150 nm *copper at 70°. In this way copper covers contact pads allowing for good electrical contact with aluminum bonding wires(seen in (c)) but does not appear at narrow groves defined in PMMA where central aluminum wire is formed. In picture (e) aluminum appears white while copper has copper-like color. To ensure good quality of contacts undergoing many cool-down-warm-up-sputtering sessions bonding wires are covered with silver epoxy (seen in (c)). Four shunting wires like the one seen at the right of (d) are scratched away after bonding wires are fixed and quality of contacts is confirmed.* **(f)** *SPM picture of* ~ 100 *nm* x 150 *nm x* 5 μm *wire.*

S.1.3. Filtering

Superconducting nanowires are very sensitive to external noise. Experimentally measured T_c is lowered significantly and the shape of the superconducting transition is strongly disturbed if no electrical filtering is used. In case of the very narrow wires they may not exhibit superconducting transition at all (heating can be so strong that the wires temperature is much higher then the base temperature of cryostat), or can be burnt after the sample stage is mounted in the dip-stick. In *Fig.S.3* the schematic of the low-pass filters used in my experiment is presented. The corresponding *SPICE* simulation (*5Spice freeware*) of the filter *V(f)* dependence is shown in *Fig.S.4*. The filter provides with the cut-off for higher frequencies enabling measurements in *DC* and *AC Lock-In* low frequency modes (in experiments I used *19* Hz).

When designing a filter it is important to satisfy at least two criteria:

1. Electromagnetic noise reaching the sample should be as small as possible to avoid heating effects and the change of investigated properties due to parasitic currents flowing in the wire.

2. The signal measured by the voltage preamplifier (depicted in schematic with *TestPointVoltmeter*) should have the same magnitude as the voltage drop on wire (depicted in schematic with *TestPointWire*).
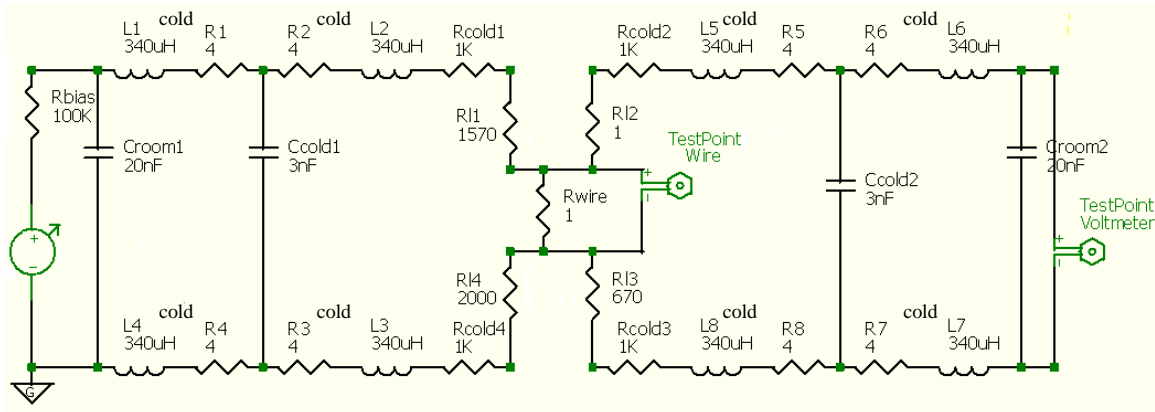
Fig.S.3. *Electrical circuit used for the 4-probe measurements of the aluminum nanowires. The wire of interest is depicted in schematic as* Rwire. *Rl1,Rl2,Rl3,Rl4 indicate resistances of the e-beam patterned electrodes and contact pads together with the bonding wires (these resistances can change during experiment).* Rbias *is used to convert the voltage source into the current source. The rest of components allow for the low-pass filtering.* 20 nF *capacitors work at room temperature while the other elements operate at the liquid helium temperatures. Additionally, at the room temperature part of the dip-stick there are ferrite coils (*L = 3 μH*) intended to filter out frequencies in the* GHz *range (in simulation they were absorbed into* L1, L2, L3, L4, L5, L6, L7, L8*).*
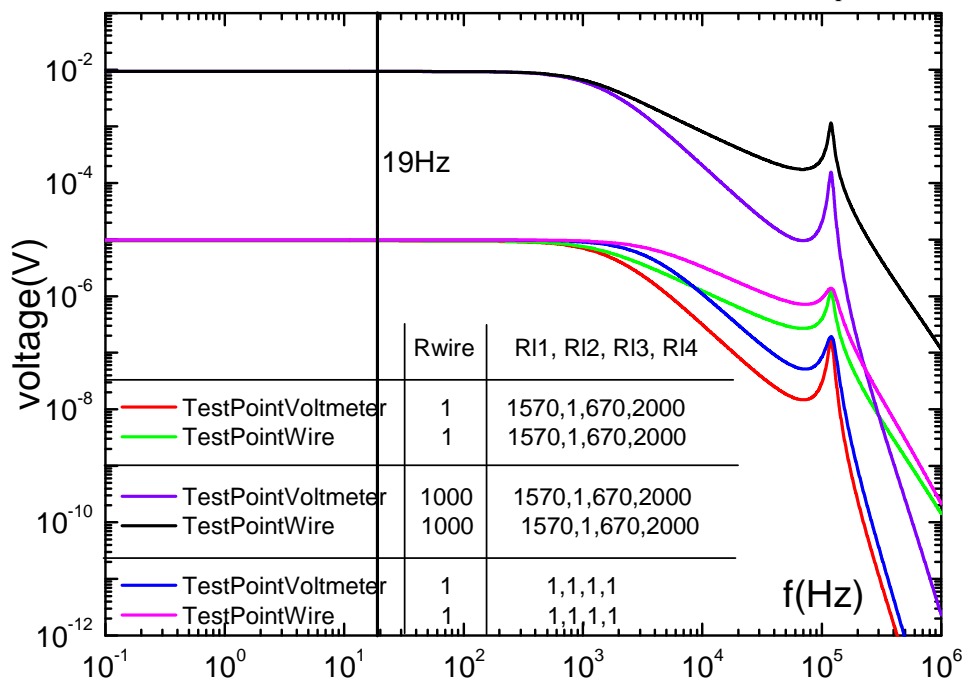
Fig.S.4. *Filter* V(f) *characteristic for the 3 various loads. For the filter description see Fig.S.3. The voltages (*TestPointWire *and* TestPointVoltmeter*) are responses to* 1 V *applied by the voltage source. At* 19 Hz *the signal measured by the voltmeter corresponds to the voltage drop on the wire.*

These two criteria must be satisfied for various loads (samples) bearing in mind that e-beam patterned electrodes connecting the wire with the measuring setup are made of the same superconducting material (Al) and hence can change their resistances in the range $\sim 0 - 2000$ kΩ. These micro-electrodes are depicted in *Fig.S.3* as *Rl1, Rl2, Rl3, Rl4*. While the first criterion seems to be obvious, the second can be easily forgotten resulting in "tricky" experimental artifacts. Example of a widely used low-pass "π" filter satisfying the first criterion, but not the second one is given in *Fig.S.5*. Corresponding *V(f)* simulation is displayed in *Fig.S.6*.
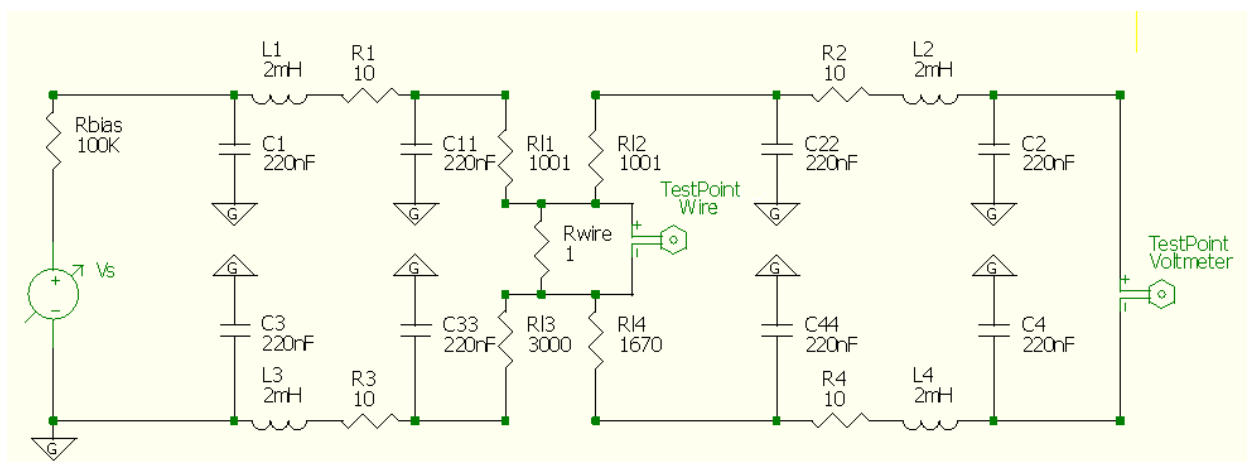
Fig.S.5. *Example of the low-pass filter design exhibiting undesired characteristic. Due to the capacitive coupling (through the ground) of the voltage and current lines the voltage measured by the voltmeter (*TestPointVoltmeter*) is different from drop of voltage on the wire (*TestPointWire*).*
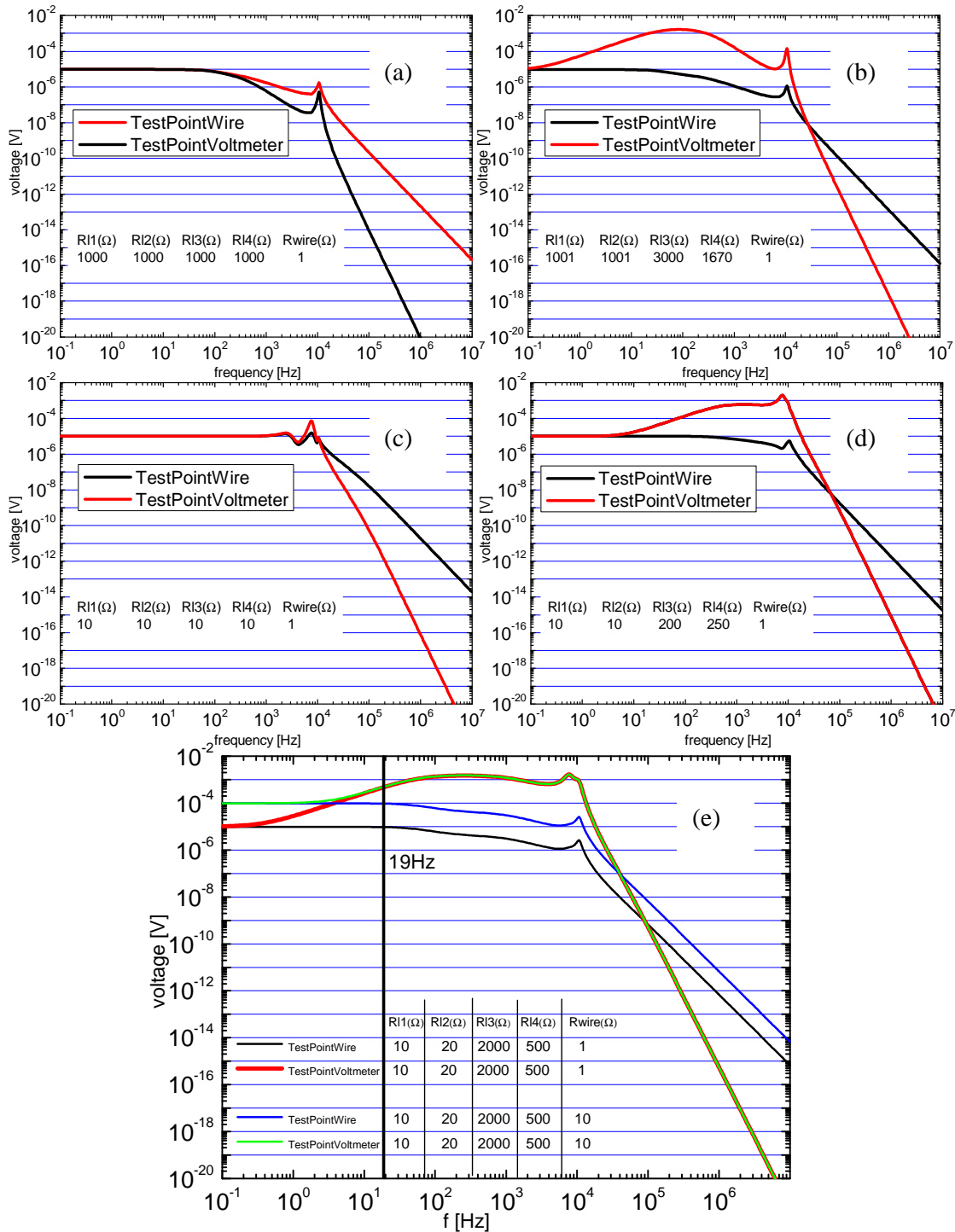
Fig.S.6. *Filter* V(f) *characteristics for different loads. For the filter description see Fig.S.5. The voltages (*TestPointWire *and* TestPointVoltmeter*) are responses to* 1 V *applied by the voltage source. While in (**a**) and (**c**) at* 19 Hz *the voltmeter measures voltage drop on the wire correctly, in (**b**) and (**d**) it is not the case: the measured voltage is 1-2 orders of magnitude larger than what should be measured. In (**e**) the wire resistance drops by one order of magnitude while voltmeter shows the same value. Such a measurement would easily broaden the observed superconducting transition of the wire and could be interpreted as a "new physics".*

Looking at *Fig.S.6* one can easily realize how an improper design of a filter can create experimental artifacts. Although it seems that the filter exhibits a nice cut-off characteristic (*Fig.S.6(a)(c)*) it should not be used. The main reason for the weird behavior of the filter is the capacitive coupling (through the ground) of the current biasing line with the voltage measuring line. In filters used in my experiment this capacitive coupling was eliminated (*see Fig.S.3*). The results of simulation at *19* Hz were confirmed in experiments in which I was varying *Rwire, Rl1, Rl2, Rl3, Rl4* replacing the actual sample with *5* potentiometers. One can easily notice that even at rather low frequencies (*~10* Hz) the "unfavorable" combination of the loads can provide an erroneous reading. Various commercial and self-made RC filters are widely used in electrical measurements. One should be extremely cautious incorporating them into the measuring setup.

S.1.4. Thermometry

The absolute measurement of temperature is the subject of metrology. For our purpose the relative accuracy of the temperature determination, being measured against some reference point, is important. In *Fig.S.7* I displayed *R(T)* dependence for the thermometer *K-22* used for temperature measurements (calibration curve as delivered by the manufacturer).

$$y = 0.93448*exp(-x/65.67797) + 28.66123*exp(-x/6.9568) + 0.52622*exp(-x/336.59416) +$$
$$+0.93448*exp(-x/65.67837) + 5.9276*exp(-x/20.28618) + 0.52622*exp(-x/336.59615) + 0.7475$$
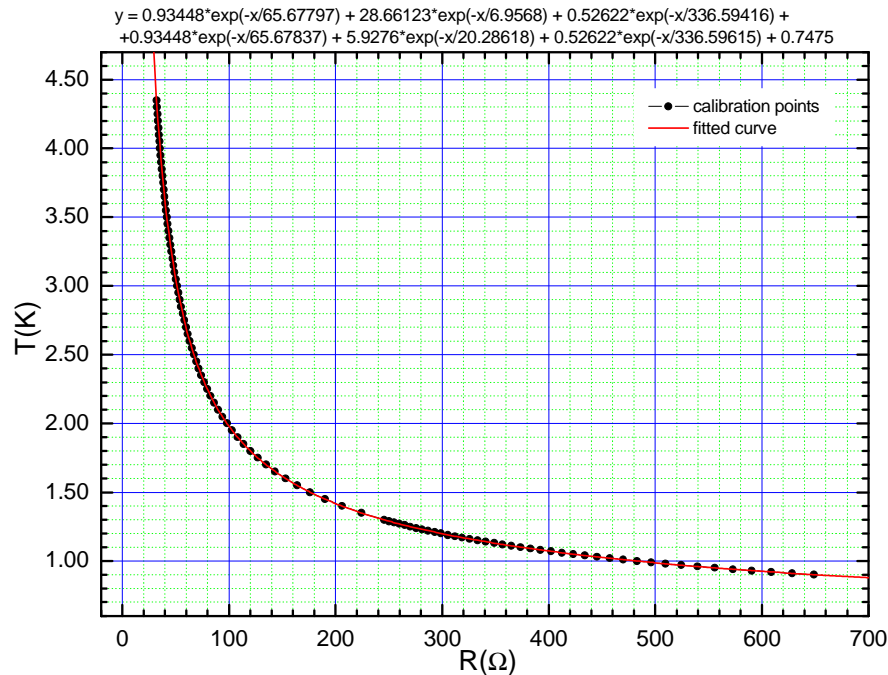
Fig.S.7. *R(T) dependence for* thermometer K-22 *used in experiments. Temperature controller* LakeShore 340 *measures the sensor resistance in the 4 probe configuration, followed by interpolation between the calibration points delivered by the thermometer manufacturer. Alternatively one could measure the resistance and use the analytic equation for curve fitted to calibration points (for example fitted sum of six exponents) to calculate the temperature. The thermometer was installed close to sample holder in the dip-stick as shown in Fig.S.2(b).*

To check the accuracy of the thermometry I installed in the sample holder (in the place where sample is usually glued) another thermometer: *Cernox CX-1050-AA* (with known calibration). It this way I could measure one thermometer against another to see consistency of the calibration data. This procedure also allows determination of the temperature stability inside our cryostat. I could measure fluctuations of the temperature readings displayed by the two thermometers (T_1 and T_2) with respect to each another. The magnitude of the temperature fluctuation is given by the width of $T_1(T_2)$ curve or alternatively T_1-T_2 *vs.* T_1 curve (*Fig.S.8*). It gives the highest attainable resolution of temperature measurements in the experimental setup.

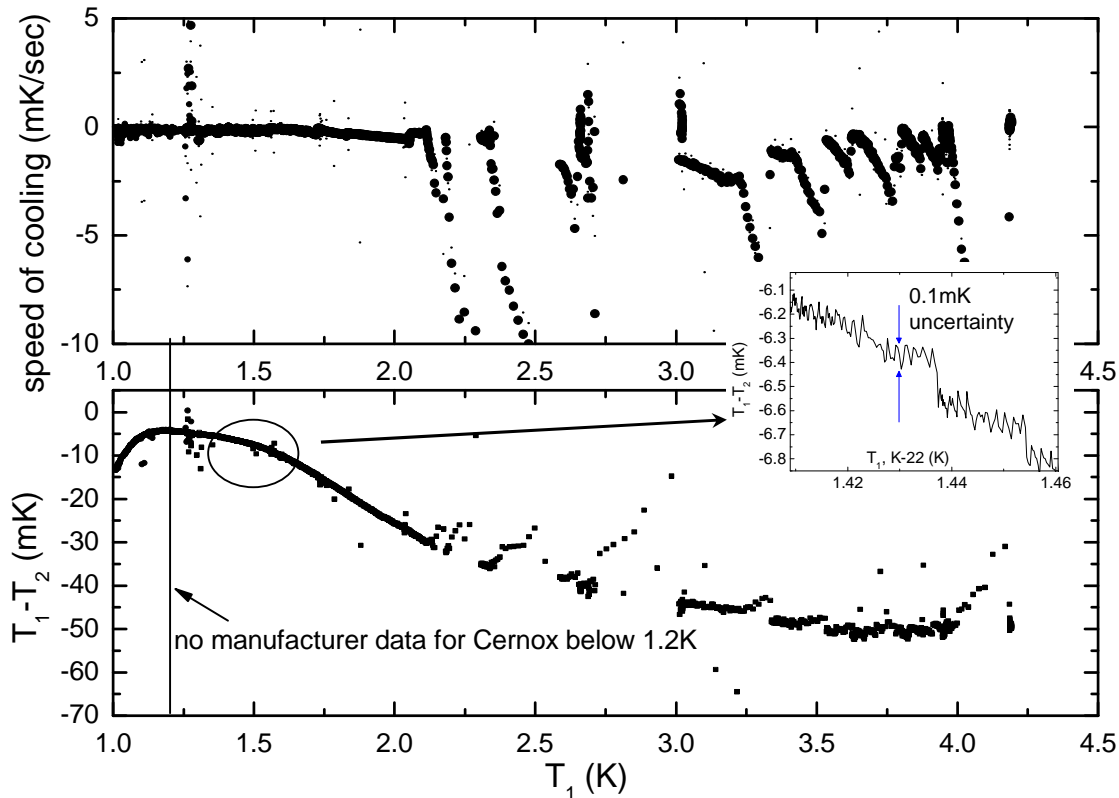**Fig.S.8.** *Cross-measurements of the two thermometers in a slow cool-down.* T_1 *(K-22) and* T_2 *(Cernox) are the temperatures determined from the measured resistance according to the calibration curves delivered by the manufacturers of two sensors.* T_2 *is stable with respect to* T_1 *with accuracy ~ 0.1 mK (inset) corresponding to the ultimate resolution of the temperature controller.*

S.1.5. Measuring derivatives of a system function

Upon application of a certain excitation to a system under study (a sample) it produces a unique response which can be treated as a characteristic of the system. The function relating excitation and response can be called the system function. When electrical properties of samples are studied one may be interested in a current response to an applied voltage *I (V)*, or a voltage response to an applied current *V(I)*. When studying a system usually as an excitation one uses the quantity which can be controlled or kept stable easier (e.g. the one which is single-valued). For example for an *S-shaped V(I)* dependence, voltage is a multi-valued function of current, but only one value of voltage can be produced in response to the applied, controlled current. However if the voltage is controlled and the current is measured, then problem with multi-valuedness disappears and the desired shape of a system function can be recorded. To get access to finite features of a system function the technique of measuring of its derivative is used (one can also measure higher order derivatives). Then *dV/dI* curve can be interpreted as the dynamical resistance and *dI/dV* as the dynamical conductance.

The idea of measuring derivative *dV/dI* is presented in *Fig.S.9.* A constant DC current I_{DC} with small sinusoidal modulation I_m is applied to a sample. If the system function can be considered linear in the probed range (defined by an amplitude of the modulation) then produced voltage is the sinusoid shifted by the constant $V_{DC}=V_{DC}(I_{DC})$ with amplitude equal to the product of the amplitude of modulating current and the slope of the system function at $I = I_{DC}$. If such a sinusoid is fed to the Lock-In amplifier the product of the slope magnitude and the *RMS* value of the modulation $abs(dV/dI) \cdot I_m^{RMS}$ is measured.

It is a good practice to check if the measured slope corresponds to the derivative of the *V(I)* curve taken in the linear (Ohmic) regime *(V ~ I)*. For superconductor it can be done significantly above T_c. Usually it is recommended to measure *V(I)* and *dV/dI* separately to eliminate the risk of "cross-talking" of the measuring devices. The less instruments connected to a sample at a time, the bigger the chance to get reliable results. Setting/calculating the modulation current (being based on the design of the set-up) and knowing the slope of the *V(I)* curve from *V(I)* measurement one should be able to predict what Lock-In should measure.

The modulating current I_m should be small enough to excite the system function *V(I)* only in the range where the response can be considered linear. In practice it is good to measure *dV/dI* at several different modulating currents, say *1* nA and *0.33* nA, to see if any difference exists. *0.33* nA can theoretically probe V(I) curve more accurately but overall signal may be more noisy. For *1* nA the situation is opposite. For too large modulating currents output signal is distorted: it does not have a one well defined frequency any more. Since Lock-In measures only one Fourier component (the one which has the same frequency as the reference signal), such a measurement has no clear physical interpretation.
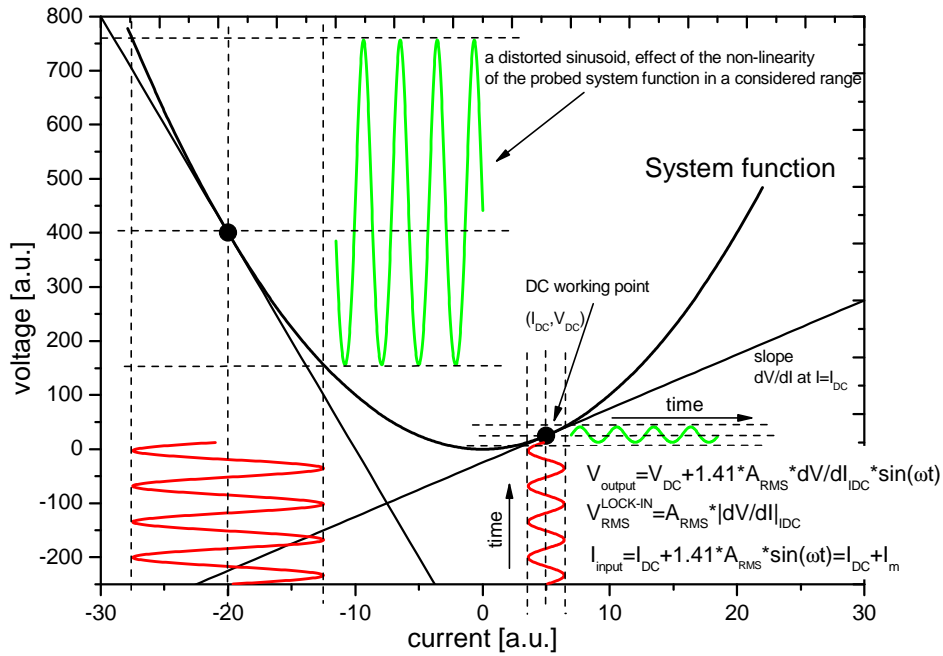
Fig.S.9. *Measuring of a system function derivative. Excitation should be modulated at sufficiently small amplitude to probe the system function within a range where the function remains linear (small sinusoids). If it is not the case the output signal is a distorted sinusoid difficult in interpretation (big sinusoids).*

Below I will describe the design of a simple mixer of *DC* and *AC* currents used in my experiments to measure *dV/dI*. The schematic of the mixer is presented in *Fig.S.10.* It consists of the *DC current source* of infinite internal resistance and *sinusoidal generator* of zero internal resistance. The final current reaching sample is calculated from superposition principle: for *DC* current analysis I short-circuit sinusoidal generator, for A*C* current analysis I open branch with *DC* current source.
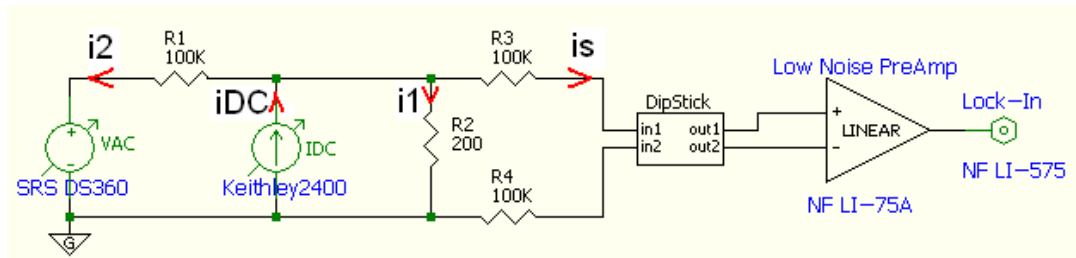
Fig.S.10. *Schematic of current mixer used in my experiments for measuring derivatives.* i_s *is the current reaching the sample. Blue labels display names of actual devices. For design of the dip-stick see Fig.S.3.*

DC current through sample:

$$i_s^{DC} + i_1 + i_2 = i_{DC}$$

$$i_s^{DC} = \frac{i_{DC}}{1003} \text{ for design from Fig.S.10.}$$

AC current through sample:

$$\frac{V_{AC}}{R_1} = i_1 + i_s^{AC} \text{ for } R_1 \gg R_2$$

$$i_s^{AC} = 10^{-8} \Omega^{-1} \cdot V_{AC} \text{ for design from Fig.S.10.}$$

S.2. Sputtering gun
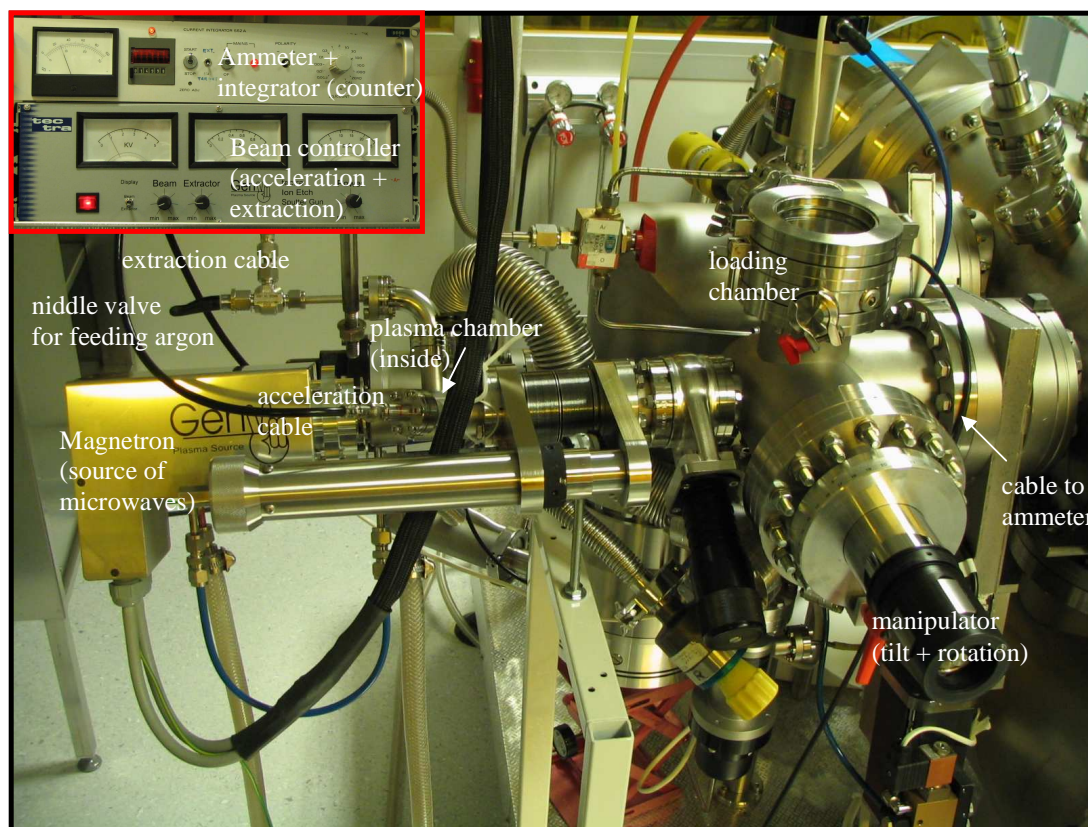
Fig.S.11. *Ion gun attached to the loading chamber of the UHV evaporator. Microwaves are fed into the small sapphire plasma chamber (~ 1 cm^3) where also Ar (or O$_2$) is delivered. Due to the microwave absorption and the successive collisions enhanced by small magnetic field plasma is created. It is kept at positive potential (e.g.1 kV). Ar$^+$ ions are extracted from chamber with negative potential (e.g. -1.3 kV) and accelerated against the grounded sample. Sample stage rotates with regulated incident Ar$^+$ ions angle allowing for homogenous sputtering. The ion current reaching the sample stage is measured with the ammeter and is integrated in time to know the total fluence (number of Ar$^+$ ions that hit the target). The argon flow is adjusted to keep the working pressure at 1 - 3 x 10^{-4} mBarr (measured in the loading chamber). The device can be used either for size reduction or for cleaning samples before they are processed in the UHV chamber for evaporation (e.g. to remove the undesired oxide layer or surface contamination).*
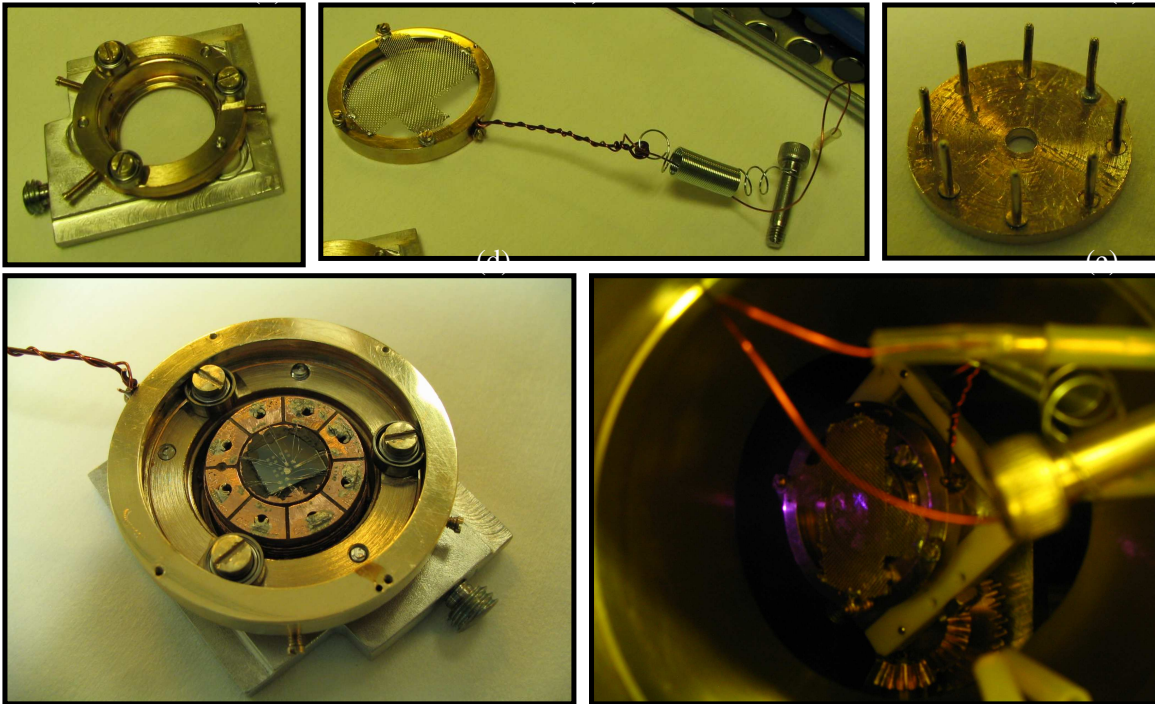
Fig.S.12. *Vacuum holder and sample holder used for sputtering.* **(a)** *Brass holder with 3 bearings and 3 fixing screws sitting at aluminum plate to be installed in rails in the loading chamber. Holder is electrically isolated from the plate via sapphire tubes.* **(b)** *Brass ring with the wire for current measurements and fixing screw preventing the ring from rotation together with the holder (the ring rolls over the bearings). One can distinguish platinum mesh mounted at the top of ring. The mesh serves as the charge neutralizer for projectiles and is of importance for insulating substrates (like mica) to prevent charging effects. For weakly conducting silicon substrates it may be removed.* **(c)** *Shunting pins to be installed at the bottom of the sample holder (They replace 8 screws shunting ring seen in Fig.S.2(c) during the sputtering).* **(d)** *Sample holder fixed in holder.* **(e)** *Picture of the sputtered sample (through window in loading chamber). Vacuum holder is tilted at* 45^0 *with respect to the incident ions (they come from left) what also allows to see the reflected image of the ion gun aperture connecting the loading chamber with plasma chamber. Violet color is typical of argon plasma.*

VI. Experiments on Ultra-Narrow Superconducting Aluminum Nanowires (E)

In this chapter I will present my main experimental findings related to superconductivity in aluminum nanowires. The basic idea of my research was to study the shape of the superconducting $R(T)$ transition as the function of the wire cross-section expecting to observe a manifestation of quantum phase slips (QPS) in the thinnest samples. I investigated *the evolution of physical properties of the same nanowire progressively reducing its cross-section by low energy ion sputtering* starting from diameters $\sigma^{1/2} \sim 100$ nm down to *sub - 10* nm scales. The technological details of sample fabrication have been presented in *Chapter 2*. Here I would like to repeat that the method enables the non-destructive reduction of the wire cross-section without introducing any significant structural defects. The low energy Ar^+ ions with acceleration energy *0.2-1* keV can alter only the very surface of aluminum $\sim$*2-3* nm, which is comparable with the thickness of the naturally grown aluminum oxide.

Aluminum has been selected as the appropriate material by several considerations. First, aluminum is a technologically easy-to-fabricate material. Second, the critical temperature of aluminum ($\sim$*1.4* K for thin films and wires) is in the experimentally convenient region: it allows conducting experiments in the directly pumped ^{4}He bath. The temperature of the superfluid helium can be stabilized with sub-mK accuracy (*section S.1.4*) and temperature gradients are negligible. From the practical point of view experiments in helium bath are much faster than in a dilution refrigerator. Third, being exposed to ambient atmosphere, aluminum is immediately covered with oxide providing a naturally-grown protecting layer. Other possible candidates (e.g. *Zn, In, Sn*) are more difficult to handle degrading too fast. Finally, since resistance due to QPS R_{QPS} satisfies relation $\log(R_{QPS}) \propto -1/K \cdot \sqrt{\xi_{BCS}}$ ($K = \rho_n \cdot l_{mean}$) (section *T.5.4*), aluminum with its parameters: $K = 6 \cdot 10^{-16}$ Ωm^2 and $\xi_{BCS} = 1.6$ µm, can be considered quite good candidate for studying QPS. Estimations predict noticeable manifestation of the QPS mechanism in aluminum wires of diameter $\sigma^{1/2} \sim 10$ nm (*section T.5*).

In the following *section E.1*, I will address the subject of inhomogeneity of realistic samples and its influence on the shape of experimentally observed superconducting transition $R(T)$. Then in *E.2* I will discuss the representative superconducting transitions of relatively thick aluminum wires. The main conclusion of the first two sections is that the inevitable variations of the wire cross-section and the corresponding changes of the size-dependent critical temperature $T_c(\sigma)$ broaden the transition making comparison with the *LAMH* model of thermally activated phase slips (*TAPS*) impossible. However, the particular property of aluminum - *the increase of T_c with the decrease of the wire cross-section* - allows *to exclude any inhomogeneity-driven extension of the R(T) dependence*

below the bulk critical temperature T_c^{bulk} ~ 1.2 K. Later, in *E.3* experiments on ultra-narrow wires will be analyzed attributing the broadening of their superconducting transition *R(T)* to the *QPS* mechanism. Finally, two reproducible, but not well understood phenomena observed exclusively in the thinnest samples will be discussed: negative magnetoresistance and "peculiar" *V(I)* characteristics.

E.1. Experimental limit on observation of phase slips – influence of sample inhomogeneity on the shape of R(T) transition

Usually the lack of abrupt superconducting transition in narrow 1D channel is associated with activation of phase slips (*see Chapter II (T)*). In the following it is shown that such an interpretation can be doubtful when the inhomogeneity of real wires is taken into account. Even if the material is clean, containing a negligible concentration of impurities capable of changing the critical temperature, the inevitable structural imperfection (e.g. variation of cross-section or size of crystalline grains) might broaden the *R(T)* dependence.

The quantitative analysis presented below is based on the fact that for many low-dimensional superconductors the critical temperature T_c differs from the one in bulk materials. Generally, T_c of films and nanowires depends on their cross-section/thickness, and morphology [3,5,11,64,65,66,67,68]. It is sensitive to the size of crystalline grains, packing of the grains, and even to the fine structure of the grains e.g. their roughness. The mentioned parameters may be affected by the supporting substrate, temperature of the film deposition, and for films covered with natural layer of oxide - the pressure of oxidization. Experimental data shows that in *Al* polycrystalline films and wires T_c grows with decreasing the size of the structure ([1,3,5], *Fig.E.1*, *Fig.E.2*) while in case of *Pb* and *Nb* it becomes smaller [11,65]. There are theoretical works which consider both enhancement [5,66] and suppression [67] of the critical temperature T_c in thin wires/films. The one generally accepted origin of this behavior remains unclear at the moment and requires further studies. An interesting explanation for variation of T_c with sample morphology was given in work [68,69,70]. The authors observed that enhancement of T_c in polycrystalline metal films is related to the average
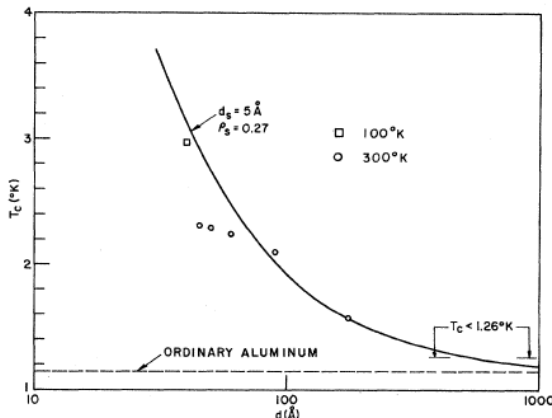

Fig.E.1. *After [68]. Variation of T_c in polycrystalline aluminum films is attributed to the different crystallite size d of the aluminum films, not the film thickness.*

crystallite size ([68], *Fig.E.1*). They attributed this effect to the increased electron-phonon interaction near the geometric boundaries of the superconductor (crystalline boundaries), suggested earlier by Ginzburg [66]. At the same time no T_c variations were observed when film thickness was varied (crystallite size was not dependent on film thickness).

The empirical dependence of T_c on cross-section for aluminum nanowires studied in this work is presented in *Fig.E.2*. One can clearly see that: (i) T_c increases with the decrease of the cross-section; (ii) the bulk value is reached only in sufficiently thick samples with $\sigma^{1/2} > 100$ nm. If to apply mentioned interpretation (*Fig.E.1*) to my experimental findings (*Fig.E.2*) one could say that narrower wires are built up from smaller crystallites, hence their T_c is higher. In my case of very narrow samples the crystallite size was dependent on the cross-section and both were reduced together in course of sputtering. However, in what follows, I will treat the variation of T_c with the wire cross-section as the empirical fact. It may happen that aluminum nanowires prepared in a different way (e.g. amorphous wires) will not follow the dependence in *Fig.E.2,* but it is not important for the following discussion.
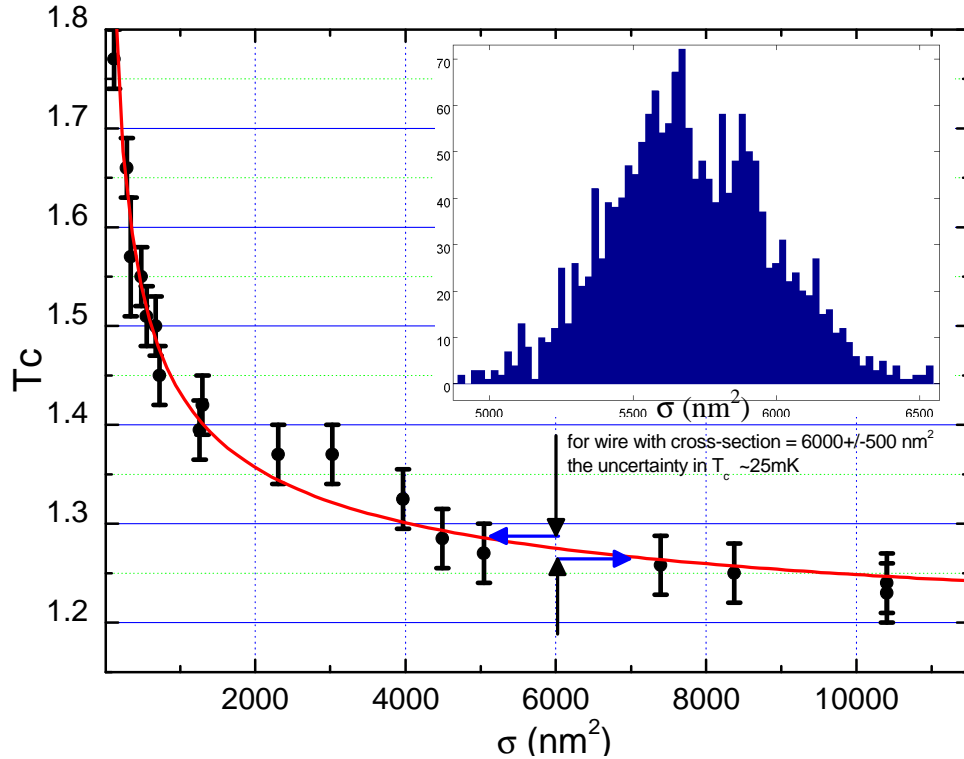
Fig.E.2. *The empirical dependence of the critical temperature T_c on the average cross-section σ for polycrystalline aluminum nanowires studied in this work [3]. T_c is defined as the temperature at which the wire resistance drops by the factor of two: $R(T_c) = R_N/2$. The line is guide for eye. Inset shows the distribution of cross-sections (histogram) for a typical lift-off e-beam fabricated nanowire with length $L = 10 \mu m$. The data were obtained from SPM topography (see Fig.E.5). The variation of the cross-section along the wire for this particular sample is displayed in Fig.E.5. The arrows indicate the margin within which the local critical temperature of the various parts of the particular sample from the inset varies.*

A wire can be characterized by a distribution of its cross-section (*Fig.E.2, inset*). Such a distribution can be obtained from *SPM* topography data (usually it resembles Gaussian distribution) and can be treated as a quantitative measure of homogeneity of the sample. Since each real nanowire is inhomogenous to a certain extent, one immediately can conclude that different sections of the wire undergo transition to superconducting state at different local T_c. The wire can be represented as a set of *"resistors"* connected in series, each with slightly different cross-section and hence different T_c. In practice, due to proximity effect, the local T_c can not change very rapidly along the wire, but in the limit $L \gg \xi$ (L - length of the wire) the distribution of cross-section implicates a smooth distribution of the local T_c (*Fig.E.3*).
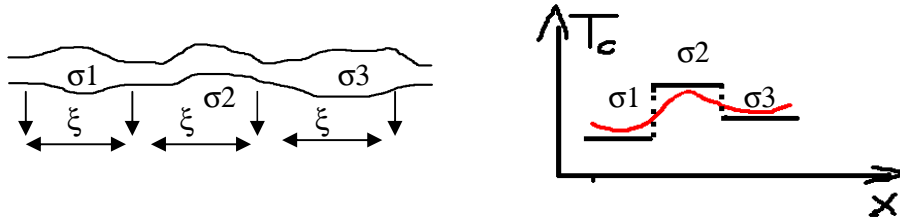
Fig.E.3. *(Left) Variation of the wire cross-section* σ *along an imaginary sample. (Right) The corresponding smooth variation of the critical temperature* T_c *due to proximity effect between the neighboring sections.*

Normal state resistance of the small section of the wire of length *dl* reads:

$$dR_N = \frac{\rho(\sigma)dl}{\sigma} \tag{E.1}$$

with cross-section σ and the cross-section dependent resistivity ρ. $\rho(\sigma)$ dependence is important in ultra-narrow samples, where the mean free path l_{mean} is limited by the physical boundaries. Being given a normalized distribution of the wire cross-section $p(\sigma)$ (e.g. *inset, Fig.E.2,* $p(\sigma)d\sigma$ is a fraction of wire with cross-section falling into range $(\sigma, \sigma + d\sigma)$), the elemental length of the wire with cross-section falling into range $(\sigma, \sigma + d\sigma)$ is $dl = p(\sigma)d\sigma \cdot L$ (L - length of the wire) and hence dR_N as the function of σ can be expressed as:

$$dR_N = \frac{\rho(\sigma) \cdot p(\sigma) \cdot L}{\sigma} d\sigma \tag{E.2}$$

Further we assume that critical temperature of the considered small section of the wire is given by the dependence $T_c(\sigma)$ based, for example, on the empirical data presented in *Fig.E.2*.

We would like also to account for possible temperature instabilities. To treat this quantitatively we assume that temperature T of the piece of the wire with cross-section σ is given by some probability density distribution $g(\sigma,T,T_m)$ with the mean value corresponding to temperature T_m measured in experiment with some thermometer (in case of overheating the mean temperature can be different from T_m). Function $g(\sigma,T,T_m)$

characterizes how well the measured value T_m reflects the actual temperature of the wire section T. It allows considering temperature fluctuations related to temperature stability of the measuring setup or resolution of the thermometer limited by different sources of noise. Existence of *Kapitza thermal resistance* between the sample, substrate and thermometer can lead to overheating of the sample (different in different places) and, hence, give rise to distribution of the local temperatures. We assume that whenever temperature inside the particular section of the wire falls below the local critical temperature this small section becomes superconducting. Hence probability for being in the normal state reads:

$$P(T > T_c(\sigma)) = \int_{T_c(\sigma)}^{\infty} g(\sigma, T, T_m) dT \qquad (E.3)$$

It follows that effective resistance produced by the fraction of the wire with cross-section σ is:

$$dR_{eff}(T_m) = dR_N \cdot P(T > T_c(\sigma)) \qquad (E.4)$$

Adding up all section of the wire we get the temperature-dependent effective resistance of the whole sample:

$$R_{eff}(T_m) = \int_0^{\infty} \left(\frac{\rho(\sigma) \cdot p(\sigma) \cdot L}{\sigma} \cdot \int_{T_c(\sigma)}^{\infty} g(\sigma, T, T_m) dT \right) d\sigma \qquad (E.5)$$

Derived formula describes the shape of superconducting transition for an inhomogenous wire provided both distribution of its cross-section and $T_c(\sigma)$ dependence are known (also knowledge of $g(\sigma, T, T_m)$ is required).

In the following we consider case when temperature during experiment is a well defined quantity: $g(\sigma, T, T_m) = \delta(T - T_m)$ (Dirac delta function). Then *eq. E.5* for the effective resistance reduces to simpler equation:

$$R_{eff}(T_m) = \int_0^{\infty} \frac{\rho(\sigma) \cdot p(\sigma) \cdot L}{\sigma} \cdot H(T_m - T_c(\sigma)) \, d\sigma = \int_{\sigma} \frac{\rho(\sigma) \cdot p(\sigma) \cdot L}{\sigma} d\sigma \qquad (E.6)$$

with $H(T_m - T_c(\sigma))$ being the *Heaviside step function*. Right hand side integral is convenient for numerical calculations and should be performed over σ for which $T_c(\sigma) < T_m$.

The resulting transition calculated using *eq. E.6* for the $T_c(\sigma)$ dependence from *Fig.E.2* and the distribution of the wire cross-section from inset of *Fig.E.2* is presented in *Fig.E.4*. Additionally $\rho(\sigma) = const$ has been assumed, which is good approximation if cross-sections do not deviate significantly from the mean value. Analyzing *Fig.E.4* one can conclude that $R(T)$ broadening resulting from inhomogeneity is much more pronounced than the one predicted by the *LAMH model of TAPS* (*section T.4, eq. T.9*). Hence, for this particular sample the effects related to thermally activated phase slips can NOT be resolved. Generally, the *LAMH* fitting can be performed only when $T_c(\sigma)$ dependence and σ distribution are known and proven to play minor role in determining the shape of superconducting transition compared to *TAPS*. The sample from the inset in *Fig.E.2* was

selected as the example representing a typical lift-off fabricated nanowire: length $L = 10$ μm and diameter $\sigma^{1/2} = 75 \pm 4$ nm. Even such a "moderate" geometrical inhomogeneity can make verification of the *LAMH* model very problematic.
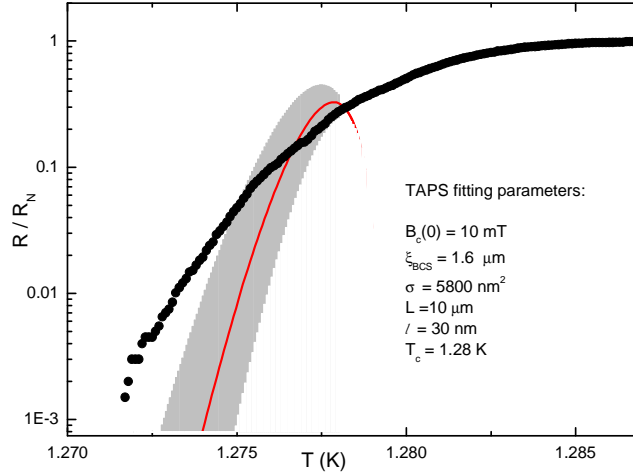
Fig.E.4. *Simulated resistive transition R(T) using equation E.6 (black curve) for the wire from the inset in Fig.E.2. The R(T) broadening results only from the geometrical inhomogeneity of the sample and the corresponding $T_c(\sigma)$ dependence. Red curve is the calculation based on TAPS (LAMH) model with reasonable parameters indicated in the figure. Shadow region corresponds to variation of the TAPS fitting parameters l and B_c within +/- 10 %. Effects arising from inhomogeneity are much more pronounced than those due to thermal phase slips [3].*

Another example of inhomogeneity of real samples is their finite size and the existence of measuring probes. It could seem that electrodes in 4-probe resistance measurement configuration contribute negligibly to measured signal. This would be true if one was able to use a non-invasive (= infinitely narrow leads) so that they would not influence the wire cross-section in the nodes regions. However, when studying ultrathin wires, electrodes are usually much bigger than the measured wire. In such case distribution of the wire cross-section is affected by the thicker sections in the very locus of electrodes. For particular case of aluminum, the thicker electrodes enter superconducting state at lower temperatures than the "body" of the wire. It follows that after almost entire wire is in superconducting state still its nodes can produce residual signal which can be misinterpreted as a "new" physics e.g. quantum phase slip manifestation (*Fig.E.5*). Such a signal in logarithmic scale can seem quite large although it is *2* or *3* orders of magnitude smaller than the normal state resistance. However, for electrical signals measured below bulk T_c this kind of mistake can be ruled out with big dose of confidence. For aluminum below the bulk $T_c \sim 1.2$ K the whole sample (including the electrodes) should be in the superconducting state and cannot produce a measurable signal, unless a really new effect comes into play.
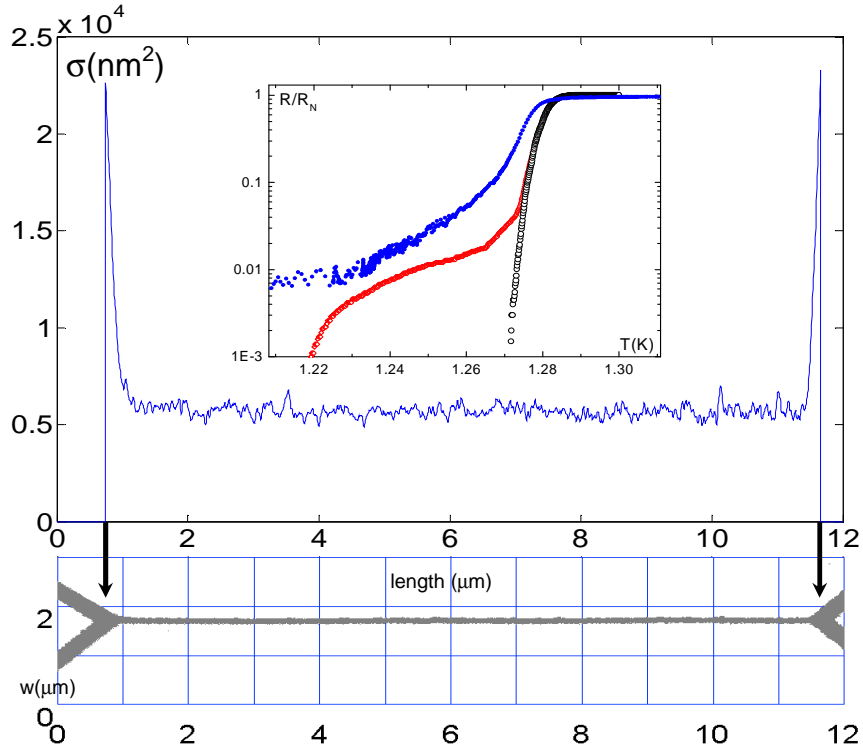
Fig.E.5. *Bottom: SPM image of a typical aluminum wire with 4 probes. Top: cross-section along the wire measured with SPM. Inset: Red curve corresponds to calculation based on eq. E.6 and $T_c(\sigma)$ dependence from Fig.E.2 performed within the limits indicated by the two arrows. Black circles are the result of similar calculation without taking into account the contact regions (peaks in cross-section) – it is the same curve as in Fig.E.4. Blue dots correspond to experimentally measured transition for the wire.*

In the limit $I \to 0$, the shape of the R(T) transition does not depend on the bias current. However, experiments with higher currents can reveal the contributions coming from narrow "body" of the sample and the thicker electrodes (*Fig.E.6*). For higher currents the central part of wire exhibits overheating: it displays non-linear (*V vs. I*) behavior at constant temperature. However contacts, being much bigger, do not suffer from overheating. They exhibit ohmic behavior even for the relatively large currents. It follows that resistance of electrodes is constant for different currents (*Fig.E.6*). It is in contrast to behavior expected for quantum phase slips, when *V(I)* curve is essentially non-linear (*cf. Fig.E.8*).

To conclude this section I would like to emphasize that sample homogeneity is the key issue for interpretation of the *R(T)* data in narrow superconducting channels. In materials where the size dependence of the critical temperature is observed, this effect can override the contributions coming from fluctuations. With the decrease of the wire cross-section σ the relative variation of its cross-section $d\sigma/\sigma$ usually increases ($d\sigma$ being standard deviation). It means that the inhomogeneity of the sample becomes larger as one

reduces the diameter. At the same moment, typically the $T_c(\sigma)$ dependence is non-linear: variations of T_c with cross-section σ are more pronounced for thinner structures (*e.g. Fig.E.2*). It possibly could explain why some authors observed broadening of the superconducting transition with decreasing the wire diameter which deviated from the *LAMH* prediction significantly [11,65]. While phase slip concept in *1D* wires seems to be an attractive explanation for the observed broadening of superconducting transition, one should not forget that in many cases experimental data can be straightforwardly explained by the sample inhomogeneity.
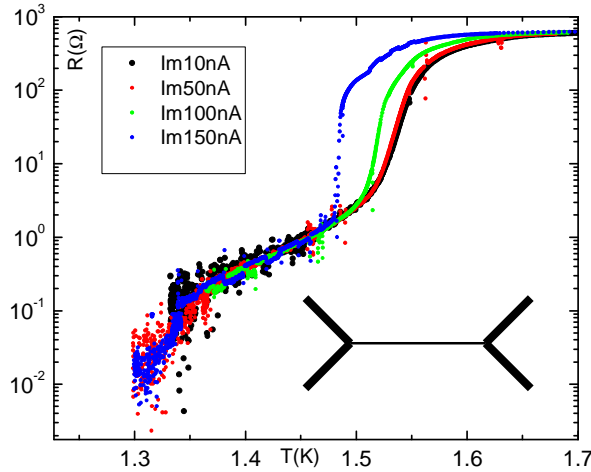

Fig.E.6. *R(T) transition for aluminum nanowire taken at various bias currents. Inset: schematics of the sample with contacts. The dominating contribution to the resistance comes from the long and narrow "body" of the sample, which can be overheated much easier than the thicker nodes.*

E.2. Thermal phase slip activation mechanism in aluminum nanowires

Thermal activation of phase slips (*TAPS*) should provide the dominating contribution to measured resistance very close to T_c , while quantum tunneling (*QPS*) should come into play at lower temperatures $T < T_c$. The crossover temperature T^* between two mechanisms is the one at which the *QPS* rate Γ_{QPS} is the same as the *TAPS* rate Γ_{TAPS}. In thicker samples the crossover temperature T^* corresponds to immeasurably small resistance meaning that no *QPS* mechanism can be observed. In thinner samples T^* is sufficiently close to T_c so that the phase slip process is still measurable allowing for *QPS* detection.

As our method enables progressive reduction of the nanowire cross-section, one might expect observation of the sharp crossover between the *TAPS* and quantum mechanisms as the function of wire diameter. In thick samples with $\sigma^{1/2} > 10 - 20$ nm the TAPS mechanism should dominate in the whole experimentally measurable range $T^* << T < T_c$, while in thinner ones the *QPS* contribution is expected to develop at $T < T^*$. In *Fig.E.7* the R(T) transitions for several aluminum wires with effective cross-section 20 nm $< \sigma^{1/2} < 40$ nm are presented. One can clearly see that the experimental width of the superconducting transitions always exceeds the theoretical predictions of LAMH model (*eq.T.13&T.12*) for homogeneous wire. Also the shapes of the measured transitions are different from those resulting from application of the model. Formally, one may postulate an existence of a short constriction in the wire responsible for almost entire measured resistance. Then the *LAMH* prediction can have the slope corresponding to the measured transition in the narrow range of temperatures what would possibly allow one to claim observation of the *TAPS* mechanism (*Fig.E.7*). However, such an interpretation is rather improbable. First, the wires were inspected with *SPM* prior to and after measurement and only those without obvious constrictions were processed. Second, T_c for such constriction had to be significantly higher than the onset of the *R(T)* transition. Third, agreement between the data and the *TAPS* model could be achieved only in a narrow range of resistances covering less then *1* order of magnitude resistance variation. Fourth, *V(I, T=const)* dependencies exhibit linear behavior (note that for different bias currents the transitions in *Fig.E.7* look the same) which is not what we expect from TAPS (*cf.eq. T.8* predicting *sinh* dependence of the *TAPS* rate on the measuring current). Finally, by no means the postulate of existence of a constriction could account for complex shape of the measured *R(T)* transition: e.g. development of the low temperature "foot". The straightforward explanation of the shape of superconducting transitions is the sample inhomogeneity, discussed in the previous section. Resuming, we may state that the *quality of the studied lift-off fabricated aluminum polycrystalline nanowires was not sufficient to resolve the TAPS contribution*. Hence, my data are not conclusive with respect to verification of the LAMH model. Eventually, only atomically perfect *1D* objects as superconducting whiskers or hypothetic superconducting 1D molecules (nanotubes?) can

be utilized for reliable verification of the TAPS model. Applicability of the TAPS model for realistic nanowires is problematic [23].

sample Cu5µm1no1
after 3rd sputtering (R_N=316 Ω, σ = 1060 nm^2, I_{mean}=9 nm, L=5µm):
- I_m = 10 nA
- I_m = 50 nA
- – – LAMH model R_N= 316 Ω, I_{mean} = 9 nm, T_c = 1.45 K, L=5µm

after 4th sputtering (R_N=965 Ω, σ = 520 nm^2, I_{mean}= 6 nm, L=5µm):
- I_m = 10 nA
- I_m = 20 nA
- – – LAMH model R_N= 965 Ω, I_{mean}= 6 nm, T_c = 1.56 K, L=5µm
- – – LAMH model R_N= 965 Ω, I_{mean}= 6 nm, T_c = 1.61 K, L=1.5µm

after 5th sputtering(R_N=1255 Ω, σ = 440 nm^2, I_{mean}= 5.5 nm, L=5µm):
- I_m = 20 nA
- I_m = 1 nA
- – – LAMH model R_N= 1255 Ω, I_{mean}= 5.5 nm, T_c = 1.53 K, L=5µm

Fig.E.7. *Typical R(T) transitions for the same aluminum wire obtained by progressive reduction of its cross-section. Predictions of the LAMH model of TAPS (eq. T.13) are provided with dashed lines. Each transition is presented for two different biasing currents proving that wires were not overheated. The broadening of the signal in resistance domain for fixed temperature for low resistances is the effect of instrumental noise (sensitivity of the front-end preamplifier was ~1 nV). Note that the sample after 5th sputtering has the lower T_c than the same sample after 4th sputtering. It is in contrast to the general tendency observed for aluminum nanowires (Fig.E.2). It suggests that not only size is important for T_c determination, but also other factors e.g. morphology (which in this particular case could have been affected by the way wire surface was oxidized after sputtering).*

E.3. Superconductivity in ultra-narrow aluminum nanowires

E.3.1. Resistive transitions of ultra-narrow nanowires

For sufficiently thick aluminum wires studied in this work their resistive transitions can be understood in terms of inhomogeneity: each $R(T)$ transition shows more or less abrupt step(s) having some finite width due to slightly different T_c for different sections of the wire and no measurable resistance below the bulk $T_c \sim 1.18$ K (*section E.1 & E.2*). However, when the wire becomes sufficiently thin (its cross-section goes below ~ 400 nm^2) the qualitatively different shape of the resistive transition has been observed, which can be understood *neither* in terms of *TAPS, nor* sample inhomogeneity (*Fig.E.8*).
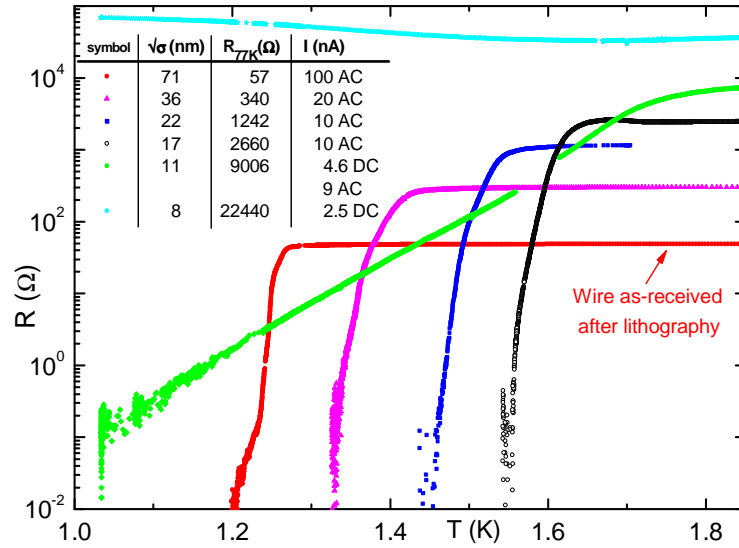
Fig.E.8. *Resistance vs. temperature for the same aluminum nanowire with length L = 10 μm after several sessions of diameter reduction. As the wire cross-section is reduced, the shape of the R(T) transition remains unchanged until the wire enters the new regime where QPS events broaden the transition (green curve). Further reduction of cross-section leads to insulating behavior (the uppermost curve)[1]. Parameters of the samples are presented in the inset.*

As was already pointed out, since T_c of aluminum nanowires increases with decrease of the diameter (*Fig.E.8*, *section E.1*), no signal measured below $T_c^{bulk} \sim 1.18$ K can be attributed to a smooth geometrical variation of the wire cross-section and resulting difference in the local T_c (*Fig.E.2*). Also, no set of realistic parameters can provide an acceptable fit using the *TAPS* model, even if to assume presence of unrealistically narrow constriction(s). The experimental $R(T)$ broadening for the samples with cross-section below $\sigma < 400$ nm^2 can be associated with the *quantum phase slip* (*QPS*) phenomenon, also often referred to as the *macroscopic quantum tunneling* (MQT).

In the following I will discuss the superconducting transitions of different thin wires which showed QPS-like behavior. They have been fitted with QPS model of single phase slip activation developed by GZ (*section T.5.3, eq. T.31*). The model is rewritten here in the form convenient for comparison with experiment:

$$R_{QPS} = D \cdot (1 - t) \cdot \exp(-C(1-t)^{1/2});$$ (T.31)

$$t = \frac{T}{T_c};$$

$$C = S_{QPS}(T = 0) = A \cdot \frac{R_q}{R_N} \cdot \frac{L}{\xi(0)};$$

$$D = B \cdot C \cdot \frac{L}{\xi(0)} \cdot R_q;$$

$$R_N = \rho_N \cdot \frac{L \cdot l_{mean}}{\sigma \cdot l_{mean}} = \frac{K \cdot L}{\sigma \cdot l_{mean}} = \frac{K \cdot L \cdot FWHM}{\sigma^2};$$

$$l_{mean} \approx h;$$

$$\sigma = h \cdot FWHM$$

$$\xi(0) = 0.85 \cdot \sqrt{\xi_0 \cdot l_{mean}}; \quad \xi_0 = 1.6 \; \mu m \quad \text{for} \quad Al;$$

$$K = \rho_N \cdot l_{mean} = 6 \cdot 10^{-16} \; \Omega \cdot m^2;$$

The two fitting parameters are *C* and *D*. Together with expression for the normal state resistance R_N they give 3 equations with 5 unknowns: R_N (normal state resistance of a wire), σ (wire cross-section), *L* (wire length), *A, B* (numerical constants of order of unity limiting accuracy of the GZ theory). I assumed that the elastic mean free path l_{mean} equals to height *h* of the wire (the cross-sections of the thinnest wires studied here look like flat trapezoids) and wrote that cross-section of the wire σ equals to the product of the height *h* and the full width at half maximum (*FWHM*). *FWHM* can be determined with sufficient accuracy from *SPM&SEM* measurements. We can express R_N, σ and *L* in terms of *A* and *B*. Such a procedure yields:

$$\sigma^{3/2} = \frac{K \cdot 0.85 \cdot \sqrt{FWHM \cdot \xi_0} \cdot C}{A \cdot R_q}$$

$$L = B^{-1} \cdot A^{-1/3} \cdot C^{-2/3} \cdot D \cdot FWHM^{-1/3} \cdot K^{1/3} \cdot (0.85)^{4/3} \xi_0^{2/3} \cdot R_q^{-4/3}$$

$$R_N = \frac{A}{B} \cdot \frac{D}{C^2}$$

σ, *L* and R_N determined in the described way can be directly compared with the values characterizing the whole wire and obtained by other means: the length of the wire can be measured with *SPM*, the normal state resistance can be measured with very good accuracy using four-probe method, and finally the wire cross-section can be estimated reasonably being based on *SPM* data and R_N value (*e.g. section W.4*). In such approach *A* and *B* are used to fit the model to experimental data assuming that phase slips can happen along the

whole wire evenly, or in other words, assuming that the wire has a uniform cross-section everywhere. This approach is widely used: e.g. [2]. However, such a procedure does not take into consideration an important consequence of the *QPS* theory: *very strong dependence of QPS rate on cross-section implicates that the narrowest part of the wire provides the overwhelming contribution to the measured resistance R_{QPS} (cf. section T.5.4, Fig.T.8 and section W.3.2, Fig.W.18&W.19).* It follows that the total length of the wire, its average cross-section and the normal state resistance are not the representative parameters when comparing the *QPS* experimental data obtained for real samples (= with cross-section variations larger than *0.5 - 1* nm) with the GZ model. These parameters give only the upper limits for the corresponding parameters characterizing the actual part of the wire (= constriction, weak link) producing phase slips predominantly (see discussion in the end of *section T.5.3*). Note that due to ambiguity of the A and B parameters it is possible to get exactly the same fit with different values of σ, L, R_N provided that the products $\sigma \cdot A^{2/3}$, $L \cdot B \cdot A^{1/3}$ and $R_N \cdot B \cdot A^{-1}$ remain unchanged. Hence, from mathematical point of view one can fit data with $\sigma = 50$ nm^2 and $A = 2.83$ as well as with $\sigma = 150$ nm^2 and $A = 0.54$. Thus I preferred to perform fitting which leaves explicit dependence of the fitted σ, L and R_N on A and B parameters to avoid playing with numbers.

Experiment conducted on one single wire scaled down with *1* keV Ar^+ sputtering is presented in *Fig.E.9*. Predictions of the *LAMH* model by no means can account for the broad transitions observed for the thinnest samples. Assuming existence of the narrow constriction in the wire, giving rise to the total wire resistance predominantly (it can be done formally by reducing wire length by one order of magnitude – see *Fig.E.9*), does not solve the problem. Effect of inhomogeneity can be ruled out below *1.18* K (*section E.1*). The reasonable explanation is provided by assuming that *R(T)* transitions for the thinnest wires are governed by the *QPS* mechanism. The values of fitted σ_fit, L_fit, R_N_fit (I associate them with parameters of constrictions producing QPS predominantly) along with values of σ_{av}, L and R_N determined by other means (I associate them with parameters characterizing the whole wire) can be found from *Fig.E.9*. σ_fit, L_fit, R_N_fit are determined within accuracy given by theory i.e. up to numerical constants or order of unity. Since the wire should finally break in one point and because of the strong dependence of the *QPS* rate on the cross-section it is logical to obtain the best fit assuming the decrease of the effective constriction length L_fit when the wire is sputtered. At first sight, the decrease in the fitted value of the constriction normal state resistance R_N_fit seems to be not reasonable, but what matters is the resistance per length (R_N_fit / L_fit). This ratio increases while the wire is sputtered and the *QPS* rate gets higher. This observation confirms the claim that what is important for the *QPS* appearance is the narrow link of small cross-section (or equivalently of large resistance per length). It may happen that the wire *No.1* with large resistance can exhibit much weaker *QPS* behavior than the wire *No.2* of the same length and significantly smaller resistance. This is the case when
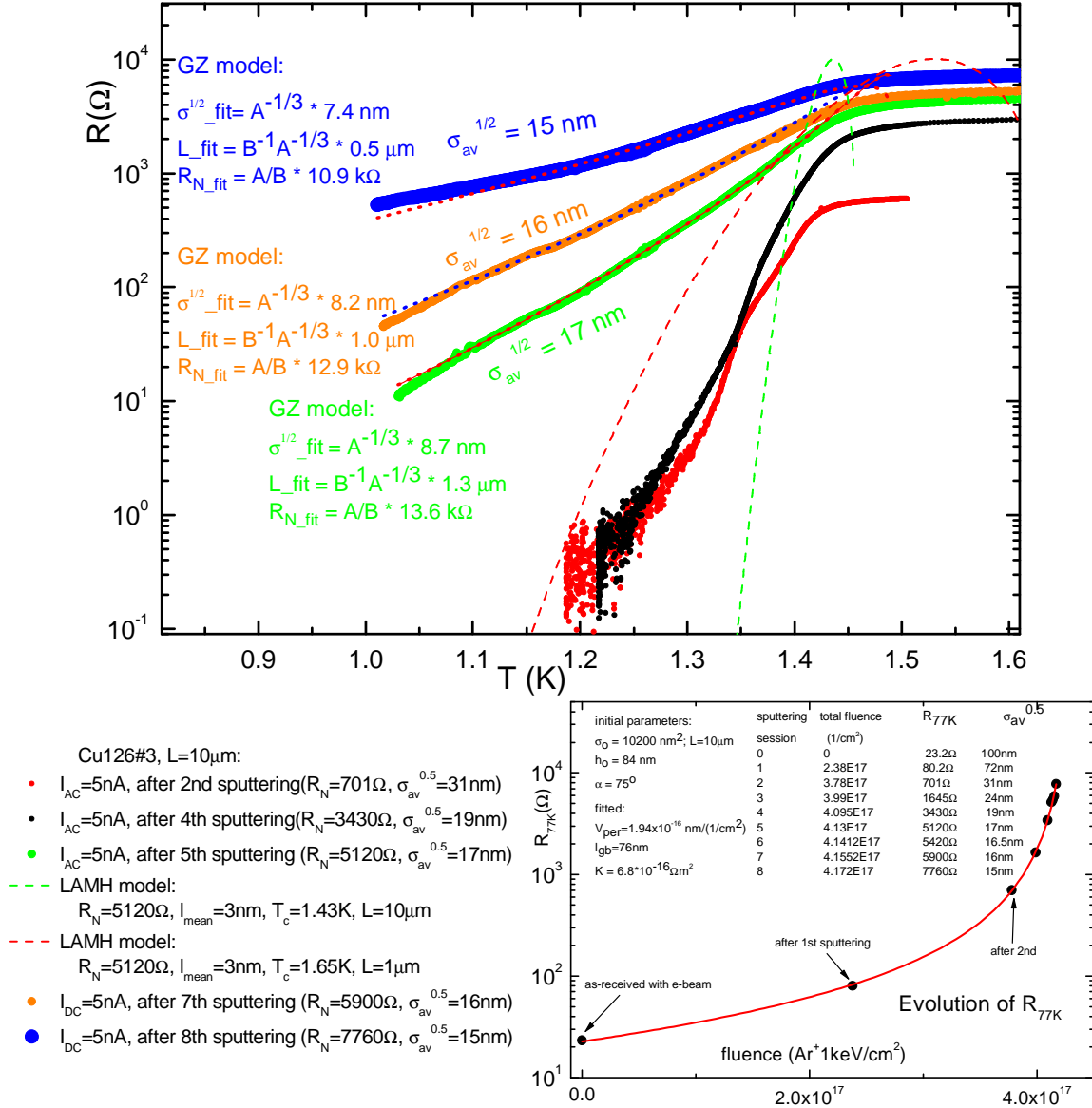
Fig.E.9. *Top panel: detailed R(T) data for the same wire (L = 10 μm) with successively reduced cross-section (1keV Ar⁺ beam). Predictions of the LAMH model of TAPS (eq.T.13) are provided with dashed lines for sample after 5th sputtering. Note that even assuming the existence of the narrow short constriction (L = 1μm, red dashed line) in the wire, one can NOT explain the data in terms of TAPS. Dotted lines (for three samples) are fits to QPS model (eq.T.31) with fitting parameters displayed in the plot. Transitions of two thicker samples can be understood in terms of inhomogeneity. The smaller panel shows evolution of the resistance measured at T = 77 K with ion fluence. Solid line is the fit to resistance formula (W.4) combined with flattening model (W.3). Three samples exhibiting QPS behavior can be found also from Fig.E.11 (transition 1,3,5) [2].*
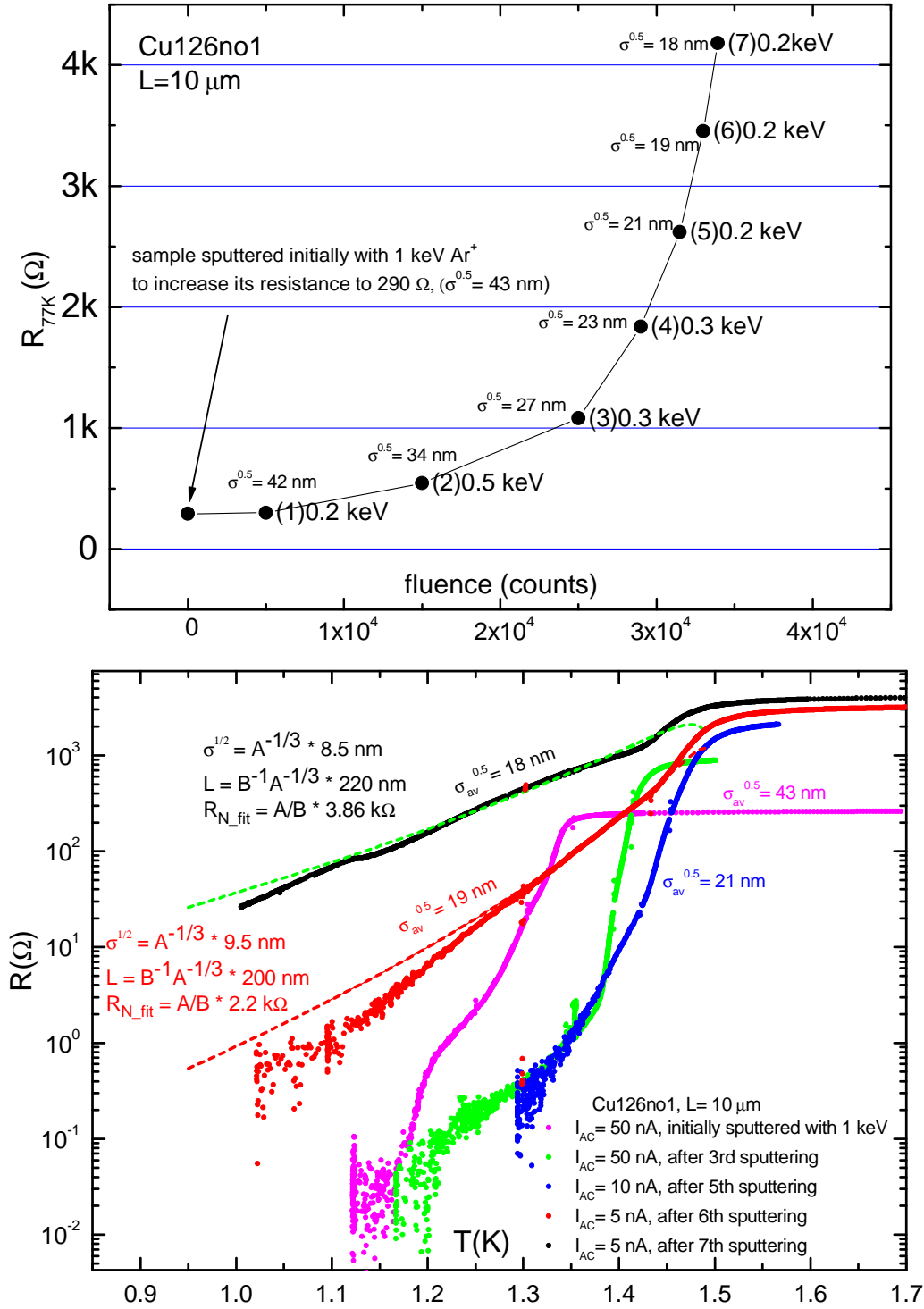
Fig.E.10. *Detailed data for one the same wire with successively reduced cross-section. Top panel shows evolution of the normal state resistance at T = 77 K after successive sessions of sputtering, bottom panel - corresponding resistive transitions. Note energies of Ar⁺ ion beam used for sputtering. Dashed lines for two the most resistive samples are fits to QPS model (eq.T.31) with fitting parameters displayed in the plot. The shape of the other transitions (not fitted with QPS model) can be explained in terms of inhomogeneity.*

wire *No.1* is uniform and its resistance is distributed evenly, while the second wire *No.2* contains a "bottle neck" responsible for the dominating fraction of the measured resistance. Similar experiment like in *Fig.E.9* is presented in *Fig.E.10*. It is shown there that the same *QPS* behavior is obtained when *200* eV ion beam energy is used. Penetration depth for *Ar⁺* ions is then ~ *1* nm which is smaller than the thickness of the surface layer of naturally formed aluminum oxide.

One can be surprised that difference in diameter between samples of the same wire exhibiting *QPS* behavior is at the level of *1* nm. Is it possible to sputter a wire with such accuracy? The answer is yes: one can get convinced exploring *Appendix 2*. It is important to note that the reduction of the wire diameter by 1 nm is responsible for huge increase in the measured resistance for the *QPS*-dominated samples. Particularly for presented aluminum nanowires R_{QPS} scales with cross-section as $exp(-a\sigma^{3/2})$ (cf. *section T.5.4 and eq.T.34*). It follows that performing the experiment on a single wire with successively reduced diameter one is able to observe the crossover between superconducting and resistive (= *QPS* dominated) behavior of the superconductor (see sequence of *R(T)* transitions in *Fig.E.9*). The crossover is governed by the wire cross-section or equivalently resistance per length and is observed in the narrow range of diameters (few nanometers wide).

Superconducting transitions of thicker samples of the same wire, not exhibiting QPS behavior, are also displayed in *Fig.E.9* (*2* samples) and in *Fig.E.10* (*3* samples). No low temperature resistance "tails" have been detected below T_c ~ *1.18* K for all of them. It follows that the shape of their superconducting transition can not be attributed to *QPS* mechanism. Instead, the shape of these transitions can be entirely understood in terms of sample inhomogeneity, e.g. "foot" observed at the low-temperature part of transitions is associated with the wider node regions (electrodes) which has the lowest local critical temperature. Note also that any trial to fit discussed "inhomogeneous" transitions with the *LAMH* model fails (cf. prediction of the *LAMH* model for width of transition of aluminum nanowires displayed in *section E.2, Fig.E.7*).

I show several representative resistive transitions of aluminum nanowires of different lengths for which *QPS* behavior has been observed in *Fig.E.11*. The values of fitted *σ_fit, L_fit, R_N_fit* along with values of σ_{av}, *L* and R_N determined by other means are attached in the table. If to assume *A = 1* and *B = 1* then for all transitions fitted cross-sections and lengths are smaller then average cross-sections and total lengths determined from *SPM / normal state resistance* measurements. In such case, however, the normal state resistance of constriction R_N_fit starts to be bigger than the normal state resistance of the wire R_N. But there exist some other values of *A* and *B* (of order of unity, e.g. *A = 0.5, B = 2*) for which *σ_fit, L_fit, R_N_fit* are smaller than σ_{av}, *L* and R_N respectively in all cases. *Fig.E.11* shows that QPS starts to be observable independently of the wire length as soon as some part of the wire is narrow enough i.e. according to fit to QPS model falls into

range of $\sigma^{1/2} = A^{-1/3} \cdot 8$ nm or as soon as $\sigma^{1/2}$ for some part of the wire is not bigger than *11 - 17* nm (according to independent estimation).

	$\sigma^{1/2}$_fit [nm]	L_fit [µm]	R_N_fit [Ω]	$\sigma_{av}^{1/2}$ [nm]	L [µm]	R_N [Ω]
(1) Cu126#3after8th	$A^{-1/3} * 7.4$	$B^{-1}A^{-1/3} * 0.5$	$A/B * 10900$	15	10	7760Ω
(2) Cu115#2after8th	$A^{-1/3} * 8.2$	$B^{-1}A^{-1/3} * 0.5$	$A/B * 10300$	15	10	7863Ω
(3) Cu126#3after7th	$A^{-1/3} * 8.2$	$B^{-1}A^{-1/3} * 1.0$	$A/B * 12900$	16	10	5900Ω
(4) Cu5µm1#1	$A^{-1/3} * 8.5$	$B^{-1}A^{-1/3} * 0.8$	$A/B * 9300$	15	5	4005Ω
(5) Cu126#3after5th	$A^{-1/3} * 8.7$	$B^{-1}A^{-1/3} * 1.3$	$A/B * 13600$	17	10	5120Ω
(6) Cu1µm1#3	$A^{-1/3} * 8.4$	$B^{-1}A^{-1/3} * 0.14$	$A/B * 1700$	11	1	2676Ω
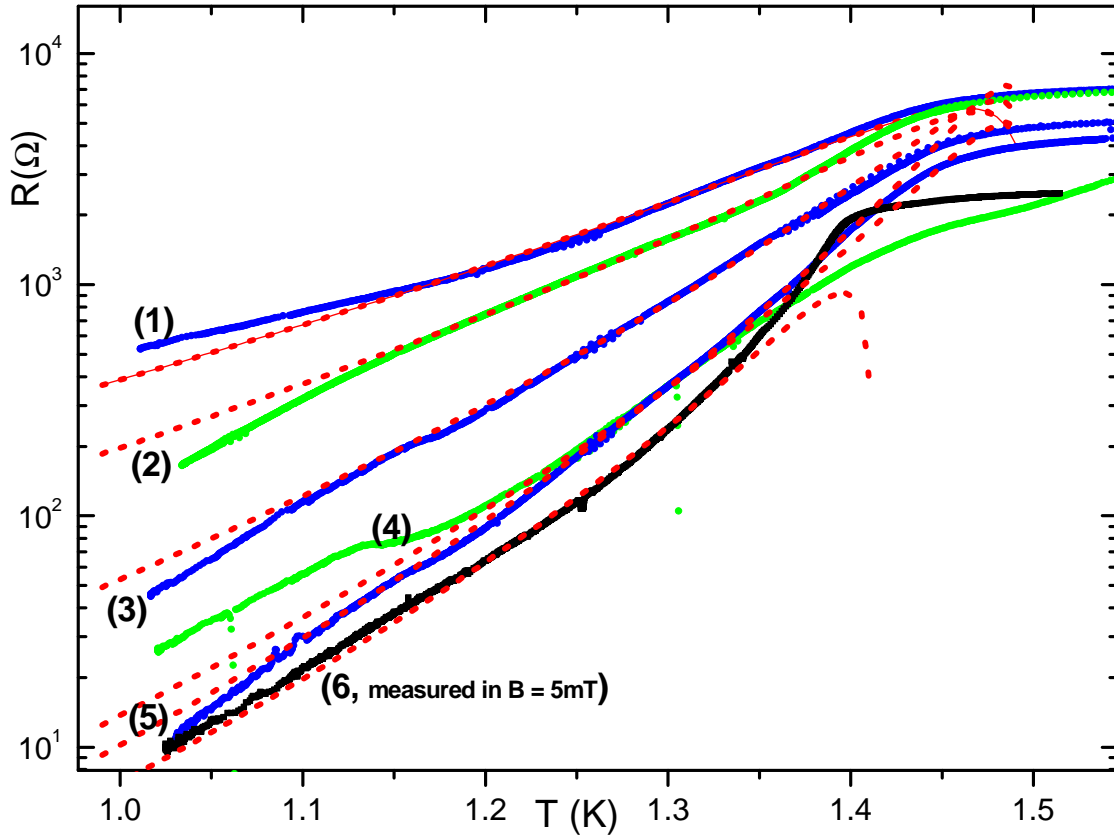
Fig.E.11. *Fitting of QPS model (eq. T.31, red dotted lines) performed for nanowires of different lengths exhibiting broadening of the R(T) transition (solid lines) reveals that their resistive behavior below T_c is governed by the nucleation of QPS in the parts of the smallest cross-section. No matter what is the actual length of the wire, as soon as some its part has cross-section small enough, QPS starts to be observable as the finite resistance below T_c. Note how sensitive is the QPS rate on the value of cross-section. In table σ_fit, L_fit, R_N_fit denote fitted parameters of constriction and σ_{av} (average cross-section), L (length) and R_N (normal state resistance) are determined for the whole wire by independent measurements. A and B are constants of order of unity.*

Presented interpretation of the data can meet some criticism if to accept that phase slip event is non-local e.g. it is sensitive to electromagnetic environment. *GZ* theory of *QPS* was derived for uniform wires taking into account dissipation inside and outside phase slip core self-consistently. One could ask to what extent the rate of *QPS* of a constriction is sensitive to existence of the thicker parts surrounding the phase slip core. Even if to assume that *QPS* is initiated in the narrowest section of the wire (which may have length of just few ξ) still it is not clear to what extent this *QPS* initiation is dependent on the thicker parts of the wire. *GZ* claimed that action related to electromagnetic field propagation out of the phase slip core is negligibly small compared to the uncertainty in the action for the core for sufficiently short wires (*section T.5.3*). It should follow that phase slippage is only sensitive to the core (constriction) parameters. However, since effect of electromagnetic environment is absorbed into *A* constant one can argue that *A* is actually not a constant but varies slightly, dependently on the environment (cf. *section T.5.4*). Since the mentioned dependence of *A* parameter on the environment is not quantitatively known I did not take it into account in the presented analysis.

I have not provided a comparison of *R(T)* data for aluminum nanowires with Giordano formula (*section T.5.2, eq. T.16*), bearing in mind that from experimental point of view it is actually the same as GZ expression (*eq. T.31*): dominating exponential dependence is the same in two models. Pre-factors are different but they play a minor role when comparing data with theories.

It is very important to stress that observation of successive development of *QPS* phenomenon is consistent with independent estimation of the wires cross-sections reduction due to sputtering (cf. *Fig.E.9* and *Appendix 2*). Eventual formation of a Josephson junction somewhere along wire is rather unlikely since all presented data were obtained for wires tailored with ion-beam sputtering in controlled (and predictable!!!) way assuming their metallic behavior typical of aluminum in normal state (section W.3.1). Also the measured normal state resistance for the thinnest wires is in agreement with *SPM*-based estimations (*section W.4*). If a Josephson junction was formed after one of the sputtering sessions the wire resistance would increase in unpredictable way. Moreover the resistance estimated from SPM measurements would be significantly lower than the directly measured value.

Resuming this section, I would like to repeat that the method of progressive reduction of the sample cross-section enabled to trace the evolution of the size-effect determining the shape of the *R(T)* transitions in narrow superconducting aluminum nanowires. For samples with diameter *20* nm $< \sigma^{1/2} < 100$ nm, the shape of the transitions can be qualitatively understood in terms of geometrical inhomogeneity. Data for these thick wires are not conclusive with respect to verification of the *LAMH* model of thermal phase slip activation. In thinner samples $\sigma^{1/2} < 20$ nm the *R(T)* transitions are much wider and can be explained neither by the *LAMH* model, nor by inhomogeneity. The model of *QPS* [34] gives a good agreement with experiment for the thinnest wires.

E.3.2. Observation of negative magnetoresistance (nMR) below T_c

Application of small magnetic field perpendicular to the plane of the structures revealed unexpected effect: negative magnetoresistance (*nMR*) (*Fig.E.12*). The phenomenon is rather counterintuitive as typically magnetic field suppresses superconductivity. It has been observed only in the thinnest samples exhibiting QPS behavior and only below ~*1.18* K, which is the T_c for bulk aluminum. The latter observation turned out to be universal for all studied samples and an interpretation should necessarily take this fact into account. Observed *nMR* exhibits strong dependence on measuring current being more pronounced for larger currents (*Fig.E.13*). Almost in all cases the nMR appearance was accompanied by a "kink" in the superconducting transition measured around $T = 1.15$ K in zero magnetic field (*Fig.E.13*, look also carefully at transitions in *Fig.E.9, E.10, E.11*). Application of few mT magnetic field removes the "kinks" completely. It is also worth pointing out that the "kinks" were more pronounced in shorter wires (compare *Fig.E.13(b), L = 5* μm and *Fig.E.13(c), L = 1* μm)).
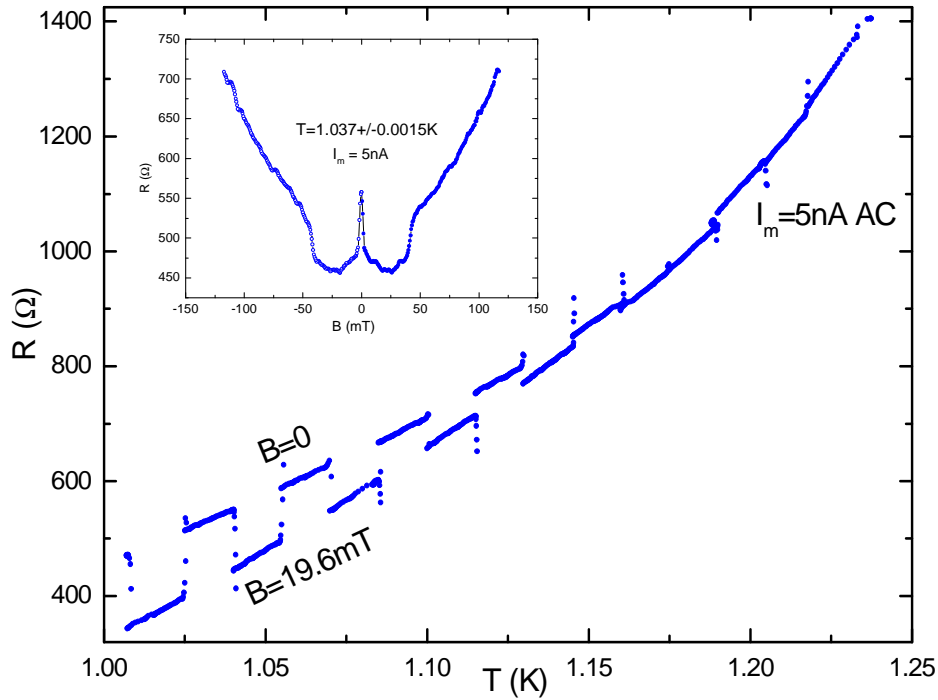
Fig.E.12. *Slowly recorded resistance vs. temperature dependence for $\sigma_{av}^{1/2}$ ~ 15 nm sample. While sweeping the temperature few times perpendicular magnetic filed B=19.6 mT was switched on and off. Top branch corresponds to the zero field, while the lower one - to the field 'on'. Inset: resistance vs. perpendicular magnetic field for the same sample measured at constant temperature and small ac current. The effect was only observed below ~1.18K. For full transition of this wire in zero field see Fig.E.11(1) [2].*

At the moment I do not have a convincing interpretation for the *nMR* data. The presence of magnetic impurities in the samples should be negligible. They were all fabricated in the *UHV* chamber where magnetic materials have never been processed. Even if to allow for Kondo impurities in aluminum wires, corresponding magnetic fields (few mT) are too small to polarize their magnetic moments. In addition, it is known that aluminum is immune to creation of localized magnetic moments with concentration of the impurities up to few at.% [71].
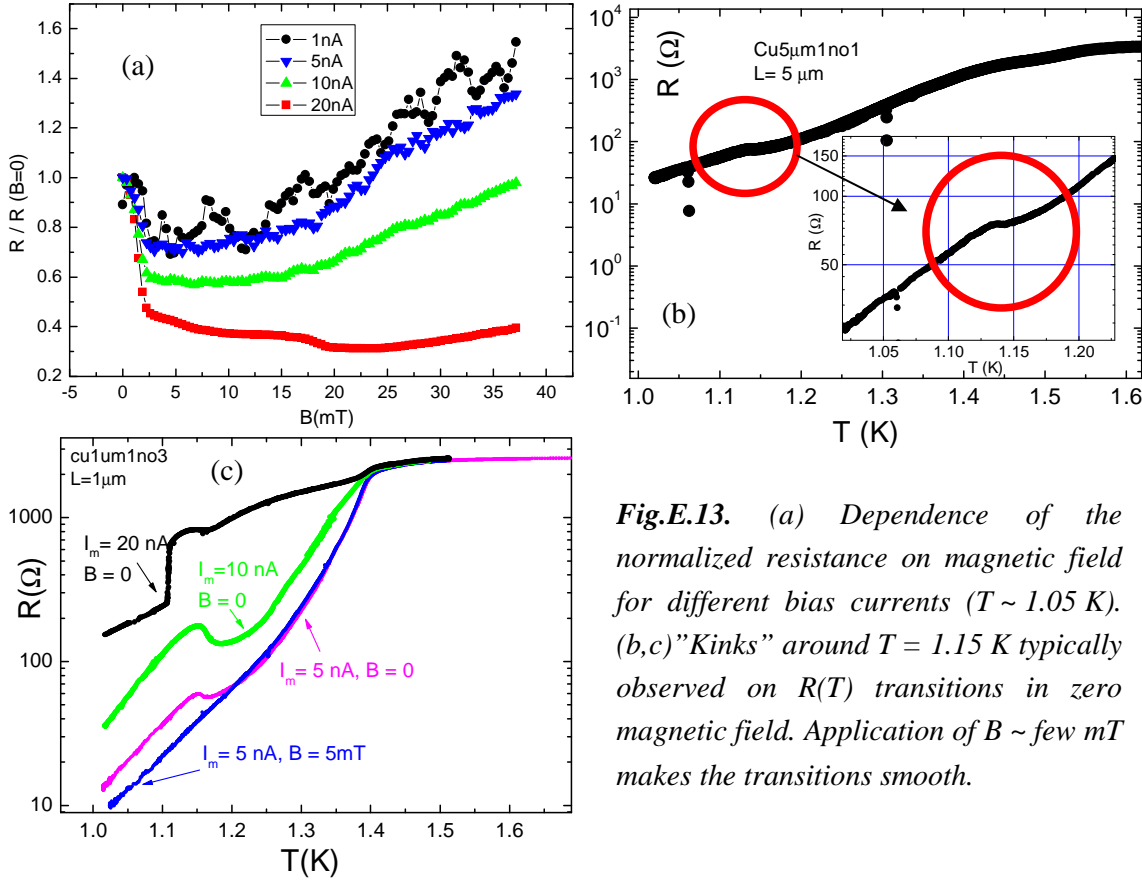

Fig.E.13. *(a) Dependence of the normalized resistance on magnetic field for different bias currents (T ~ 1.05 K). (b,c)"Kinks" around T = 1.15 K typically observed on R(T) transitions in zero magnetic field. Application of B ~ few mT makes the transitions smooth.*

Possible explanations for nMR in thin wires:

1. A plausible explanation of the *nMR* effect could be related to the reduction of the energy gap Δ_0 in the magnetic field [32]. Such reduction should reduce the core action ($S_{core} \sim \sqrt{\Delta_0}$, *cf. eq.T.24*), just leading to enhanced *QPS* rate (implicating larger effective resistance measured in QPS regime). However, suppression of the gap also results in the increase of thermally excited quasiparticles ($n_{qp} \sim \sigma_{qp} \sim \exp(-\frac{\Delta_0}{k_B \cdot T})$, σ_{qp}-conductivity of the "normal" channel) leading to stronger dissipation in the phase slip process ($S_{core} \sim \sigma_{qp}$, *cf.eq.T.24*). Dissipation effects due to quasiparticles inside the *QPS* core (and also outside it) are expected to reduce the probability of *QPS* events similarly to the standard problem

86

of quantum tunneling with dissipation [31]. If second effect dominates *nMR* should be expected. This explanation also implicates that *nMR* should not be observed at sufficiently low temperatures (when no quasiparticles are excited). In this limit $T << T_c$ application of magnetic field should lead to the conventional suppression of superconductivity and increase of the measured resistance. However I performed measurements only down to *0.95* K which was not low enough to verify the validity of the described scenario.

2. Negative magnetoresistance in aluminum nanowires is believed to appear as a result of *magnetic field dependent boundary conditions*: around T = *1.15 - 1.18* K the leads connecting the sample with the measuring setup enter superconducting state what is manifested in all measured transitions by a "kink". Application of small magnetic field (~ few mT) prevents the leads from going to the superconducting state and then smooth transitions are observed.

This observation can actually suggest that overheating is responsible for the observed *nMR*. It is known fact that superconducting leads are ideal insulators against conventional thermal conduction [72,73]. It follows that when electrodes are in superconducting state, heat removal from the nanowire is significantly reduced due to suppressed diffusion of hot quasiparticles out of the structure produced in each phase slip event. Experimentally it should be measured as a shift of *R(T)* transition to lower temperatures with respect to the transition recorded when heat is removed more efficiently (i.e. leads in normal state, magnetic field "on").

The boundary conditions are also important if to consider the propagation of electromagnetic waves (*Mooij-Schön mode*) generated at each phase slippage. Then it could be claimed that boundary conditions can influence the reflection of electromagnetic waves at contacts (leads), thus modifying the QPS action (interaction of single phase slips with electromagnetic field initiated by another phase slip). It would be desirable to use normal metal electrodes (e.g. *Au*) instead of aluminum ones to see if *nMR* is still observed. It would be also interesting to vary the geometry of the contact pads to alter the heat and electric transport conditions at the sample-electrode interface (e.g. increase area of contact pads to see if excess heat (if exists) can be reduced).

3. Another idea employs possible dependence of a charge imbalance region on magnetic field [74]. This non-equilibrium region accompanying each phase slip event should provide dissipation outside the core of a phase slip, possibly modifying the *QPS* action. However at the moment the validity of the charge imbalance concept is not theoretically justified in case of *QPS* observed well below T_c.

Negative magnetoresistance was also found in lead nanowires [75]. Probably a related effect - increase of the critical current by magnetic field - was observed in *MoGe* and *Nb* nanowires [76]. The suggested explanations related to localized magnetic momenta is not applicable to our aluminum nanowires, where existence of active magnetic impurities is questionable.

E.3.3. V(I) and dV/dI characteristics of narrow aluminum nanowires

Current applied to a wire leads to reduction of the free-energy barrier opposing formation of current-reducing phase slips, thus enhancing the phase slip rate (*cf. Ch.II (T), eq.T.6* and *Fig.T.6*). It follows that narrow *1D* superconducting channel is essentially a non-Ohmic element: strong non-linearity in *V(I)* curve is expected for wires exhibiting phase-slip behavior. In *Fig.E.14* I present superconducting transitions for the same wire measured at different biasing currents.
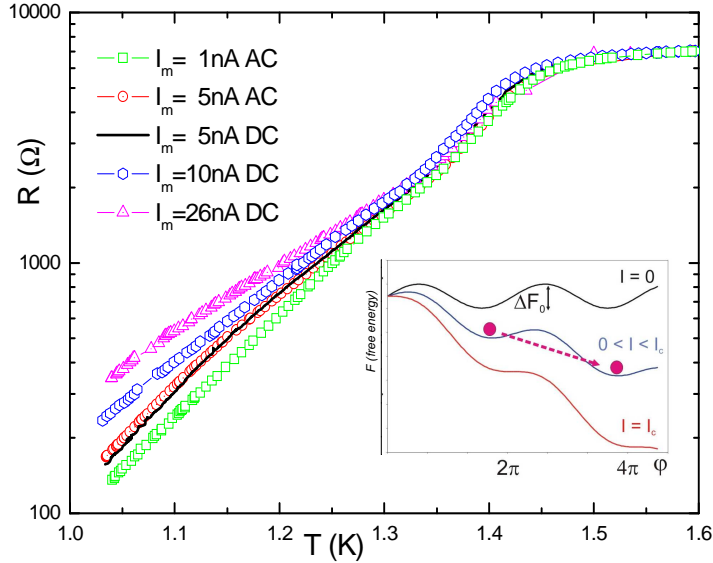

Fig.E.14. *R(T) transitions for thin* ($\sigma_{av}^{1/2} \sim 15$ nm) *aluminum nanowire with length L=10 μm (Cu115#2after8th) measured for different DC and AC currents. The top parts of the transitions show ohmic behavior while the bottom parts exhibit pronounced non-linearity. Inset shows schematically physical process underlying non-linearity - reduction of free energy barrier with applied current leading to enhanced activation rate for QPS (see also caption of Fig.T.3 and corresponding comments in the section T.1). At the critical current I_c the potential barrier disappears. Note consistence of data measured with two different techniques (red dots - 5nA RMS AC Lock-In 19Hz and solid black line – 5nA DC Nanovoltmeter)[2].*

Hyperbolic sine dependence of measured voltage on applied current is predicted both in case of thermally activated (*TAPS*) and quantum phase slips (*QPS*). Example of nonlinear *V(I)* curve in case of TAPS [38] has been presented in *section O.1 (Fig.O.3)*. Below I will show my experimental efforts to observe a non-linearity also in case of QPS. We can rewrite *eq. T.29* in the form convenient for direct comparison with experiment:

$$V = \frac{\hbar}{2e} \cdot 2\pi \cdot \Gamma_{QPS} = \Omega \cdot \frac{h}{e} \cdot \sinh(I / I_0) \cdot \exp(-\frac{\Delta F_o}{\Delta(T)})$$

(E.7)

where $\Delta(T)$ is the temperature dependent superconducting energy gap and $I_0 = 4e\Delta(T)/h$ is the characteristic current, below which one can expect linear response of the system ($I << I_0$ allows to approximate *sinh()* with its argument). For fixed temperature one gets:

$$\log(V) = \log(\sinh(I/I_0)) + \text{constant.} \tag{E.8}$$

Last equation predicts that for sufficiently high currents $I >> I_0$, *log(V) vs. I* should exhibit constant slope:

$$\frac{d\log(V)}{dI} = \frac{\log(e)}{I_0} \tag{E.9}$$

For aluminum with $T_c \sim 1.45$ K the superconducting energy gap is $\Delta(T=0) = 1.76 k_B T_c = 220$ µeV. In *Fig.E.15* the data was collected at $T = 1.04$ K while the $T_c \sim 1.45$ K (the corresponding superconducting transition can be found in *Fig.E.11(3)*). It follows that the gap should be suppressed by $\sim 20\%$ (for the actual value of the gap at given temperature see *appendix A.5*). Then for $I >> I_0 (T = 1.04K) = 27nA$ (for aluminum) we expect to see constant slope in *log(V) vs. I* dependence equal to 0.0160/nA. The model fits experimentally measured *V(I)* curve for low currents (up to *12* nA). For higher currents measured voltage is higher then predicted.

Formally one should also consider the additional current dependencies of the barrier height $\Delta F_0(I)$ and the attempt frequency $\Omega(I)$. For currents comparable and bigger than I_0 the energy barrier ΔF_0 (in exponent of *eq. E.7*) should be treated as current dependent [16,25]. We can take this effect into account doing following replacement:

$$\Delta F_0 -> \Delta F_0 + \frac{4 \cdot \Delta(T)}{3\pi^2} \frac{I^2}{I_0 \cdot I_c} \tag{E.10}$$

with I_c being critical current defined according to *eq. T.14*: $I_c = \frac{4e\Delta F_0}{h}$. For fixed temperature we predict voltage:

$$V \sim \sinh(I/I_0) \cdot \exp(-\frac{4I^2}{3\pi^2 I_0 I_c}) \tag{E.11}$$

I need to stress here that the additional current dependence discussed here considers modification of ΔF_0 itself with the applied current. It has nothing in common with ΔF_1 responsible for asymmetric shape of the actual potential (*cf. Fig.T.6, section T.3*) and accounted for in *sinh(I/I_0)* term (*cf. eq. T.8*). Taking into account the current-dependent ΔF_0 allows reproducing the slope of experimental *V(I)* for higher currents (*Fig.E.15*). But due to "oscillating" nature of *V(I)* barely visible in *Fig.E.15,* but well pronounced for *dV/dI* (to be described below), it is not possible to fit the data in the entire current range. Situation looks much better for higher temperature *T=1.23* K. The application of the model with $I_0=21.6$ nA (see *appendix A.5* to get estimation for the gap) and $I_c = 80$ nA yields agreement with experiment up to *70* nA (*Fig.E.16*)).
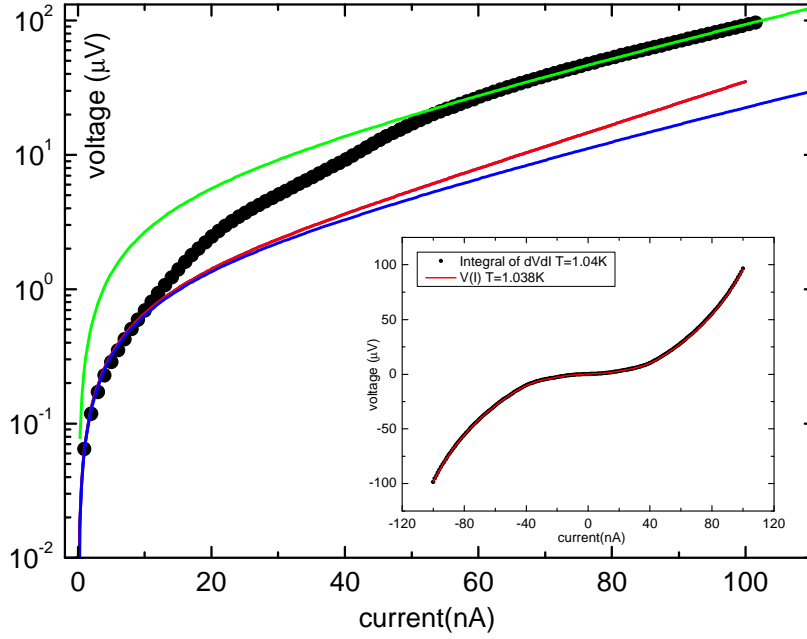
Fig.E.15. *Experimentally measured V(I) dependence (black dots) for sample Cu126#3after7th ($\sigma_{av}^{1/2}$ ~ 16 nm, L = 10 μm, T = 1.04 K) compared to the model (eq.E.8) with current- independent ΔF_0 (red line) and the model (eq.E.11) with current-dependent ΔF_0 (blue line). Both models could have been fitted for low currents with only one fitting parameter corresponding to the vertical shift (the shapes of theoretical curves were defined by estimations of parameters appearing in theory - $I_0=27$ nA, $I_c=120$ nA). The model (E.11) applied for higher currents gives the same slope as the measured data points, however then discrepancy for small currents occurs (green line). Inset shows the same experimental curve measured in two different ways to show consistency of data: V(I) and integrated dV/dI.*
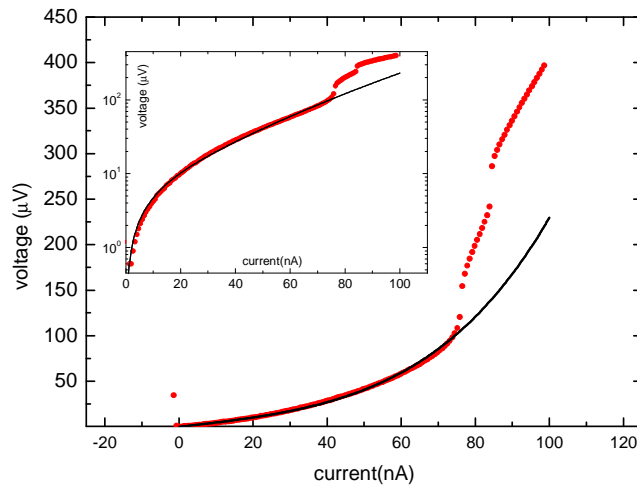

Fig.E.16. *V(I) curve of the same sample as in Fig.E.15 recorded at 1.23 K (T_c ~ 1.45 K) can be fitted with eq. E.11 assuming dependence of ΔF_0 on applied current. Before the wire is driven to normal state sequence of steps is observed. Inset shows the same data in semi-log presentation.*

The sequence of steps appearing above $I \sim 70$ nA (*Fig.E.16*) can be attributed to development of current induced phase slips which can show up just before the critical current I_c is reached. The topic of the current-induced phase slip activation has been intensively studied in *1970s* in superconducting whiskers and microbridges [77,78] as well as more recently in nanowires [79,80,81]. However it is also possible to consider formation of "hot spots", nucleated at different values of the local critical current and then spreading out [41,42,82]. Actually this kind of scenario is very probable in narrow polycrystalline wires where weak links with different local I_c are unavoidable. I have not investigated the current induced phase slip regime in details to draw any final conclusions on the observed steps. The reason was that I was afraid to burn thin wires by the strong current.

I used the described model with current dependent ΔF_0 (*eq. E.11*) to fit $V(I)$ dependencies measured at different temperatures for another sample *Cu115#2after8th* (*Fig.E.17*, for corresponding superconducting transition see *Fig.E.11 (2)*). In principle it is possible to obtain reasonable fits at temperatures above $T \sim 1.18$ K taking critical current I_c as the fitting parameter and calculating I_0 as given in *eq. E.7*. I would like to note that since the $R(T)$ transitions for very thin wires are rather broad, the critical temperature and the critical current are not well-defined quantities. At large currents the *QPS* rate is enhanced and the effective wire resistance in a fluctuation - dominated superconducting wire can approach the normal state value in a gentle way. However, at lower temperatures (below $T \sim 1.18$ K) significant departure from the expected behavior appears (see *Fig.E.17* and also *Fig.E.15*). This departure is better seen when $dV/dI(I)$ curve is measured (*Fig.E.17(c)*), namely, instead of expected "smooth" behavior a set of bumps is observed. The behavior of these bumps for sample *Cu126#3after8th* is displayed in *Fig.E.18* in details. As temperature is reduced the bumps appear at higher currents (*Fig.E.18(a)*). Interestingly they disappear upon application of ~ 20 mT perpendicular magnetic field (*Fig.E.18(b)*). If to plot differential conductance vs. voltage ($dI/dV(V)$) bumps occur at quite regular intervals $\Delta V = (5 \pm 1)$ µV (*Fig.E.18(c)*). The effect was reproducible exclusively only in the thinnest (sub-*15* nm) wires and at temperatures below $T \sim 1.18$ K. Note that negative magnetoresistance (*nMR, section E.3.2*) has been observed also only below this temperature. In general dV/dI bumps were more pronounced at lower temperatures. Hence it seems mandatory to perform experiments in the dilution refrigerator to see the effect more clearly. At the moment I do not have solid justification for this observation. However there are several speculations.

1. First one is based on analogy with the usual *quantum particle in a box* problem. When the diameter of a metal wire starts to be comparable to the conducting electron de Broglie wavelength, size quantization phenomena might come into play resulting in a quantized spectrum of the energy states (e.g. quantum well). The effect is usually observed in semi-conductors where the de Broglie wavelength can be of order of *30* nm. In conventional metals (as aluminum) the de Broglie wavelength is smaller then *1* nm. It makes observation of quantization of electron modes rather difficult, but in principle still

possible if one is able to create constriction narrow enough. One can claim heuristically that the free energy potential of *1D* current-carrying dissipating nanowire can be viewed as system of quantum wells each exhibiting quantization of energies (*Fig.E.14, inset*). Applied current can shift energy levels with respect to each other just allowing for the resonant tunneling to occur.

2. Second explanation is somehow related to the first one. One can speculate that electromagnetic modes propagating in a wire (possibly standing waves originating from reflection of the Mooij-Schön plasmons from the wire boundaries [83]) have a discrete energy spectrum with eigen-energies changing appropriately to boundary conditions. It can be heuristically argued that applied current can tilt the free energy washboard potential allowing for resonant tunneling in Hilbert space at values matching the energy of the standing waves. The process would be analogous to tunneling between two quantum wells (each with discrete energy levels) in Euclidean space. This explanation takes into account the important experimental fact: the peculiarities in *dV/dI* curves have been exclusively observed below temperatures $T \sim 1.18$ K. It is the T_c for bulk aluminum. Since contacts (e.g. bonding wires, contact pads, leads) are made from aluminum I believe that their superconducting transition has something in common with "weird" nature of the measured *V(I)* and *dV/dI* curves. Contacts either in normal or superconducting state could define here boundary conditions defining phase slip activation.

3. Another explanation would rely on some resemblance with the current induced phase slip centers (*PSC*) [78]. Unlike intrinsic phase slips studied in this thesis appearing at all values of current, *PSC* appear only for sufficiently strong currents. It is claimed [79], that for thin superconducting wires two different critical currents exist: j_{c2} at which the pure superconducting state becomes unstable and $j_{c1} < j_{c2}$ at which the current-induced phase slip state is realized in the system. It is not excluded that the *dV/dI* "bumps" observed in my experiments are the consequence of successive switching of the current-induced phase slip centers at different values of the bias current.

4. There exist a well-known *Shapiro effect* [84]: formation of current steps on I(V) characteristics in *RF*-irradiated Josephson junctions. Much weaker, but of the same origin, is the *Fiske effect*: formation of the current steps due to re-absorption of the Josephson radiation coming from the junction. Recently it has been shown theoretically that a current-biased superconducting nanowire in the QPS regime is dual to the voltage-biased Josephson junction [9]. Hence, it is not excluded that the equally-spaced peaks of conductivity observed for the nanowires (*Fig.E.18(c)*) are the manifestation of an effect similar to Fiske steps.

Homogeneity of quasi-1D samples is a central issue in interpretation of results. Of particular importance is the presence of weak links capable to mimic non-Ohmic behavior due to Coulomb and Josephson effects. *V(I)* curves exhibit linear (ohmic) behavior above T_c. As T_c is approached one can see a nucleation of superconductivity (*concave-up dV/dI(I) curve at I=0, Fig.E.18(b)*) giving rise to enhanced differential conductivity at small
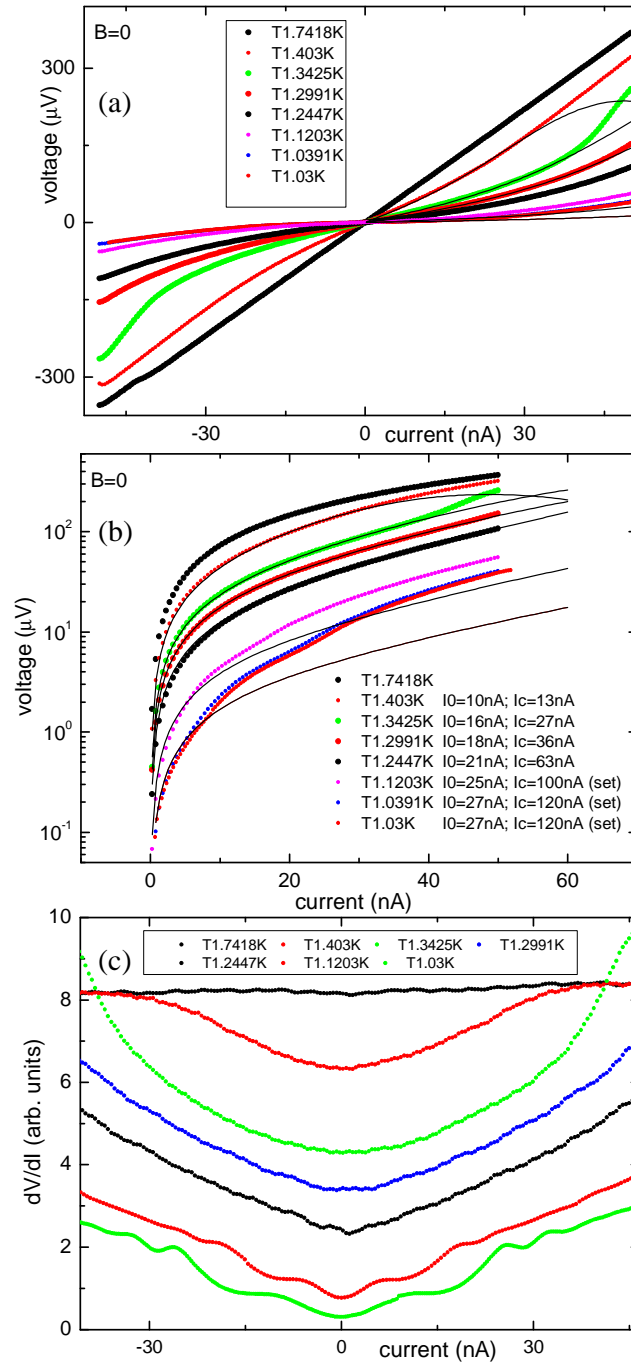
Fig.E.17. *V(I) (a - linear scale, b - semi-log scale) and dV/dI (c) curves recorded for the sample (Cu115#2after8, $\sigma_{av}^{1/2} \sim 15$ nm, L = 10 μm). Thin solid black lines in (a) and (b) are fits to the model (eq. E.11) with two fitting parameters: multiplicative constant (corresponding to vertical shift in logarithmic scale) and the critical current I_c. See legend in (b) for calculated I_0 and I_c fitted for higher temperatures and set to reasonable value for lower temperatures.*

currents (*Fig.E.18(c)*). If there were a junction formed somewhere along a wire then one would expect to observe suppressed conductivity. Hence, I consider the studied wires to be continuous without random junctions which could give rise to Coulomb blockade. However, one can claim that resistance of wires is too small to clearly see the hypothetical Coulomb blockade.
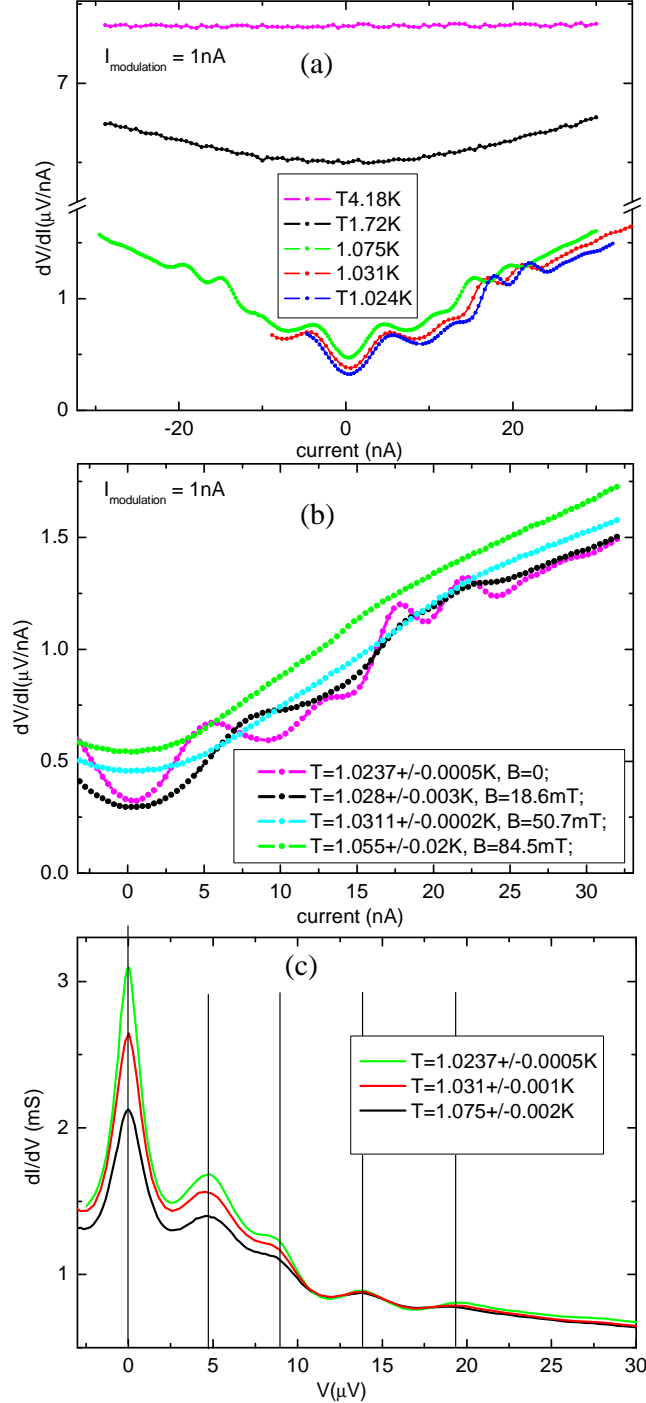

Fig.E.18. *dV / dI(I) curves recorded for the sample Cu126#3after8 ($\sigma_{av}^{1/2}$ ~ 15 nm, L = 10 μm): effect of temperature (a); effect of applied magnetic field (b); recalculation of data from (a) in terms of dI / dV(V)(c). For corresponding superconducting transition see Fig.E.11 (1).*

94

Conclusions (C)

Low energy Ar^+ sputtering has been utilized to progressively reduce cross-sections of lift-off fabricated polycrystalline aluminum nanowires. The strategy for tailoring the samples in a desired way has been described. $V(T,I,B)$ dependencies have been measured for obtained nanowires.

It has been demonstrated that experimental verification of existence of the *Thermally Activated Phase Slip* (*TAPS*) mechanism in polycrystalline aluminum nanowires is not possible. The broadening of the $R(T)$ superconducting transition in thick aluminum samples (with cross-section > 250 nm^2) due to inevitable inhomogeneity can be much larger than the one resulting from the *TAPS* contribution.

It has been shown that **Quantum Phase Slip** (*QPS*, also called *Macroscopic Quantum Tunneling* (*MQT*)) **in thin superconducting polycrystalline aluminum wires (with cross-section < 250 nm^2) is the mechanism responsible for dissipation below the critical temperature T_c.** The finite resistance associated with the *QPS* phenomenon has been measured at temperatures much lower than T_c where thermal activation of phase slips (*TAPS*) is prohibited. **The $R(T)$ transitions for thin wires have much weaker temperature dependence compared to *TAPS* prediction**. It has been proven that inhomogeneity of the studied thin samples can NOT account for the collected experimental evidence. **The physical parameter controlling the QPS rate is the resistance per unit length, or equivalently – the wire diameter**. It has been observed that the *QPS* rate increases progressively as the wire diameter is reduced. It is manifested in experiment as a strong exponential dependence of the effective resistance below the T_c on the wire cross - section. Performing the experiment on a single wire with successively reduced diameter **the gradual crossover between superconducting and quasi-normal (= QPS dominated) behavior has been demonstrated**: in *sub - 15* nm scales the reduction of the wire diameter by few nanometers effectively suppresses superconductivity bringing the wire to the QPS - dominated regime where its effective resistance measured below the T_c approaches the normal state value. Strong dependence of the QPS rate on the wire diameter implicates that **the narrowest section of the sample provides an overwhelming contribution to the measured resistance**. The above observations are in a good agreement with the theoretical model [34].

Unexpected observation of the negative magnetoresistance and the non-monotonous $dV/dI(I)$ dependencies in the QPS regime requires further studies. Particularly measurements down to mK temperatures would be advisable to follow the evolution of the effects in a wider temperature range.

So far mainly studies on amorphous and polycrystalline superconducting nanowires have been reported in literature. To establish existence of the QPS phenomenon measurements on atomically pure samples (e.*g.* MBE-grown) would be recommended.

According to theoretical predictions [35] there are materials (e.g. *Ti)* for which the *QPS* mechanism should be observed at much larger cross-section than for *Al* [1,2] or *MoGe* [26,45]. The investigation of nanowires made of such materials would be highly desired.

Apart from the basic scientific importance for understanding the physics of non-equilibrium superconductivity, the presented study is very significant for numerous applications setting the fundamental limitations for miniaturization of superconducting elements in electronic nanocircuits. *QPS* phenomenon is expected to bring up a new exciting physics. It has been already suggested to use *QPS* junctions as building blocks for quantum bits [8] and quantum standard of current [9].

Appendix 1: Sputtering: evolution of cross-section

The purpose of this appendix is to give a sketch for derivation of functional dependence of *wire cross-section* on the *applied fluence*. As it has been assumed in section W.2.6, the shape of cross-section of a typical lift-off fabricated nanowire can be roughly approximated with a trapezoid. First I will show that the area of the trapezoid decreases with sputtering like a parabola, and then I will derive parameters for the parabola in terms of experimentally measured (or calibrated) quantities.

$$-\frac{dN_{surf}}{d\phi} \propto perimeter$$

Number of atoms removed from the surface N_{surf} is proportional to the perimeter of the structure cross-section exposed to the ion beam bombardment.

$$-\frac{dN_{surf}}{d\phi} \propto -\frac{dN}{d\phi} \propto -\frac{d\sigma}{d\phi}$$

Number of atoms removed from the surface is also the number of atoms removed from cross-section N and is proportional to the decrease in cross-section σ.

$$\sigma \propto perimeter^2$$

If shape of the wire is *kept constant* during sputtering (then one says that successive cross-sections are *similar*). You can easily verify this for triangle or square, and then think that any arbitrary shape can be represented as a sum of triangles or squares.

From above proportionalities we get the differential equation with corresponding initial conditions:

$$-\frac{d\sigma}{d\phi} = A \cdot \sqrt{\sigma}$$
$$\sigma(\phi = 0) = \sigma_o$$
$$\sigma(\phi_o) = 0$$

A is a proportionality constant to be expressed in terms of the physically meaningful parameters: σ_0 – initial cross-section (before 1st sputtering) and fluence ϕ_0 required to just sputter away the whole structure.

The final result for the evolution of the cross-section of the *structure preserving its shape* during sputtering is:

$$\sigma = \sigma_o \cdot (1 - \frac{\phi}{\phi_o})^2$$

For the *flattening model* introduced in *Chapter IV (W)* we deal with the non-constant shape (the trapezoid becomes flatter as it is sputtered). However it is possible to show that the evolving trapezoid in this case can be
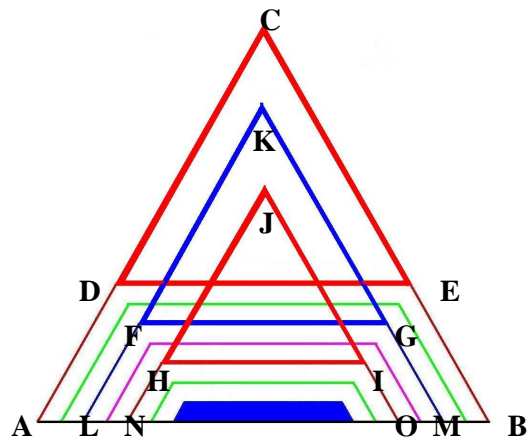

Fig.A.1. Geometrical model used in the derivation.

considered as a difference of two triangles, each of them evolving according to equation derived above for similar figures (see two families of triangles in *Fig.A.1*: *ABC, LMK, NOJ* and *DEC, FGK, HIJ*). It follows that the cross-section of the trapezoid is the difference of two terms with different σ_0 and ϕ_0 for each triangle family:

$$\sigma = \sigma_1 \cdot (1 - \frac{\phi}{\phi_1})^2 - \sigma_2 \cdot (1 - \frac{\phi}{\phi_2})^2 = a\phi^2 + b\phi + c$$

For the sharpening scenario we get the parabolic dependence like the one just derived until triangle is formed for the first time. Then it is sputtered according to formula derived for similar structure.

Since we know that evolution is parabolic we need *3* boundary conditions to determine parameters of parabola*: a*, *b* and *c* in terms of experimentally measurable quantities:

$\sigma(\phi = 0) = \sigma_0 = c$ Initial wire's cross-section is equal to σ_0.

$\sigma(\phi = \phi_0) = 0$ ϕ_0 is fluence required to just sputter whole wire: $\phi_0 = h_0/V_{per}$

$\sigma'(\phi = 0) = b$ *b* is derivative of σ at $\phi = 0$.

Derivative is calculated as follows (DE and EB are given in figure):

$$b = \frac{d\sigma}{d\phi}\Big|_{\phi=0} = \lim_{\Delta\phi \to 0} \frac{V_{per} \cdot DE \cdot \Delta\phi + 2 \cdot V_\alpha \cdot EB \cdot \Delta\phi}{\Delta\phi} = V_{per}(w_0 - \frac{2 \cdot \sigma_0}{h_0}) - V_\alpha \cdot \frac{2 \cdot h_0}{\sin \alpha}$$

where h_0, w_0, σ_0, α - initial height, width, cross-section and side wall angle of trapezoid. These parameters can be determined from *SPM* measurements, we need only *3* of them since 4th is not independent. V_{per} - speed of sputtering for the top part of the trapezoid, V_α -speed of sputtering for the sides of the trapezoid. The speeds can be calibrated for given ion gun).

From third boundary condition the parameter *a* can be expressed in terms of *b*, σ_0 and ϕ_0:

$$a = \frac{-\sigma_0 - b \cdot \phi_0}{\phi_0^2}$$

In analogous way the expression for the sharpening case can be derived.

Appendix 2: Sputtering - layer by layer removal of material

The purpose of this appendix is to give a feeling how accurate sputtering can be. *Fluence ϕ* is defined as the total number of projectiles (in my case Ar^+ ions) that hit *1* cm^2 of a target surface during experiment. Each argon ion on average removes a certain number of aluminum atoms. It is denoted by *yield Y*. Knowing the yield (e.g. from SRIM simulation, e.g. *Fig.W.6*) and the total fluence to sputter the whole wire ϕ_0 , one can

calculate the number of eroded *target* atoms (in my case aluminum) from $S = 1 \times 1$ cm^2 area or equivalently the number of sputtered atomic monolayers *N*:

$$\phi \cdot Y = N \cdot S \cdot \rho$$

where ρ is the *surface atomic density* of the target.

Let's consider sputtering experiment performed on aluminum nanowire (*Fig.A.2*). *1* mol of aluminum (= N_A = *6.02* • *10^{23}* atoms) has the weight of *27* g and aluminum density is *2.7* g/cm^3. It follows that average distance between aluminum atoms in crystalline lattice is *0.26* nm and the corresponding surface density ρ is *1.5* • *10^{15}* atoms/cm^2. The yield read out from *Fig.W.6* for incident angle *40^0* is *Y = 2.5*. If the total fluence is *4* • *10^{17}* at./cm^2 (see asymptote in *Fig.A.2*), then *N = 670* monolayers is the estimation for the initial wire thickness. It should be compared with value *N = 370* coming from the direct recalculation of the initial wire height (h_0 = *97* nm) in terms of the number of atomic monolayers. Taking into account that the total fluence has been calculated with some error it is quite satisfactory agreement. The error for the fluence estimation comes from the fact that we measure the total amount of charge that flows through the sample stage and divide it by the conductive area of the whole sample holder. This conductive area can not be specified very accurately. Even if it was, still there would be uncertainty related to the fact that ion beam has a different local density over the sample stage. Also secondary electrons emitted from bombarded targets can give rise to the measured total current. Another source of error is related to the fact that SRIM considers amorphous targets, hence the used yield is only approximate. Since in calculation I used the average distance between aluminum atoms (= *0.26* nm), the particular crystalline lattice orientation has not been taken into account. After 7th sputtering session sample resistance was *3620* Ω and after *8th* sputtering session sample resistance was *7863* Ω (*Fig.A.2*). The fluence applied between these two data points is *0.049* • *10^{17}* which corresponds roughly to *4 - 8* atomic monolayers, just giving diffe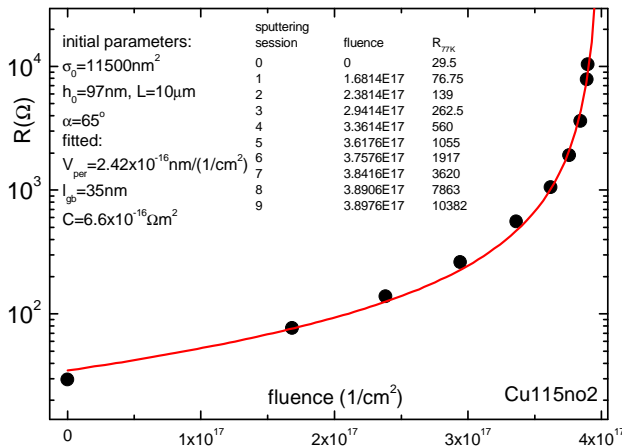rence of *1-2* nm in height of the structure between two sputtering sessions. This estimation is in good agreement with the independent estimate of the wire cross-section based on the normal state resistance. The estimate shows that cross-section changed from ~*350* nm^2 to ~*230* nm^2 (wire was flat, say with width = *70* nm, and whole cross-section change can be attributed to the height reduction). The difference between the *7863* Ω sample and the *10382* Ω (*Fig.A.2*) sample corresponds to just one monolayer sputtered.

Fig.A.2. *Evolution of the wire resistance with Ar$^+$ 1keV fluence.*

Appendix 3: Determination of material constant $K = \rho \bullet l_{mean}$

In my experiments with aluminum nanowires the best fit material constant $K = \rho \bullet l_{mean}$ was found to be equal to $(6 \pm 2) \bullet 10^{-16} \, \Omega m^2$. In various experiments found in literature it varies from 5 to $12 \bullet 10^{-16} \, \Omega m^2$. Here I will calculate its theoretical value. The easiest way is to start with Drude formula for resistivity: $\dfrac{1}{\rho} = \dfrac{n \cdot e^2 \cdot \tau}{m_e}$ with $\tau = \dfrac{l_{mean}}{V_F}$. It immediately yields: $K = \rho \cdot l_{mean} = \dfrac{m_e \cdot V_F}{n \cdot e^2}$. Particularly for aluminum $K = 4 \bullet 10^{-16} \, \Omega m^2$ ($n = 1.8 \, x \, 10^{29}/m^3$, $V_F = 2 \bullet 10^6$ m/s, $e = 1.6 \bullet 10^{-19}$ C, $m_e = 9.1 \, x \, 10^{-31}$ kg).

One can also start with Einstein relation for degenerate conductor: $\dfrac{1}{\rho} = e^2 \cdot N_F \cdot D; \; N_F = g(E_F) = \dfrac{1}{2 \cdot \pi^2} \cdot (\dfrac{2m}{\hbar^2})^{3/2} \cdot \sqrt{E_F}$ (N_F - density of states at Fermi level). Diffusion constant D can be expressed as $D = 1/3 \cdot V_F \cdot l_{mean}$. Combining these two formulas one arrives at: $K = \rho \cdot l_{mean} = \dfrac{3}{V_F \cdot e^2 \cdot N_F}$. It is the same like the one derived from Drude formula if to notice that concentration of electrons $n = \int\limits_0^{Ef} g(E)dE$.

If to assume that K for sample is known with good accuracy then product of the wire cross-section σ and the elastic mean free path l_{mean} is easily calculated: $\sigma \cdot l_{mean} = \dfrac{K \cdot L}{R}$. However additional assumption is needed to split this product into separate components. In my work I usually assumed the trapezoid shape of the nanowire cross-section giving $\sigma = h \bullet FWHM$ (h - height, $FWHM$ - Full Width at Half Maximum) and $l_{mean} = h$ for sufficiently thin (= flat) wires. Assumption $l_{mean} = h$ is quite reasonable keeping in mind that at these scales and temperatures elastic scattering is mainly determined by the physical boundaries: the smallest dimension sets the scale for the mean free path. Both $FWHM$ and h can be estimated reasonably with SPM.

Appendix 4: Elastic mean free path in thin granular wires

Studied wires were granular. At low temperatures for sufficiently thick wires (grain size << transverse dimension of the wire) the momentum relaxation can be considered to happen mainly at the grain boundaries and impurities. However, when the diameter of the wire is reduced below the average grain size (~ 40 nm in our samples) the surface scattering can not be neglected.

In the following section elastic mean free path for diffusive wire is derived. We assume scattering on the impurities and grain boundaries which is exactly the same as it

would be in the bulk material. Additionally we take into account the scattering due to sample boundaries. Electron moves inside the sample with Fermi velocity V_F. Equipartition of kinetic energy requires that average speed in each of the equivalent directions is the same and equal to $V_x = V_y = V_z = V_F / \sqrt{3}$. Total momentum relaxation time is τ. This time multiplied by Fermi velocity gives average distance traveled between any kinds of elastic scatterings which we call the elastic mean free path l_{mean}. $1/\tau$ is the number of scatterings per unit time. It accounts for all kinds of elastic scattering: $1/\tau_{gbx}=1/\tau_{gby}=1/\tau_{gbz}$ scatterings due to the grain boundaries and impurities in x-, y- and z- directions, $1/\tau_y$ scatterings due to sample boundaries in y direction and $1/\tau_z$ scatterings due to sample boundaries in z direction (in the x direction the wire has no boundary). On multiplying each of these times by the average velocity in one direction we get elastic mean free path with respect to particular kind of scattering:

$$\tau_{gbx} \cdot \frac{V_F}{\sqrt{3}} = \tau_{gby} \cdot \frac{V_F}{\sqrt{3}} = \tau_{gbz} \cdot \frac{V_F}{\sqrt{3}} = l_{gb} = linear\ size\ of\ grain$$

$$\tau_y \cdot \frac{V_F}{\sqrt{3}} = FWHM = Full\ Width\ at\ Half\ Maximum\ of\ the\ WIRE$$

$$\tau_z \cdot \frac{V_F}{\sqrt{3}} = h = height\ of\ the\ wire$$

FWHM is defined such that: $FWHM \cdot h = \sigma = cross\ section\ of\ the\ wire$. Total number of scatterings in unit time reads:

$$\frac{1}{\tau} = \frac{1}{\tau_{gbx}} + \frac{1}{\tau_{gby}} + \frac{1}{\tau_{gbz}} + \frac{1}{\tau_y} + \frac{1}{\tau_z}$$

On substituti on :

$$\frac{1}{\tau} = \frac{1}{\dfrac{l_{mean}}{V_F}} = 3 \cdot \frac{1}{\dfrac{\sqrt{3} \cdot l_{gb}}{V_F}} + \frac{1}{\dfrac{\sqrt{3} \cdot h}{V_F}} + \frac{1}{\dfrac{\sqrt{3} \cdot FWHM}{V_F}}$$

$$\frac{\sqrt{3}}{l_{mean}} = \frac{3}{l_{gb}} + \frac{1}{h} + \frac{1}{FWHM}$$

Final result :

$$l_{mean} = \frac{\sqrt{3} \cdot l_{gb} \cdot \sigma}{3 \cdot \sigma + l_{gb}(\sigma / h + h)} \quad or \quad \frac{1}{l_{mean}} = \frac{1}{l_{mean\_bulk}} + \frac{1}{l_{mean\_meso}} = \frac{1}{\dfrac{\sqrt{3}}{3} \cdot l_{gb}} + \frac{1}{\dfrac{\sqrt{3} \cdot \sigma}{\sigma / h + h}} \quad (A.4.1)$$

It can be checked that in the limit $h<<l_{gb}$ and $h<<FWHM$ (flat wire) formula for l_{mean} reduces to:

$$l_{mean} = \sqrt{3} \cdot h$$

If $h << FWHM$ and $l_{gb} << FWHM$, which was usually the case in studied wires term $\sim 1/FWHM$ can be neglected and mean free path is given by expression:

$$l_{mean} = \frac{\sqrt{3} \cdot l_{gb} \cdot h}{3 \cdot h + l_{gb}}$$

In our nanowires at low temperatures the bulk mean free path (= before sputtering in thick wires) was about *30 - 60* nm being mainly determined by the grain size. Usually, in ultra-narrow samples, I assumed $l_{mean} = h$ which gives very similar result as the above rigorous estimation. However, for modeling of the wire resistance as a function of the ion fluence I used the full formula for l_{mean} (*eq. A.4.1*) since it exhibits desired crossover between macroscopic and mesoscopic limits (cf. *section W.3*).

Appendix 5: BCS superconducting gap

The implicit relation for the *temperature-dependent superconducting gap* reads [85]:

$$\frac{1}{N(0) \cdot V} = \int_{-\hbar \omega_D}^{\hbar \omega_D} \frac{\tanh\{ \left[e^2 + \Delta^2(T) \right]^{1/2} / (2 k_B T) \}}{2 \cdot \left[e^2 + \Delta^2(T) \right]^{1/2}} de$$

At $T = 0$ for the weak electron-phonon coupling $N(0)V << 1$ the following two relations hold:

$$\Delta(0) = 2 \cdot \hbar \omega_D \cdot e^{-1/N(0)V}$$
$$\Delta(0) = 1.76 \cdot k_B T_c$$

It allows rewriting the BCS gap equation in dimensionless form convenient for numerical calculation:

$$\frac{1}{N(0) \cdot V} = \int_{-\exp(1/N(0)V)/2}^{\exp(1/N(0)V)/2} \frac{\tanh\{ \left[e'^2 + \Delta'^2(t) \right]^{1/2} / (2 \cdot t/1.76) \}}{2 \cdot \left[e'^2 + \Delta'^2(t) \right]^{1/2}} de'$$

where $N(0)V << 1$ (weak coupling); $e' = e / \Delta(0)$; $\Delta'(t) = \Delta(T) / \Delta(0)$; $t = T / T_c$

The equation was solved self-consistently for the gap parameter. The result is presented in *Fig.A.3*. The handy simple approximate formula for variation of the gap with temperature takes the form:

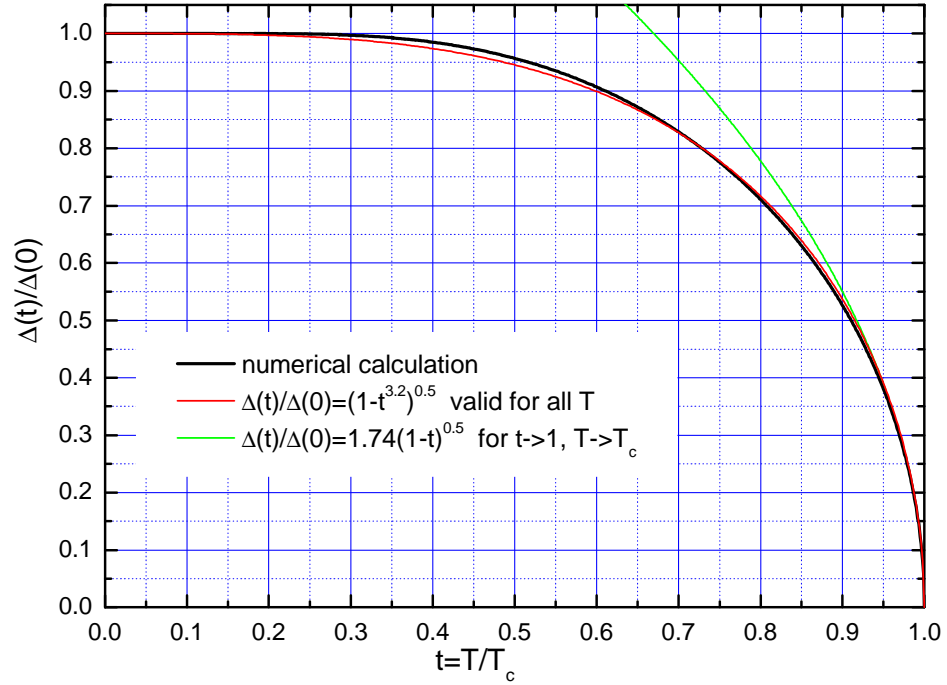$$\Delta(T) / \Delta(0) = (1 - (T / T_c)^{3.2})^{1/2}$$

Fig.A.3. *Temperature dependence of the BCS superconducting energy gap: numerically solved gap equation (1/N(0)V=15), fitted approximate formula and the asymptotic relation.*

Acknowledgements

References

1. M. Zgirski, K-P. Riikonen, V. Touboltsev, and K. Arutyunov, *Size Dependent Breakdown of Superconductivity in Ultranarrow Nanowires*, NanoLetters, 5, 1029 (2005)

2. M. Zgirski, K.-P. Riikonen, V. Touboltsev, K. Arutyunov, *Quantum fluctuations in ultranarrow superconducting aluminum nanowires*, Phys. Rev. B 77, 1 (2008)

3. M. Zgirski, K. Arutyunov, *Experimental limits of the observation of thermally activated phase-slip mechanism in superconducting nanowires*, Phys. Rev. B 75, 172509 (2007)

4. M. Zgirski, K.-P. Riikonen, V. Touboltsev, P. Jalkanen, T. Hongisto, K. Arutyunov, *Ion beam shaping and downsizing of nanostructures*, Nanotechnology 19, 055301 (2008)

5. A. Shanenko, M. Croitoru, M. Zgirski, F.M. Peeters, K. Arutyunov, *Size dependent enhancement of superconductivity in Al and Sn nanowires: shape-resonance effect*, Phys. Rev. B 74, 052502 (2006)

6. J.M. Martinis, M.H. Devoret, J. Clarke, *Experimental tests for the quantum behavior of a macroscopic degree of freedom: The phase difference across a Josephson junction*, Phys. Rev. B 35, 4682 (1987)

7. A.J. Leggett, J.Phys (Paris), *Colloq. 39*, C6-1264 (1978); *Les Houches Summer School on Chance and Matter*, (North-Holland, Amsterdam, 1986);
   Shin Takagi, *Macroscopic Quantum Tunneling*, Cambridge University Press (2002)

8. J.E. Mooij, C. Harmans, *Phase slip flux qubits*, New Journal of Physics 7, 219 (2005)

9. J.E. Mooij, Yu.V. Nazarov, *Superconducting nanowires as quantum phase-slip junctions*, Nature Lett. 2, 169 (2006)

10. L.G. Aslamazov, A.I. Larkin, *Effect of fluctuations on properties of a superconductor above critical temperature*, Sov. Phys. Solid State 10, 875 (1968)

11. F. Sharifi, A.V. Herzog, and R.C. Dynes, *Crossover from Two to One Dimension in In Situ Grown Wires of Pb*, Phys. Rev. Lett. 71, 428 (1993)

12. W.A. Little, *Decay of Persistent Currents in Small Superconductors*, Phys. Rev. 156, 396 (1967)

13. G. Schön, *Superconducting nanowires*, Nature 404, 948 (2000)

14. J.E. Mooij and G. Schön, *Propagating Plasma Mode in Thin Superconducting Filaments*, Phys. Rev. Lett. 55,114(1985)

15. R.P. Feynmann, R.B. Leighton, M. Sands, *The Feynman Lectures on Physics*, vol.3, ch.21

16. J.S.Langer and V. Ambegaokar, *Intrinsic resistive transition in narrow superconducting channels*, Phys. Rev.164,498 (1967)

17. L.P. Gor'kov, *On the energy spectrum of superconductors*, J. Exp. Theoret. Phys. (U.S.S.R.) 34, 735-739 (1958)

18. B.D. Josephson, *Possible new effects in superconductive tunnelling,* Physics Letters 1, 251-253 (1962)

19. S. V. Panyukov and A.D. Zaikin, *Correlation functions and transport properties of granular arrays with ohmic dissipation*, Phys. Lett. A 156, 119 (1991)

20. D.E. McCumber and B.I. Halperin, *Time scale of intrinsic resistive fluctuations in thin superconducting wires*, Phys. Rev. B 1,1054(1970)

21. C.N. Lau, *PhD Thesis*, Harvard University, 2001

22. M. Tinkham, *Introduction to Superconductivity*, McGraw Hill, New York (1996)

23. D. Meidan, Y. Oreg, G. Refael, *Sharp superconductor-insulator transition in short wires*, Phys. Rev. Lett. 98, 187001 (2007)

24. J.E. Lukens, R.J. Warburton, W.W. Webb, *Onset of Qunatized Thermal Fluctuations in "One-Dimensional" Superconductors*, Phys. Rev. Lett. 25, 1180 (1970)

25. R.S. Newbower, M.R. Beasley, M. Tinkham, *Fluctuation Effects on the Superconducting Transition of Tin Whisker Crystals*, Phys. Rev. B 5, 864 (1972)

26. C.N. Lau, N. Markovic, M. Bockrath, A. Bezryadin, M. Tinkham, *Quantum Phase Slips in Superconducting Nanowires*, Phys. Rev. Lett. 87, 217003(2001)

27. A.J. van Run, J. Romijn, J.E. Mooij, *Superconducting phase coherence in very weak aluminum strips,* Jpn. J. Appl. Phys. Part 1 26, 1765 (1987) – regular papers, short notes & review papers

28. N. Giordano, *Evidence for Macroscopic Quantum Tunneling in One-Dimensional Superconductors*, Phys. Rev. Lett. 61, 2137 (1988)

29. S. Saito, Y. Murayama, *Effect of dissipation on macroscopic quantum tunneling in thin superconducting wires*, Phys. Lett. A 139, 85 (1989)

30. N. Giordano, *Superconducting fluctuations in one dimension*, Physica B 203 (1994)

31. A.O. Caldeira, A.J.Leggett, *Influence of Dissipation on Quantum Tunneling in Macroscopic Systems,* Phys. Rev. Lett. 46, 211 (1981)

32. A. Zaikin, D. Golubev, A. van Otterlo and G.T. Zimanyi, *Quantum Phase Slips and Transport in Ultrathin Superconducting Wires*, Phys. Rev. Lett. 78,1552 (1997)

33. A. Zaikin, D. Golubev, A. van Otterlo and G.T. Zimanyi, *Quantum Fluctuations and Dissipation in Thin Superconducting Wires*, Usp. Fiz. Nauk. 168, 244 (1998)

34. D. Golubev, A. Zaikin, *Quantum tunneling of the order parameter in superconducting nanowires*, Phys. Rev. B 64, 014504 (2001)

35. K.Yu. Arutyunov, D. Golubev, A. Zaikin, *Superconductivity in one dimension*, Phys.Rep. 469, 1 (2008), arXiv:0805.2118v2

36. J.M. Duan, *Quantum Decay of One-Dimensional Supercurrent: Role of Electromagnetic Field*, Phys. Rev. Lett. 74, 5128 (1995)

37. V.S. Berezinskii, *Destruction of long-range order in one-dimensional and two-dimensional systems having a continous symmetry group 1- classical systems*, Sov. Phys. JETP 32, 493 (1971);
J.M. Kosterlitz, D.J. Thouless, *Ordering, metastability and phase transitions in 2-dimensional systems,* J. Phys. C – Solid State Physics 6, 1181 (1973)

38. J.E. Lukens, R.J. Warburton, W.W. Webb, *Onset of Qunatized Thermal Fluctuations in "one-Dimensional" Superconductors*, Phys. Rev. Lett. 25, 1180 (1970)

39. R.S. Newbower, M.R. Beasley, M. Tinkham, *Fluctuation Effects on the Superconducting Transition of Tin Whisker Crystals*, Phys. Rev. B 5, 864 (1972)

40. K. Arutyunov*, Fabrication of Quasi-One-Dimensional Superconducting Micro- and Nanostructures*, Recent Patents in Nanotechnology 1, 129 (2007)

41. W.J. Skocpol, M.R. Beasley and M. Tinkham, *Self heating hotspots in superconducting thin-film microbridges*, J. Appl. Phys. 45, 4054 (1974)

42. T.M. Klapwijk, M. Sepers and J.E. Mooij, *Regimes in the behavior of superconducting microbridges*, J. Low T. Phys. 27, 801 (1977)

43. A.M.Kadin, W.J. Skocpol and M. Tinkham, *Magnetic field dependence of relaxation times in nonequilibrium superconductors*, J. Low T. Phys. 33, 481 (1978)

44. B. Huard, H. Pothier and D. Esteve, *Electron heating in metallic resistors at sub-Kelvin temperature*, Phys. Rev. B 76, 165426 (2007)

45. A.Bezryadin, C.N. Lau, M. Tinkham, *Quantum suppression of superconductivity in ultrathin nanowires*, Nature 404 (2000)

46. A. Bezryadin, *Quantum suppression of superconductivity in nanowires*, J. Phys.:Cond. Mat. 20, 043202 (2008)

47. A.T. Bollinger, A. Rogachev, M. Remeika, A. Bezryadin, *Effect of morphology on the superconductor-insulator transition in one-dimensional nanowires*, Phys. Rev. B 69, 180503(R) (2004)

48. A.T. Bollinger, A. Rogachev, A. Bezryadin, *Dichotomy in short superconducting nanowires: Thermal phase slippage vs. Coulomb blockade*, Europhys. Lett. 76 (3), pp.505-511 (2006)

49. M. Tian et al., *Dissipation in quasi-one-dimensional superconducting single-crystal Sn nanowires*, Phys. Rev. B 71, 104521 (2005)

50. F. Altomare, A. Chang, M. Melloch, Y. Hong, Ch. Tu, *Evidence for Macroscopic Quantum Tunneling of Phase Slips in Long One-Dimensional Superconducting Al Wires*, Phys. Rev. Lett. 97, 017001 (2006)

51. K. Bouzehouane et al., *Nanolithography based on real-time electrically-controlled indentation with an atomic force microscope for nanocontacts elaboration*, arxiv.org/ftp/cond-mat/papers/0306/0306068.pdf

52. D.M. Eigler and E.K. Schweizer*, Positioning Single Atoms With a Scanning Tunneling Microscope*, Nature 344, 524 (1990)

53. S. Nishimura, Y. Takemura and J. Shirakashi*, SPM local oxidation nanolithography with active control of cantilever dynamics*, Journal of Physics: Conference Series 61 (2007) 1066–1070

54. S. Michotte et al., *Development of phase-slip centers in superconducting Sn nanowires*, Appl. Phys. Lett., 85, 3175 (2004)

55. M. Tian et al., *Synthesis and characterization of superconducting single-crystal Sn nanowires*, Appl. Phys. Lett., 83, 1620 (2003)

56. E.J. Menke, Q. Li, and R.M. Penner, *Bismuth Telluride (Bi2Te3) Nanowires Synthesized by Cyclic Electrodeposition/Stripping Coupled with Step Edge Decoration*, NanoLetters 4, 2009 (2004)

57. M. Savolainen, K. Arutyunov *et al.*, *Ion beam sputtering for progressive reduction of nanostructures dimensions*, Appl. Phys. A. 79, 1769 (2004)

58. N. Giordano, *Dissipation in a one-dimensional superconductor: Evidence for macroscopic quantum tunneling*, Phys. Rev. B, 41, 6350 (1990);
    N. Giordano, *Superconductivity and dissipation in small diameter Pb-In wires*, Phys. Rev. B, 43, 160 (1991)

59. A. Yurgens, D. Winkler, T. Claeson, N. Zavaritsky, *In situ controlled fabrication of stacks of high-Tc intrinsic Josephson junction*, Appl. Phys. Lett. 70, 1760 (1997);
    L.X. You, M. Torstensson, A. Yurgens, D. Winkler, C.T. Lin, B. Liang , *Single intrinsic Josephson junction with double-sided fabrication technique*, Appl. Phys. Lett. 88, 222501 (2006)

60. J.F. Ziegler, J.P. Biersack, M.D. Ziegler, *The Stopping and Range of Ions in Matter (SRIM)*, freeware http://www.srim.org/

61. M. Moseler et al., *The Ultrasmoothness of Diamond-like Carbon Surfaces*, Science, 309, 1545 (2005)

62. e.g. P. Santhanam, S. Wind, D. Prober, *Localization, superconducting fluctuations, and superconductivity in thin films and narrow wires of aluminum,* Phys. Rev. B, 35, 3188 (1987)

63. H.G. Scott, *Sputtering of Gold by Low Energy Inert Gas Ions*, J. Appl. Phys.33, 2011 (1962)

64. I.A. Parshin, I.L. Landau and L. Rinderer, *Conductivity onset and superconducting properties of quench-condensed gallium films deposited onto different substrates,* Phys. Rev. B 54, 1308 (1996)

65. A. Rogachev, A. Bezryadin, *Superconducting properties of polycrystalline Nb nanowires templated by carbon nanotubes*, Appl. Phys. Lett. 83, 3 (2003)

66. V.L. Ginzburg, *On surface superconductivity*, Phys. Lett. 13, 101 (1964)

67. Y. Oreg, A. Finkelstein, *Suppresion of T_c in superconducting amorphous wires*, Phys. Rev. Lett. 83, 191 (1999)

68. B. Abeles, R.W. Cohen and G.W. Cullen, *Enhancement of superconductivity in metal films*, Phys. Rev. Lett. 17, 632 (1966)

69. W. Buckel, R. Hilsch, *Einfluss der kondensation bei tiefen temperaturen auf den elektrischen widerstand und die supraleitung fur verschiedene metalle*, Z. Physik 138, 109 (1954)

70. I.S. Khukhareva, *The superconducting properties of thin aluminum films*, Sov. Phys. JETP 16, 828 (1963); I.S. Khukhareva, *Superconducting properties of freshly deposited mercury films*, Sov. Phys. JETP, 14, 526 (1962)

71. P. Jalkanen, V. Touboltsev, A. Virtanen, K. Arutyunov, J. Raisanen, O. Lebedev, G.V. Tendeloo, *Critical temperature modification of low dimensional superconductors by spin doping,* Sol. St. Comm., 142,407 (2007)

72. M. Meschke, W. Guichard, J. Pekkola, *Single-mode heat conduction by photons*, Nature 444, 187(2006)

73. B. Huard, *PhD Thesis*, SPEC-CEA Saclay (2006), p.248

74. K. Arutyunov, *Negative magnetoresistance of ultra-narrow superconducting nanowires in the resistive state,* Physica C 468, 272 (2008)

75. P. Xiong, A. Herzog, R. Dynes, *Negative Magnetoresistance in Homogeneous Amorphous Superconducting Pb Wires*, Phys. Rev. Lett. 78, 927 (1997)

76. A. Rogachev et.al., *Magnetic enhancement of superconductivity in ultranarrow wires*, Phys. Rev. Lett. 97, 137001-1 (2006)

77. J.D. Meyer, G.V. Minnigerode, *Instabilities in transition curve of current carrying one-dimensional superconductors*, Phys. Lett. A 38, 529 (1972)

78. R. Tidecks, *Current-Induced Nonequilibrium Phenomena in Quasi-One-Dimensional Superconductors*, Spriger, NY, 1990

79. D.Y. Vodolazov *et al.*, *Current-voltage characteristics of quasi-one-dimensional superconductors: An S-curve in the constant voltage regime*, cond-mat/0304193v2

80. S. Michotte *et al.*, *Development of phase-slip centers in superconducting Sn nanowires*, Appl. Phys. Lett. 85, 3175 (2004)

81. S. Michotte *et al.*, *Condition of the occurrence of phase slip centers in superconducting nanowires under applied current or voltage*, cond-mat/0309699v1

82. M. Stuivinga, C.L.G. Ham, T.M. Klapwijk, J.E. Mooij, *Phase slip centers in superconducting aluminum strips*, J. Low Temp. Phys. 53, 633 (1983); M. Stuivinga, T.M. Klapwijk, J.E. Mooij, A. Bezuijen, *Self-heating of phase slip centers*, J. Low Temp. Phys. 53, 673 (1983)

83. Yu. Nazarov, private communication

84. S. Shapiro, *Josephson currents in superconducting tunneling: the effect of microwaves and other observations*, Phys. Rev. Lett. 11, 80 (1963)

85. T. van Duzer, Ch.W. Turner, *Principles of Superconductive Devices and Circuits*, Prentice Hall (1999), 2nd ed.